MICROCOPY RESOLUTION TEST CHART

NATIONAL BUREAU OF STANDARDS – 1963 – A

ARL-TR-85-21

Copy No. *11*

AD-A160 900

GENERATION OF UNDERWATER SOUND BY A MOVING HIGH-POWER LASER SOURCE

Yves H. Berthelot

APPLIED RESEARCH LABORATORIES
THE UNIVERSITY OF TEXAS AT AUSTIN
POST OFFICE BOX 8029, AUSTIN, TEXAS 78713-8029

1 August 1985

Technical Report

Prepared for:

OFFICE OF NAVAL RESEARCH
DEPARTMENT OF THE NAVY
ARLINGTON, VA   22217

DTIC
ELECTE
NOV 0 4 1985
E

85 11 04 119

REPORT DOCUMENTATION PAGE		READ INSTRUCTIONS BEFORE COMPLETING FORM
1. REPORT NUMBER	2. GOVT ACCESSION NO. AD. A160 7CC	3. RECIPIENT'S CATALOG NUMBER
4. TITLE (and Subtitle) GENERATION OF UNDERWATER SOUND BY A MOVING HIGH-POWER LASER SOURCE		5. TYPE OF REPORT & PERIOD COVERED technical report
		6. PERFORMING ORG. REPORT NUMBER ARL-TR-85-21
7. AUTHOR(s) Yves H. Berthelot		8. CONTRACT OR GRANT NUMBER(s) N00014-82-K-0425
9. PERFORMING ORGANIZATION NAME AND ADDRESS Applied Research Laboratories The University of Texas at Austin Austin, Texas 78713-8029		10. PROGRAM ELEMENT, PROJECT, TASK AREA & WORK UNIT NUMBERS
11. CONTROLLING OFFICE NAME AND ADDRESS Office of Naval Research Department of the Navy Arlington, VA 22217		12. REPORT DATE 1 August 1985
		13. NUMBER OF PAGES 204
14. MONITORING AGENCY NAME & ADDRESS(If different from Controlling Office)		15. SECURITY CLASS. (of this report) UNCLASSIFIED
		15a. DECLASSIFICATION/DOWNGRADING SCHEDULE

16. DISTRIBUTION STATEMENT (of this Report)

Approved for public release; distribution unlimited.

17. DISTRIBUTION STATEMENT (of the abstract entered in Block 20, If different from Report)

18. SUPPLEMENTARY NOTES

19. KEY WORDS (Continue on reverse side If necessary and Identify by block number)

thermoacoustics	moving source	convolution
optoacoustics	Doppler shift	exponential shading
laser-induced sound	transonic velocity	line source
arrays	impulse response	

20. ABSTRACT (Continue on reverse side If necessary and identify by block number)

The generation of underwater sound by a high-power laser pulse is analyzed both theoretically and experimentally. The mechanism of sound generation is the thermal expansion of the water caused by heat imparted by the laser. The basic physical properties of such a laser-induced thermoacoustic source are investigated with a time domain approach which is valid in the nearfield of the source. Results are then extended to the case of a thermoacoustic source moving at subsonic, transonic, or supersonic velocities on the surface of the water. Special attention is paid to the case of a source roving at a velocity close to

20. (cont'd)

the speed of sound in the water, because, at such a velocity, high pressure transients can be generated, making the thermoacoustic mechanism of sound generation more attractive for practical applications. Experimental results were obtained with a laser system providing up to 5 joules of energy over a pulse duration of approximately 1 ms, during which the intensity was modulated at a single frequency between 5 and 80 kHz. The laser emitted either in the infrared region of the spectrum (Neodymium:Glass rod, optical wavelength 1.06 μm) or in the visible region of the spectrum (Ruby rod, optical wavelength 0.6943 μm). Most of the experimental results presented in this study were obtained with the Neodymium:Glass laser. Four kinds of results were obtained: pressure waveforms, directivity patterns, sound level dependence on source velocity, and spreading curves. In general, the experimental results are in good agreement with the theoretical predictions.

FOREWORD

This report is an adaptation of Yves H. Berthelot's Ph.D. dissertation (same title). The degree was granted in August 1985 by the Graduate School of The University of Texas at Austin.

Accession For	
NTIS GRA&I	☒
DTIC TAB	☐
Unannounced	☐
Justification	
By	
Distribution/	
Availability Codes	
Dist	Avail and/or Special
A-1	

QUALITY INSPECTED 5

Ilene J. Busch-Vishniac
Supervisor

TABLE OF CONTENTS

Table of Contents (Cont.)

Table of Contents (Cont.)   <u>Page</u>

LIST OF FIGURES

List of Figures (Cont.)   Page

LIST OF TABLES

LIST OF IMPORTANT SYMBOLS

a	laser beam radius
A	optical transmissivity between air and water
c	sound speed
c_p	specific heat at constant pressure
D	Doppler factor
$D_\nu(.)$	parabolic cylinder function of order ν
f	frequency
f_0	laser modulation frequency
f_d	Doppler shifted frequency
G	Doppler gain
h	height of the rotating mirror above the water surface
$h(.)$	impulse response of a thermoacoustic source
$h_\theta(.)$	horizontal impulse response
$h_L(.)$	vertical impulse response
$H(\omega)$	Fourier transform of $h(t)$
$H_\theta(\omega)$	Fourier transform of $h_\theta(t)$
$H_L(\omega)$	Fourier transform of $h_L(t)$
I	Laser intensity (z-component)
$\mathbf{I}$	Laser intensity vector
I_0	envelope of laser pulse
k	wave number ω/c
k_d	Doppler shifted wave number
K	constant of proportionality ($A\beta c\alpha/4\pi c_p$)

L	$1/e$ length of the thermoacoustic source $(1/\alpha)$
M	Mach number v/c
$\mathbf{M}$	$M \sin\theta_0 \cos\phi_0$
$\mathbf{p}, p_0, p$	total pressure, ambient pressure, acoustic pressure
$p(t)$	acoustic pressure
$p_i(t)$	elementary acoustic pressure (see page 63)
$p_T(t)$	total acoustic pressure
q	heat added into the medium per unit time and volume
r_0	initial range
R_0	$r_0/c\tau_p$ nondimensional range
r_m , r_M	see page 115
s, s_0, s	total entropy, ambient entropy, acoustic entropy
S	laser beam cross section
t	time coordinate
t_R, t_m, t_M	see pages 97 and 115
T, T_0, T	total, ambient, and acoustic temperature
v	source velocity
$V_{1/2}$	half-wave voltage of the Pockels cell
V	voltage applied to the Pockels cell
x, y, z	spatial coordinates
x_t, x_c, x_N	see page 100
α	coefficient of absorption of light
β	coefficient of thermal expansion

Γ	nondimensional parameter $\alpha r_0 \cos\theta_0$
$\delta(.)$	Dirac delta function
θ_0	initial angle of observation
θ_{HP}	half-power beamwidth in the directivity pattern
θ_{max}	tilt angle of the main lobe in the directivity pattern
Θ	angle of observation between source and receiver
λ	wavelength
λ_d	Doppler shifted wavelength
$(\lambda + 2\mu)$	coefficient of viscosity
ρ, ρ_0, ρ	total density, ambient density, acoustic density
σ	nondimensional wavenumber k/α
$\tau(.)$	vertical diffraction time
τ_p	laser pulse duration
τ_p	received pulse duration
ϕ_0	initial azimuthal angle
ψ	deflection angle between the laser beam and the vertical
ω	angular frequency
ω_d	Doppler shifted angular frequency
ω_0	angular frequency of the laser modulation
Ω	nondimensional frequency $f_0/(c/a \sin\theta_0)$

CHAPTER I

INTRODUCTION

The generation of sound by a source of light was investigated experimentally more than one hundred years ago by Bell,[1] who came to the conclusion that "sonorousness, under the influence of intermittent light, is a property common to all matter". Bell's experiment resulted in the construction of a "photophone" or apparatus for the production of sound by light. Bell's invention of the photophone was neglected for many years, but recently it has received more attention because new developments in high power laser technology make this type of sound generation more suitable for practical applications. There is an obvious advantage to opto-acoustic generation of sound: it does not require any physical transducer in the medium in which one wants to generate sound. This unique property of laser-induced sound has prompted intensive research in the past twenty years in various fields such as nondestructive testing, molecular spectroscopy, and sonar applications to name only a few. Tam[2] lists more than 400 references on laser-induced sound and Pierce's recent bibliography[3] on the same subject is more than twelve pages long.

There are several ways to produce sound with a laser. The most common mechanisms of optical to acoustical transduction are, by order of increasing efficiency, electrostriction, thermal expansion, surface evaporation, explosive boiling and optical breakdown. Electrostriction is

the result of polarization of molecules due to the electromagnetic input in the medium. The polarization of molecules induces changes in density and therefore produces sound which propagates in the medium. The thermal mechanism relies on heating of the medium by the laser. Changes in temperature produce changes in density and subsequently an acoustic wave. Surface evaporation may occur if the energy density of the laser at the point of impact on the medium is sufficiently high. In this case momentum transferred into the medium generates a sound wave. At even higher energy densities, it is possible to have bubble formation in the medium, and the collapse of the bubbles radiates noise. Finally, for extremely high laser energy densities, such as in the case of a focused high power laser, a very hot plasma is formed locally around impurities in the liquid and "rapidly expanding cavities appear in the focal region, followed by shock wave propagation, cavity deceleration, localized cavitation, and eventual bubble collapse."[4] This is known as sound generation by optical breakdown. The earliest experimental detections of laser-induced sound were reported in 1963.[5,6]

In this study, we restrict our attention to the specific mechanism of thermal expansion. A sound source which relies on heating of the medium by a light source is referred to as a thermoacoustic source (TS) or optoacoustic antenna. Most thermoacoustic sources are created by shining a laser into a medium (usually water). The intensity of the laser is amplitude modulated at a fixed frequency so that it induces a periodic heating of the medium and therefore a fluctuation of density. This in turn generates an acoustic wave whose frequency is equal to the frequency at which the

2

laser intensity is modulated. The wave equation describing the sound field of a lossless medium containing heat sources was first derived by Ingard.[7] A few years later Westervelt and Larson[8] showed theoretically that very directive sound beams of low frequency can be achieved by exploiting the thermoacoustic conversion of energy in water. The first experimental verifications of the directional properties of thermoacoustic sources were made by Muir, Culbertson and Clynch,[9] who confirmed the validity of the theoretical model. As expected, the efficiency of the conversion of electromagnetic energy into acoustic energy was found to be very small (of the order of 10^{-8}) and they concluded that, "for potential applications of practical interest, (...) megawatts of optical power would probably be required in the megahertz frequency region, with gigawatts of power required in the kilohertz region, and terawatts of power necessary in the low audio band." This low efficiency barrier was investigated in detail by Soviet physicists and they showed[10,11,12] that motion of the TS is expected to significantly increase the peak amplitude of the thermoacoustic signal, especially for a source moving at velocities close to the speed of sound for the medium. Such high source velocities are easily achieved experimentally. Since there is no physical transducer in the medium, drag force and flow noise are non-existent.

The main objective of the present study is to investigate the basic physical properties of a laser-induced TS and to extend the results to the case of a moving thermoacoustic source (MTS). Previous studies of MTS have been limited by experimental apparatus. They are also restricted to farfield radiation, and theoretical models generally break down when the

3

MTS is moving at a velocity close to the speed of sound in the medium. The sophisticated experimental apparatus used in our investigation yielded very clean thermoacoustic signals. The theoretical study is based on a new approach which provides information about the nearfield of a TS and about the acoustic signature when the source is moving at transonic velocity.

The experimental apparatus is described in the second chapter of this study. A detailed analysis of a stationary TS, both theoretical and experimental, is presented in the third chapter. The theoretical approach is to obtain the impulse response of a TS. The time domain approach is used because it can be very easily extended to the case of a TS moving at any velocity, including at transonic velocity. It also yields some interesting results about the nearfield. Diffraction effects due to the finite width of the laser beam are also discussed in this third chapter, and the comparison between theory and experiment is shown for pressure waveforms, directivity patterns and spreading curves.

The fourth chapter deals with thermoacoustic radiation by a moving source, both theoretically and experimentally. In addition to presenting pressure waveforms, directivity patterns and spreading curves, for subsonic, transonic and supersonic source velocities, we investigate the dependence of the thermoacoustic sound level on source velocity.

Chapter five is an analysis of the Doppler shift of a moving source. The aim is to understand certain farfield approximations often made in the case of a transonic source. Specifically, we derive in this chapter an expression for the Doppler shift which is valid whether the angle of observation between the source and the receiver is fixed or a function of time.

The main conclusions of this study are given in the last chapter along with ideas about possible theoretical and experimental work that would be interesting to develop in the future.

CHAPTER II

EXPERIMENTAL APPARATUS

The experimental apparatus involved in our study of moving thermoacoustic sources consisted basically of a high power laser, a means of deflecting the beam so that motion of the source over a water surface could be achieved, and a receiving and analyzing system. A block diagram of the experimental system is shown in Fig. 1, and a description of the main components of the system is given below. More information on the experimental apparatus can be found in reference 13.

A. Laser

The laser used in this study was designed and built by Apollo Lasers. It is the same laser described in reference 14 . Figures 2 and 3, which are taken from reference 14, show the components of the modulated laser system. The laser head assembly consists of an interchangeable rod, either (Neodymium) Nd:glass or ruby. Optical pumping of the rod is achieved by a flashlamp , and the wavelength of the light emitted by the laser is 1.06 μm (infrared) for Nd:glass and 0.6943 μm (red) for ruby light. The laser beam is polarized in order to achieve modulation of its intensity. The polarizing

6
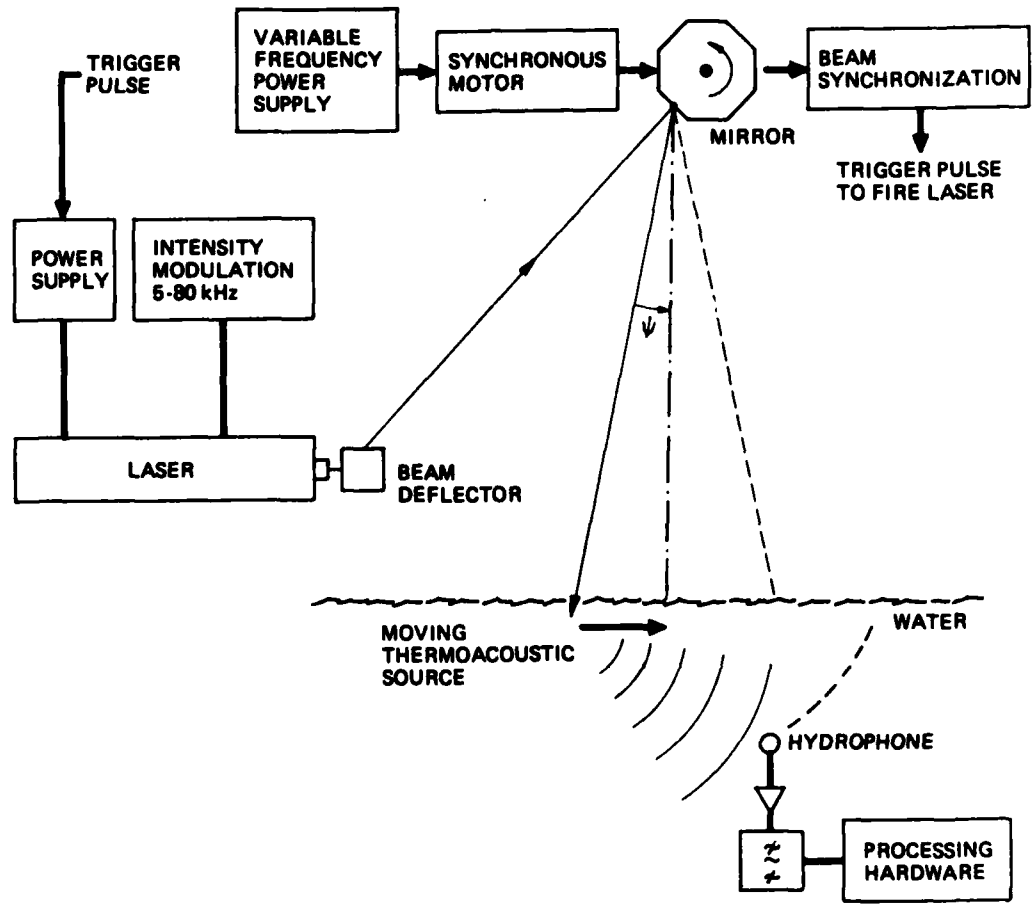
FIGURE 1
BLOCK DIAGRAM OF EXPERIMENTAL SYSTEM
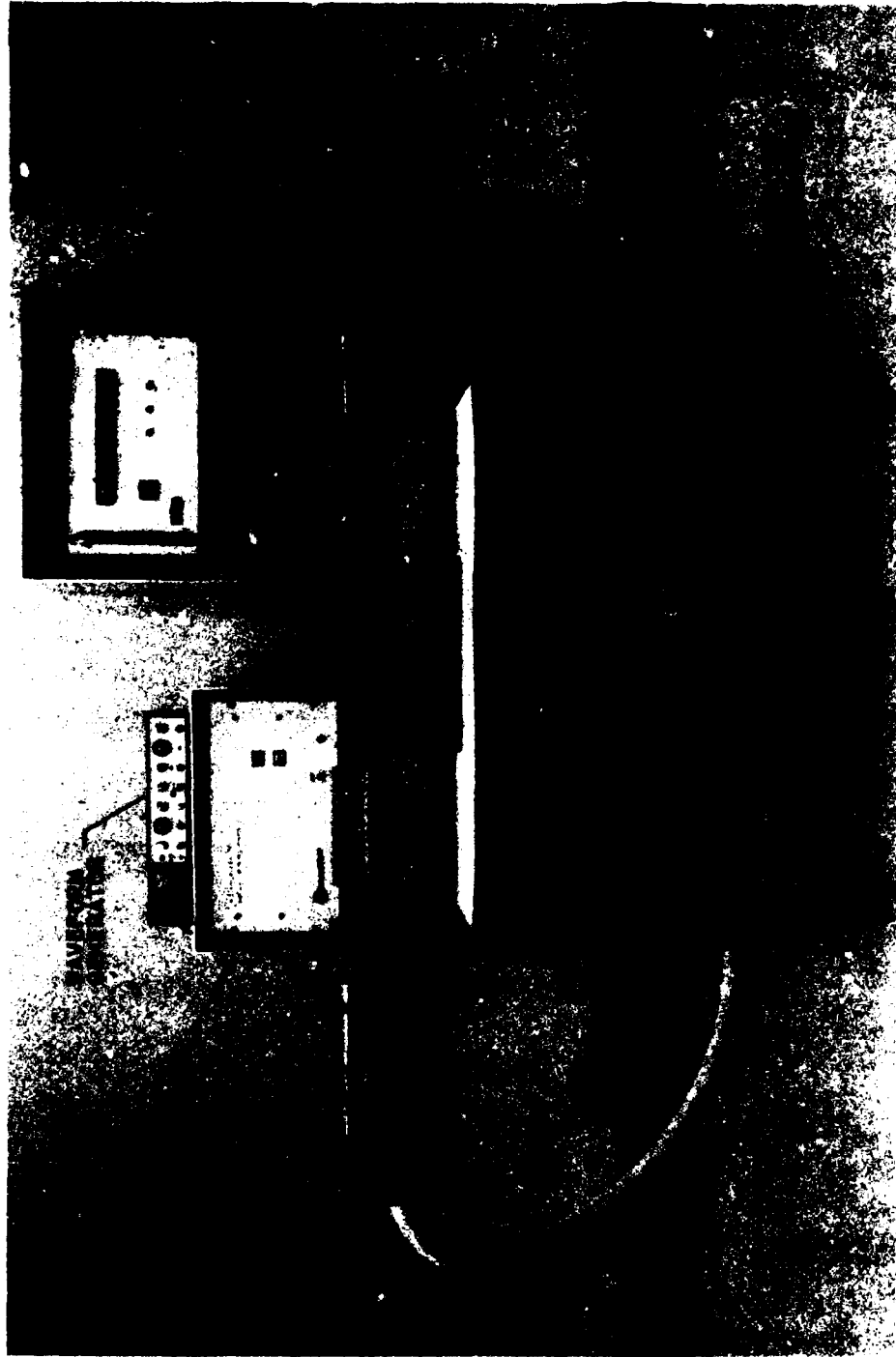
FIGURE 2
MODULATED LASER SYSTEM

0166(15)-1

8
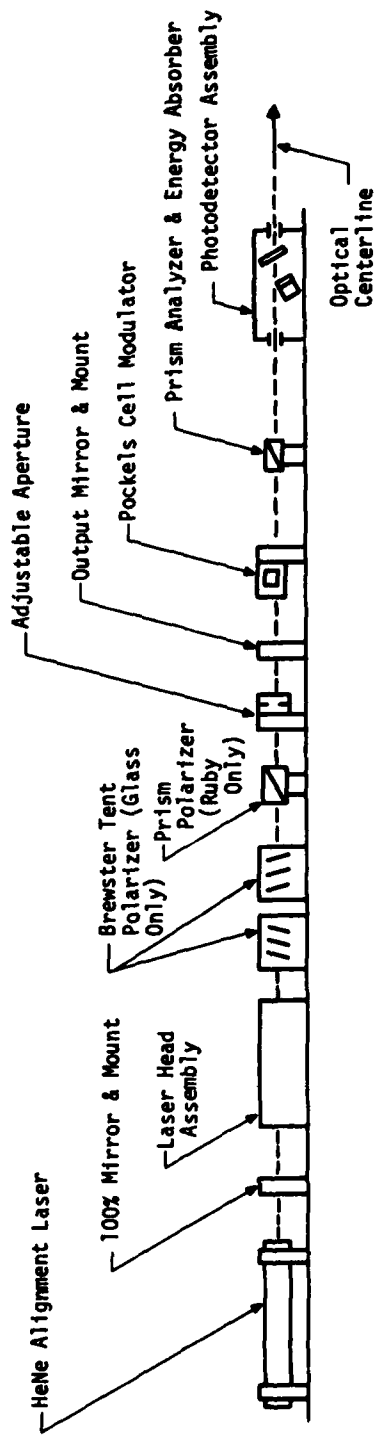
FIGURE 3
OPTICAL TRAIN CONFIGURATION

- HeNe Alignment Laser
- 100% Mirror & Mount
- Laser Head Assembly
- Brewster Tent Polarizer (Glass Only)
- Prism Polarizer (Ruby Only)
- Adjustable Aperture
- Output Mirror & Mount
- Pockels Cell Modulator
- Prism Analyzer & Energy Absorber
- Photodetector Assembly
- Optical Centerline

AS-75-1616
CRC-0207-2

9

element is a Brewster stack in the case of the Nd:glass rod and a calcite prism analyzer in the case of the ruby rod. The laser cavity is formed as usual by a 100% reflective back mirror and an output front mirror whose coating depends on the optical wavelength being emitted.

The laser is used in the conventional non-Q-switched mode so that its output is a series of very short (20-100 ns) Gaussian pulses, characteristic of the normal modes distributed statistically in space and time. The envelope of the laser pulse is denoted $I_0(t)$, and the equivalence between a modulated uniform pulse and a modulated series of dense random spikes has been established in reference 9.

In order to achieve periodic heating of the column of water being illuminated by the laser beam, one has to modulate the intensity of the laser beam. The modulation is achieved by a Pockels cell and a prism analyzer. The principle of the modulation of the laser is shown in Fig. 4. When a voltage is applied to the electrodes of the Pockels cell, it rotates the plane of polarization of the light passing through it by an amount which is nonlinearly related to the applied voltage. The prism analyzer is a polarizer with a fixed plane of polarization and the relationship between the transmitted light intensity $I(t)$ and the incident light intensity $I_0(t)$ is given by

$$I(t) = I_0(t) \, \sin^2(\pi V/2V_{1/2}) \qquad , \qquad (2.1)$$

where V is the voltage applied to the Pockels cell and $V_{1/2}$ is the
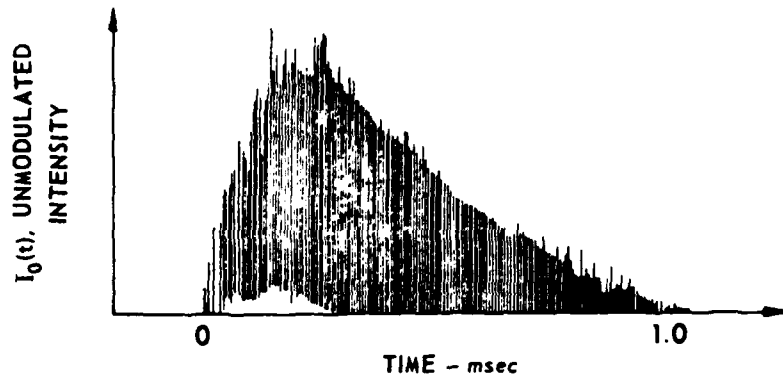
(a) NORMAL MODE LASER PULSE
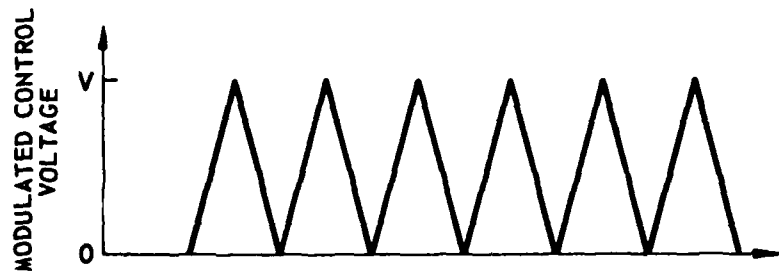
(b) MODULATION CONTROL SIGNAL
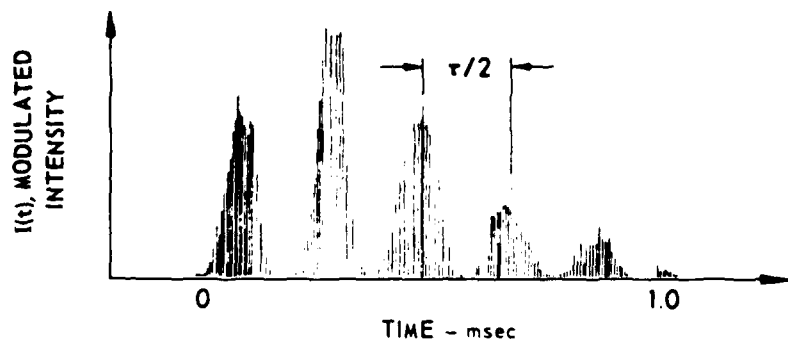
(c) MODULATED NORMAL MODE LASER PULSE

FIGURE 4
REPRESENTATIVE OPERATION OF MODULATED LASER SYSTEM

11

half-wave voltage of the modulation system. Typical peak values of V are 7.0 kV when using the Nd:glass rod and 4.5 kV when using the ruby rod. If the voltage V is chosen to be a triangular function of time with an amplitude of $V_{1/2} \omega t/\pi$, as indicated in Fig. 4(b), the resulting modulation yields a transmitted intensity of the form

$$I(t) = 0.5 \ I_0(t) \ (1 - \cos \omega_0 t) \qquad . \qquad (2.2)$$

The amplitude modulation of the laser intensity is expected to achieve a periodic heating of the column of water being illuminated by the laser beam, and therefore periodic changes in density, and subsequently sound at a frequency $f_0 = \omega_0/2\pi$. The normalized envelope $I_0(t)$ of the laser intensity in the experiment is adequately described by

$$I_0(t) = (10.8 \ t/\tau_p) \ \exp(-5.0 \ t/\tau_p) \qquad , \qquad (2.3)$$

where τ_p is the laser pulse duration. The specifications of the modulated laser system are given in Table I, reprinted from reference 14 . The average laser pulse duration varies between 0.75 ms and 1.25 ms. The laser can deliver up to 5 joules, and in most experiments the laser beam was focused so that the spot diameter on the surface of the water was about 1 cm. The triangular signal used to monitor the modulation of the laser intensity was provided by an Exact model 126 signal generator, and the modulation frequency f_0 could be varied between 5 kHz and 80 kHz. The repetition rate of the laser pulse was limited to four pulses per minute

12

TABLE I

MODULATED LASER SYSTEM SPECIFICATIONS

	RUBY	Nd:GLASS
Optical wavelength (μm)	0.6943	1.06
Unmodulated output energy (J) / power (kW)	25 J 25 kW	30 J 30 kW
Modulated output energy (J) / power (kW)	5 J 5 kW	5 J 5 kW
Pulse duration (ms)	1 ms	1 ms
Modulation frequency (kHz)	5 to 80	5 to 80
Beam divergence (mrad)	1.7	2.2

because of the time constant needed to charge the capacitors of the laser power supply.

B. Experimental set-up

The experiments were conducted at Applied Research Laboratories, The University of Texas at Austin (ARL:UT) in its 18.29 m x 4.57 m x 3.66 m (60 ft x 15 ft x 12 ft) fresh water tank. Figures 5 and 6 show the mechanical arrangements for the experiment. The laser is mounted on a table near the water tank. Shock mounts are used to prevent mechanical vibrations which occur after the laser discharge, from being transmitted to the water. After deflection of 90^0 by a total internal reflection prism, the laser beam passes through a pipe to a rotating mirror. There are three major reasons for using a pipe on the light path: (1) it is obviously safer as far as eye damage is concerned; (2) the rotating mirror can be mounted directly on the pipe rather than on the ceiling so that alignment problems are simplified; and (3) it provides a rigid support where optical lenses can be installed in order to focus the laser beam to the desired size on the surface of the water.

C. Rotating mirror

The rotating mirror was procured by Lincoln Laser Company. The specifications are given in Table II. Special attention was given to environmental conditions such as relative humidity (77% in the tank room)

14
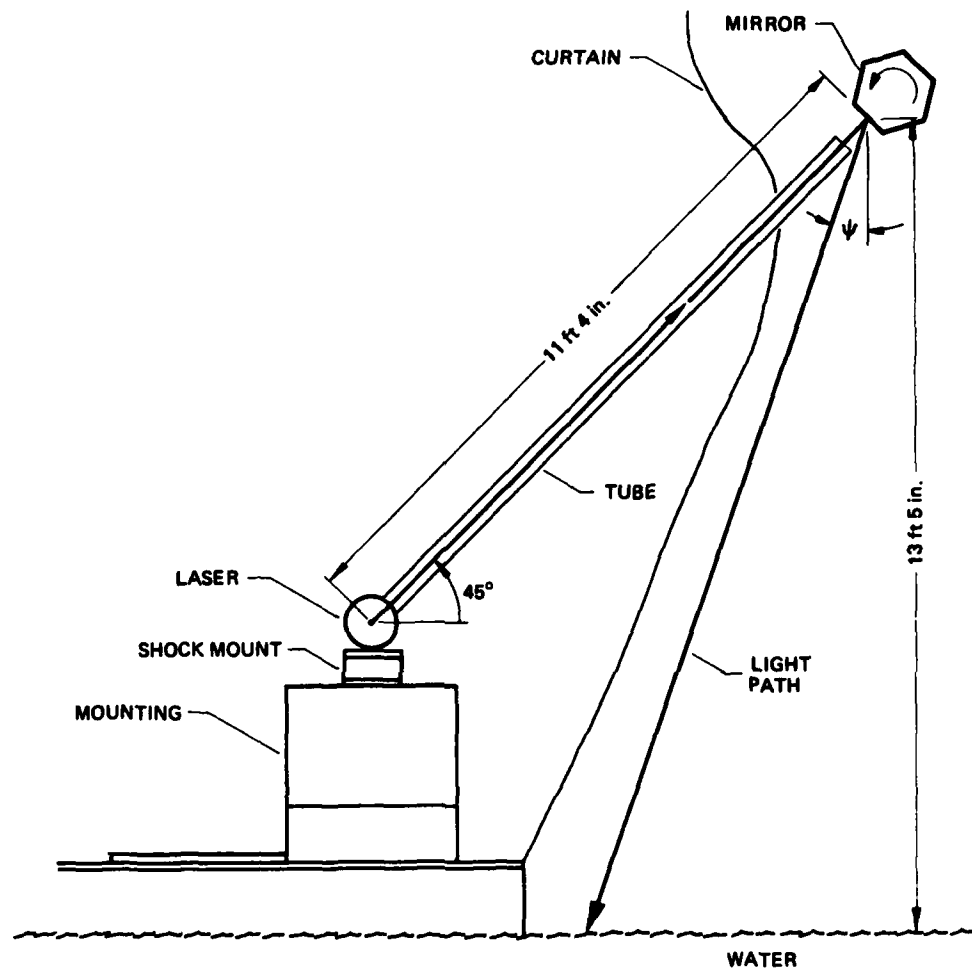
FIGURE 5
MECHANICAL ARRANGEMENT — I
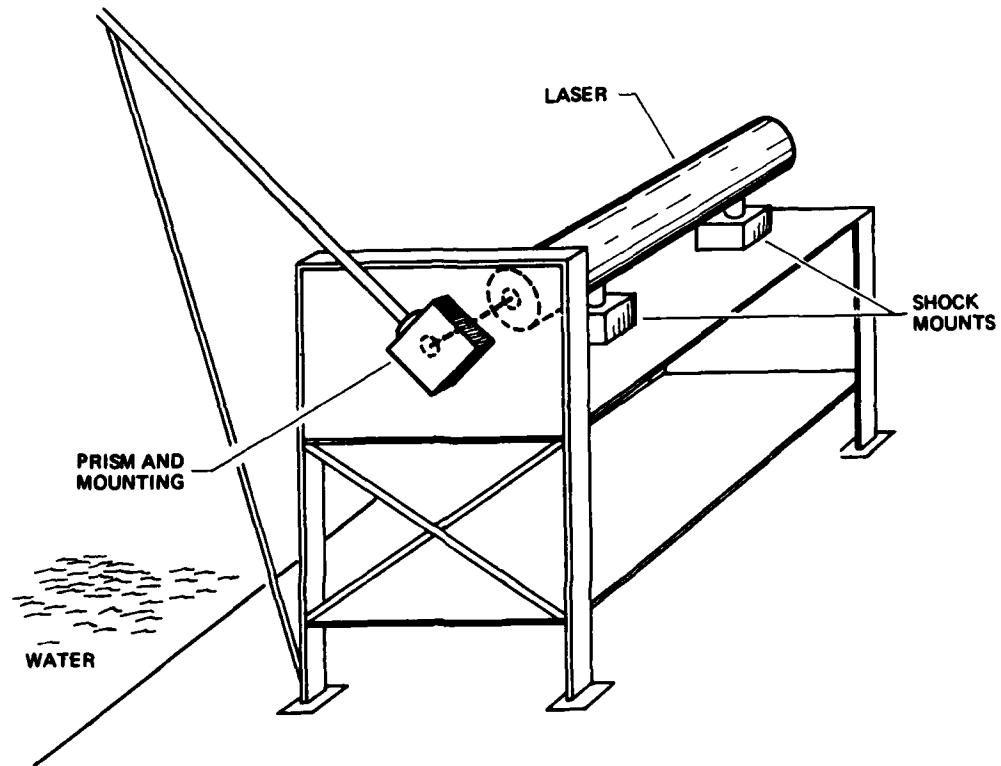
**FIGURE 6
MECHANICAL ARRANGEMENT – II**

16

TABLE II

SPECIFICATIONS FOR THE ROTATING MIRROR SYSTEM

Mirror substrate material:	aluminum and thorium flouride
Number of facets:	6
Circumscribed circle diameter:	15.2 cm (6 in.)
Facet width:	3.2 cm (1.25 in.)
Facet length:	7.6 cm (3 in.)
Surface flatness:	1/4 optical wavelength
Surface reflectivity:	82 % at 0.6943 μm
	88 % at 1.06 μm
Speed of rotation:	150 – 3500 rpm ± 0.1 %
Linear source speed:	$\approx$ Mach 0.1 to Mach 2.6

and dust accumulation. The rotational speed of the mirror was adjustable between 150 and 4500 rpm so that source velocities on the water surface could be varied between $M \approx 0.1$ and $M \approx 2.6$, where M is the Mach number of the source with respect to the sound speed in water. The stability of the angular velocity of the rotating mirror was given to be $\pm 0.1 \%$ between 150 and 3500 rpm, i.e., between $M \approx 0.1$ and $M \approx 2$. In this design the source velocity on the water surface is not truly constant because the angle the beam makes with the water is not constant, i.e., the laser beam is not always perpendicular to the water surface. It is estimated that the error $\Delta v / v$, where v is the source velocity, is less than 3% at Mach 1, and decreased with lower Mach number. It was also estimated that the maximum tilt angle of the thermoacoustic source in water was less than 8^0 at Mach 1 and decreased with lower Mach number. This estimate takes into account the refraction of the laser beam at the air-water interface. A detailed discussion is given in Appendix A, where it is shown that these secondary effects can safely be ignored.

D. Synchronization

The firing of the laser must be synchronized with the angular position of the rotating mirror so that the laser beam is deflected to a known and repeatable position on the surface of the water. One way to know the angular position of the rotating mirror is to use a light emitting diode (LED) and a phototransistor, both combined in a small reflective transducer. When the light beam emitted by the LED is perpendicular to a facet of the

18

mirror, it is reflected to the phototransistor and an electrical impulse of a few microseconds duration is produced. When the mirror rotates at constant speed, the reflective transducer delivers a series of short impulses giving an indication of the angular position of the mirror. Any one of these impulses may be delayed in time and used to trigger the firing of the laser. A digital circuit has been designed and built in order to compute the required time delay to trigger the laser at the appropriate time. A photograph of the laser rotation firing controller circuit is shown in Fig. 7.

The manually controlled settings in the firing control circuit are a set of three dip switches (DS). The input to the circuit is a pair of analog signals provided by two LED/phototransistor reflective transducers located in the rotating mirror housing. Outputs of the firing control circuit include signals from connectors labeled "T.P.A.", "OUTPUT", and "FIRE". The fire signal is a pulse of approximatively 100 µs duration and amplitude of 12 volts to trigger the discharge of the capacitors used to fire the laser. The T.P.A signal is a series of impulses delivered by the LED/phototransistor. It can be used to accurately check the mirror angular velocity and its stability. The OUTPUT signal is a single pulse of about 1 ms duration, slightly delayed after the FIRE pulse. The amount of the time delay is manually controlled by the dip switch DS3 (see Fig. 7). The reason for this time delay is that there is an intrinsic time interval between the discharge of the capacitor bank and the actual lasing of the rod. This time delay is about 180 µs for the Nd:glass rod and 340 µs for the ruby rod. Calibration curves for values of the binary number N_{DS3} associated with the dip switch DS3 controlling the time delay , indicate

19

FIGURE 7
LASER ROTATION FIRING CONTROLLER

4587-20A

that N_{DS3} should be 101 when using the Nd:Glass rod and 1010 when using the ruby rod. The OUTPUT signal is intended to be used to trigger the intensity modulator external signal provided by the Exact signal generator.

The firing control circuit contains two other dip switches, DS1 and DS2, that are manually controllable. These are indicated in Fig. 7. The decimal numbers associated with DS1 and DS2 are, respectively, N_{DS1} and N_{DS2}. These integer numbers are used to select the initial angle ψ between the vertical and the laser beam (see Fig. 5) at the beginning of the laser pulse. The initial angle ψ is given by

$$\psi = \pm 120^0 \, (N_{DS1}/N_{DS2}) - 32^0 + (n \, 120^0) \quad , \quad (2.4)$$

where the "plus" sign is to be used when the laser beam is moving away from the bench and similarly, where the "minus" sign has to be used when the beam is moving towards the bench. In Eq. (2.4), n is a positive integer accounting for the periodicity of the facets on the rotating mirror. As an example, if one wants to use the Nd:glass rod in such a way that the initial angle ψ is zero, N_{DS3} should read "101", N_{DS1} should read "100" (i.e., 4 in decimal), and N_{DS2} should read "1111" (i.e., 15 in decimal).

E. Receiving system

The signal emitted by the thermoacoustic source is received by a hydrophone, amplified and filtered, before being stored and analyzed on a digital oscilloscope which is interfaced with a mainframe computer for

21

more advanced signal processing.

The hydrophone used in most experiments described in this study is a USRD type H-56 hydrophone. This hydrophone is very sensitive ($\sim$ - 163 dB re 1 V/μPa at 60 kHz) but its bandwidth is limited to frequencies below 100 kHz. Therefore in some cases an H-23 hydrophone was preferred. Calibration curves for the frequency response and directivity patterns of the hydrophone (H-56) at several frequencies, are given in Appendix B.

The signal received by the hydrophone was amplified by two battery operated Burr-Brown model 100 AC-decade amplifiers, with a calibrated total gain of 40.5 dB. The amplified signal was bandpass filtered by a Krohn-Hite filter. The signal was then transferred to a Nicolet 4094 digital oscilloscope. This oscilloscope provides two input channels (expandable to four channels) with simultaneous 12 bit digitizers that sample at a rate of 2 MHz. The data is stored on floppy diskettes in the external disk recorder. Special diskettes are available from Nicolet for performing valuable signal processing functions on the oscilloscope. For example, the rms value of a signal over a specified time interval can be calculated. Similarly, programs to compute Fourier transforms, digital filtering, integration, etc. are available. In general the sound level measured from an experimental waveform was obtained from the peak-to-peak values of the pressure. Also, the Nicolet 4094 was interfaced to the mainframe CYBER-CDC computer at ARL:UT via an RS-232 interface, so that experimental data could be transferred to the computer and compared with theoretical predictions. The software required for such a transfer consists essentially of two programs, whose binary version are called "NICOLT" and "CNVRT". The

22

program NICOLT creates a file on the CYBER that contains integer numbers representing the signal being transferred from the Nicolet to the CYBER. Program CNVRT is used to convert these numbers into their real values. Note that NICOLT can also be used to transfer waveforms from the CYBER to the Nicolet. More information on the procedure for data transfer is given in Appendix C.

In general the sound pressure level measured from an experimenal waveform was obtained by taking 20 times the logarithm based 10 of the ratio of the peak-to-peak pressure to a reference pressure of 1 μPa.

CHAPTER III

STATIONARY THERMOACOUSTIC SOURCES[15]

The sound field radiated by a stationary thermoacoustic source is analyzed in this chapter by introducing the impulse response of the thermoacoustic system. This approach has four main advantages: (1) it can easily be extended to the case of a TS moving at any velocity through the medium, and this will be done in Chapter IV, (2) the model is valid in the nearfield of the source, (3) it can be used, in principle, for any spatial and temporal laser intensity profiles, and (4) transforms are not needed to get time information.

In the first section of this chapter we describe the physical problem of thermoacoustic radiation and derive the impulse response of a TS. The second, third, and fourth sections deal, respectively, with the pressure waveform, the directivity, and the spreading characteristics of the radiation from a TS, both theoretically and experimentally. The last section is a summary of the important features of this chapter.

A. Impulse response

Consider the thermoacoustic source shown in Fig. 8. A laser beam is shined at normal incidence in the +z direction into an optically absorbing medium. The heat produced by the laser beam generates almost
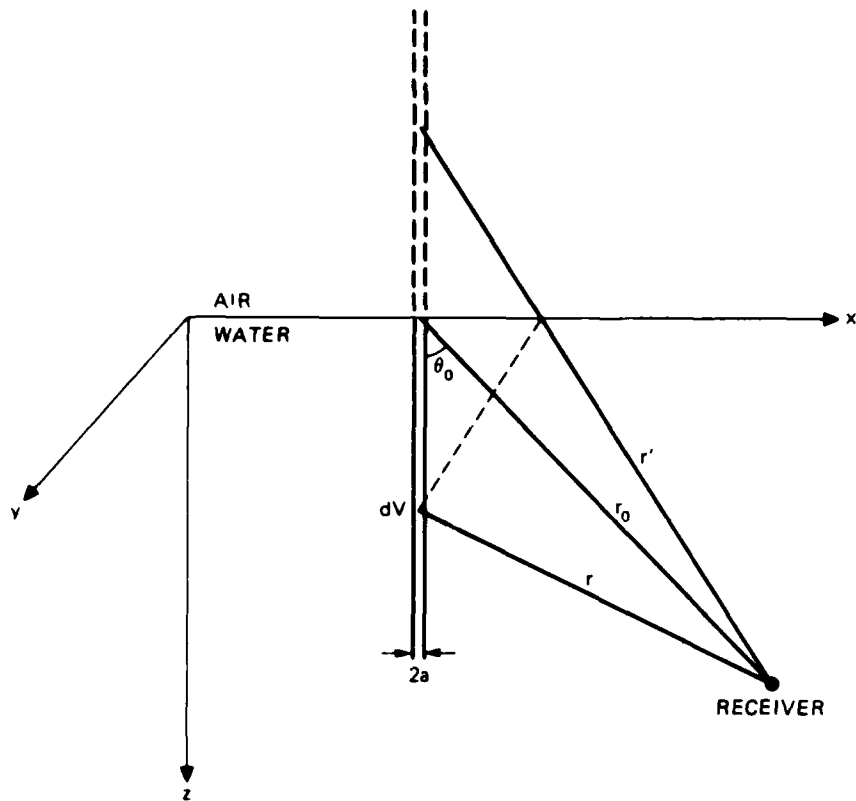
FIGURE 8
STATIONARY THERMOACOUSTIC SOURCE GEOMETRY – I

25

instantaneously a density disturbance due to thermal expansion which induces a pressure fluctuation which is observed as an acoustic wave. The objective of this study is to relate in the most general way the spatial and temporal characteristics of the laser to the acoustic pressure observed at any point in the field.

Larson[16] has shown that the wave equation describing thermoacoustic radiation is, in the case of an inviscid and non-heat-conducting fluid, given by

$$\nabla^2 p - c^{-2} p_{tt} = -(\beta/c_p) q_t \quad , \quad (3.1)$$

where the subscript t denotes a time derivative, p is the acoustic pressure generated by the thermal expansion mechanism, c is the small signal sound speed, c_p is the specific heat of the medium at constant pressure, β is the logarithmic coefficient of thermal expansion of the medium, and q is the heat energy per unit volume per unit time added to the medium. It is related to the laser intensity vector I by the relation

$$q = -\nabla \cdot \langle I(x,y,z,t) \rangle \quad . \quad (3.2)$$

A derivation of the wave equation for thermal generation of sound in a viscous medium is given in Appendix D. For practical reasons, we consider the medium to be a liquid having a constant optical coefficient of absorption α, so that the z-component of the laser beam intensity I decreases with depth according to the exponential shading $\exp(-\alpha z)$. With a

26

different absorption law, the following analysis would still be workable, although more complicated and not necessarily more realistic .

When Eqs. (3.1) and (3.2) are combined it is clear that the thermoacoustic source function is proportional to the time derivative of the laser intensity. It is therefore convenient to define the impulse response h(t) of the thermoacoustic system in the following manner:

$$p(t) = h(t) * I_t(t) \quad , \quad (3.3)$$

where the asterisk denotes convolution over time. In this formulation h(t) contains all of the spatial characteristics of the system at any arbitrary range r, and $I_t(t)$ contains all of the temporal information of the source. The spatial characteristics of the system can be decomposed into its vertical component (x-z plane) and its horizontal component (x-y plane). Let us denote by $h_L(t)$ and $h_\theta(t)$, respectively, the vertical and horizontal impulse responses of the TS. Then $h_L(t)$ represents the response of an infinitely narrow TS (a→0 in Fig. 8) of effective length L=1/α. Thus $h_L(t)$ is the response of an exponentially tapered semi-infinite line source below a pressure release boundary such as the air-water interface. On the other hand $h_\theta(t)$ represents the response of an infinitely short TS (L→0). In other words, $h_\theta(t)$ is the impulse response of a cross-section of the source. With these notations Eq. (3.3) can be rewritten as

$$p(t) = h_L(t) * h_\theta(t) * I_t(t) \quad . \quad (3.4)$$

27

It is therefore necessary to evaluate $h_L(t)$ and $h_\theta(t)$ in order to find the pressure response of a given medium excited by a laser beam of intensity $I(t)$. This analysis is carried out below.

1. Vertical impulse response $h_L(t)$

The vertical impulse response is obtained by imagining that the laser beam diameter is so small that sound coming from an entire beam cross section S is received instantaneously. This has the effect of setting the horizontal impulse response in Eq. (3.4) to a delta function in time: $h_\theta(t) \to S\,\delta(t)$. In this case the heat q is related to the laser intensity by

$$q = - d/dz\,[\,A\ I(t)\ e^{-\alpha z}\,]\ S\,\delta(x-x_c)\,\delta(y-y_c) \quad , \qquad (3.5)$$

where A is the coefficient of transmission of light across the interface, and where x_c and y_c denote the center coordinates of the beam. The solution of Eq. (3.1) for a pressure release boundary condition at the interface is then obtained by integrating the Green's function of the problem over the source volume as follows.

$$p(t) = C_1 \int_0^\infty (r)^{-1} e^{-\alpha z}\ I_t(t-r/c)\ dz$$

$$- C_1 \int_{-\infty}^0 (r')^{-1} e^{-\alpha z}\ I_t(t-r'/c)\ dz \qquad , \qquad (3.6)$$

28

where the coordinates z, r, and r' are shown in Fig. 8, and where $C_1 = (A\beta\alpha Sc/4\pi c_p)$. The second integral in Eq. (3.6) represents the contribution of the mirror image above the pressure release boundary. From Eqs. (3.4) and (3.6), then, the vertical impulse response is given by

$$h_L(t) = (C_1/S) \int_0^\infty (r)^{-1} e^{-\alpha z} \delta(t - r/c)\, dz - \text{mirror image} \quad , \quad (3.7)$$

where $\delta(t)$ is the Dirac delta function. Shifting the integration variable from z to r, yields

$$h_L(t) = K \int_r (r)^{-1} e^{-\alpha z} \delta(r - ct)\,(dz/dr)\, dr - \text{mirror image} \quad , \quad (3.8)$$

where $K = (A\beta\alpha c/4\pi c_p)$. Equation (3.8) provides a means for evaluating the vertical impulse response of a TS once the relationship between the depth z of the receiver and its radius of observation r is known. Assuming that the laser beam strikes the medium at normal incidence, one may divide the source into four regions. These are indicated in Fig. 9. For each region the relationship between z and r can easily be found. Equation (3.8) can then be written in terms of separate integrals over the four regions as follows.
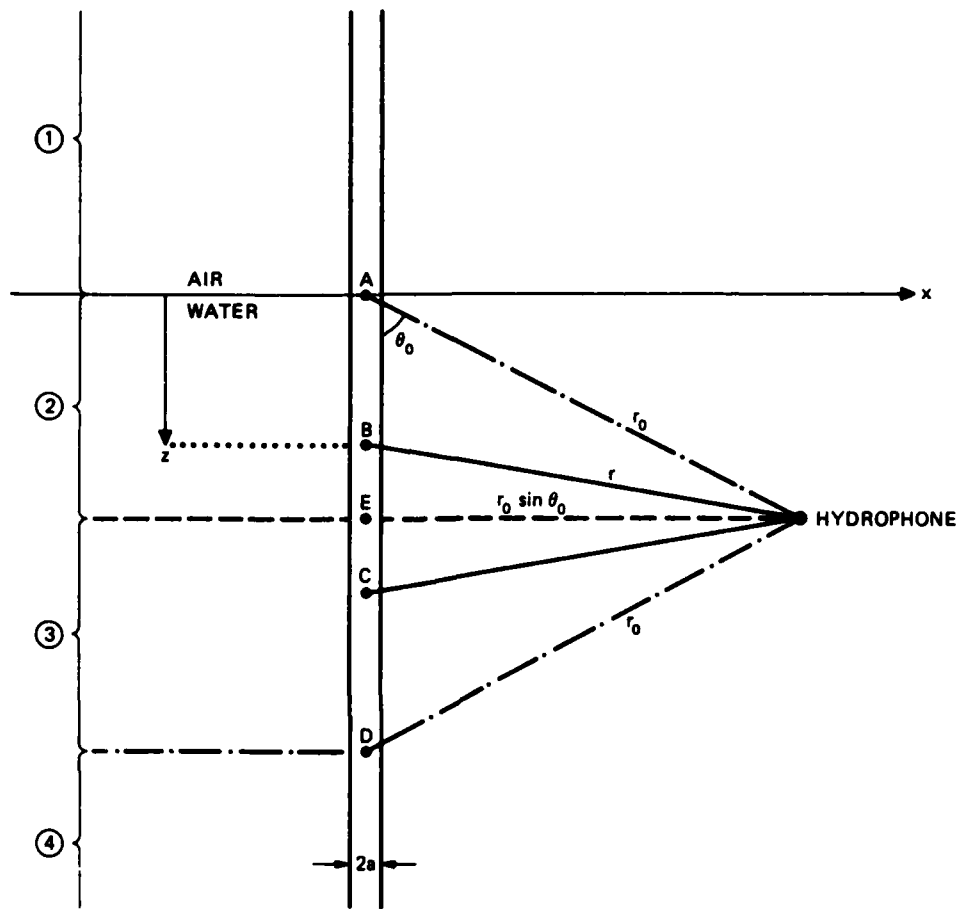
FIGURE 9
STATIONARY THERMOACOUSTIC SOURCE GEOMETRY – II

30

$$h_L(t) = K \int_{r_0}^{r_0 \sin\theta_0} (1/r)\, \delta(r-ct)\, \exp[-\alpha(r_0\cos\theta_0 - s)]\, (-r/s)\, dr$$

$$+ K \int_{r_0 \sin\theta_0}^{r_0} (1/r)\, \delta(r-ct)\, \exp[-\alpha(r_0\cos\theta_0 + s)]\, (r/s)\, dr$$

$$+ K \int_{r_0}^{\infty} (1/r)\, \delta(r-ct)\, \exp[-\alpha(r_0\cos\theta_0 + s)]\, (r/s)\, dr$$

$$- K \int_{r_0}^{\infty} (1/r)\, \delta(r-ct)\, \exp[-\alpha(-r_0\cos\theta_0 + s)]\, (r/s)\, dr$$

(3.9)

where $s = \sqrt{r^2 - (r_0\sin\theta_0)^2}$.

The four integrals in Eq. (3.9) represent the contributions to the acoustic signal from the four source regions shown in Fig. 9. However, it is more meaningful to distinguish the array response by regions in time rather than in space. The limits of integration indicate that the analysis of the impulse response should be divided into five time regimes as follows.

a) $t < r_0 \sin\theta_0/c$: In this time region, the impulse response reduces to

$$h_L(t) = 0 \quad , \tag{3.10}$$

which states that the acoustic emission from the array has not yet had time to reach the receiver. The first disturbance emitted by the TS has to travel a distance $r_0 \sin\theta_0$ before reaching the observation point. Therefore the impulse response is identically zero for any time $t < r_0 \sin\theta_0/c$.

b) $t = r_0 \sin\theta_0/c$: This particular instant corresponds to the time of arrival of the first wavelet at the receiver. This wavelet originated at a distance of $r_0 \sin\theta_0$ from the receiver, that is to say, at a depth $z_0 = r_0 \cos\theta_0$ below the pressure release boundary. Consequently the impulse response is simply, from Eq. (3.7),

$$h_L(t) = K (r_0 \sin\theta_0)^{-1} \exp (-\alpha r_0 \cos\theta_0) \quad . \tag{3.11}$$

c) $r_0 \sin\theta_0/c < t < r_0/c$: From Fig. 9, it is obvious that the first wavelet which will reach the receiver emanates from point E. An instant later, wavelets emitted from points B and C will arrive simultaneously at the receiver. The progression continues with wavelets eventually coming from points A and D. These are all the wavelets received during the interval $r_0 \sin\theta_0/c < t < r_0/c$ which resulted from sound radiation at time $t=0$. The disturbances coming from regions 2 and 3 of the TS therefore add by pairs at the observation point. The only non-zero contribution to the

32

impulse response is given by the first two integrals in Eq. (3.9), which may be evaluated to give

$$h_L(t) = \frac{2K \exp(-\alpha r_0 \cos\theta_0)}{\sqrt{(ct)^2 - (r_0 \sin\theta_0)^2}} \cosh\left(\alpha\sqrt{(ct)^2 - (r_0 \sin\theta_0)^2}\right) \quad . \qquad (3.12)$$

d) $t = r_0/c$: There are two points on the array that are located at a distance r_0 from the receiver. These two points are denoted by A and D in Fig. 9. However, the pressure release boundary condition at the free surface of the liquid implies that the acoustic contribution from point A is null, so that in fact the acoustic response at time $t = r_0/c$ is simply given by the wavelet coming from D, i.e., from the point of the source that is located at a depth $z = 2r_0 \cos\theta_0$. Equation (3.7) yields an expression for the impulse response at $t = r_0/c$:

$$h_L(t) = K \; r_0^{-1} \; \exp(-2\alpha r_0 \cos\theta_0) \quad . \qquad (3.13)$$

e) $t > r_0/c$: The disturbances emitted by regions 1 and 4 of the TS will arrive by pairs at the observation point. In this case, however, the boundary condition at the air-water interface implies that signals coming from region 1 (the mirror image region) are inverted. Hence the only non-zero contribution to the impulse response is given by the last two integrals in Eq. (3.9). These may be evaluated to give

33

$$h_L(t) = \frac{-2K \, \exp\left(-\alpha\sqrt{(ct)^2-(r_0\sin\theta_0)^2}\right)}{\sqrt{(ct)^2 - (r_0\sin\theta_0)^2}} \, \sinh(\alpha r_0\cos\theta_0) \quad . \qquad (3.14)$$

The vertical impulse response of a TS is therefore given by Eq. (3.15a-e).

$$h_L(t) = \begin{cases} 0 & \text{for } t < t_1 \quad , & (3.15a) \\[2mm] K\, e^{-\Gamma} (r_0\sin\theta_0)^{-1} & \text{for } t = t_1 \quad , & (3.15b) \\[2mm] 2K\, e^{-\Gamma} \mu^{-1} \cosh(\alpha\mu) & \text{for } t_1 < t < t_0 \quad , & (3.15c) \\[2mm] K\, e^{-2\Gamma} (r_0)^{-1} & \text{for } t = t_0 \quad , & (3.15d) \\[2mm] -2K\, \mu^{-1} e^{-\alpha\mu} \sinh(\Gamma) & \text{for } t > t_0 \quad , & (3.15e) \end{cases}$$

where $t_0 = r_0/c$, $t_1 = r_0\sin\theta_0/c$, $\Gamma = \alpha r_0\cos\theta_0$, and $\mu = c\sqrt{t^2-t_1^2}$.

Figure 10 shows how the shape of $h_L(t)$ changes as the nondimensional parameter Γ varies from 0.02 to 100. Γ can be regarded as the ratio of the depth of the receiver to the effective length $L = \alpha^{-1}$ of the TS. It is assumed in Fig. 10 that the laser is shined into fresh water where c=1486 m/s. Note that no farfield assumptions were required to derive the analytical expressions above. Figure 11 is a three dimensional representation of the impulse response $h_L(t)$ as a function of time and Γ.
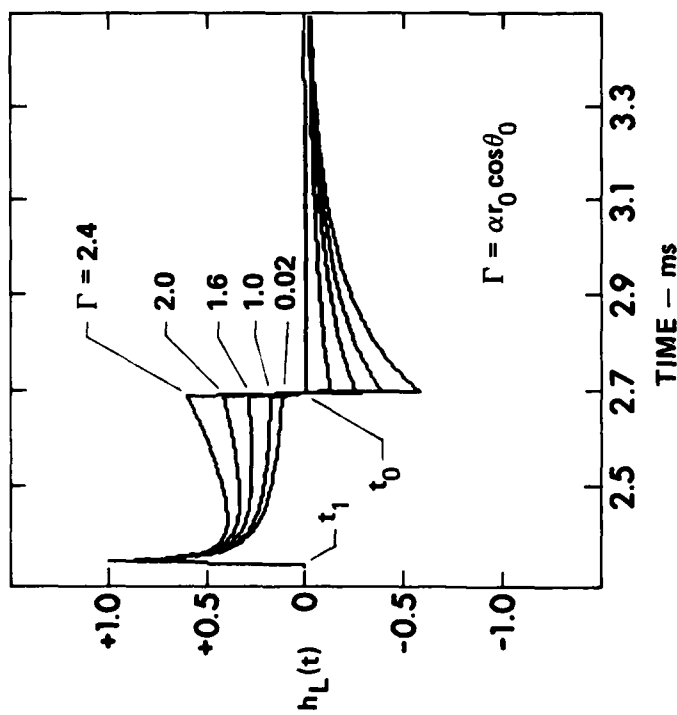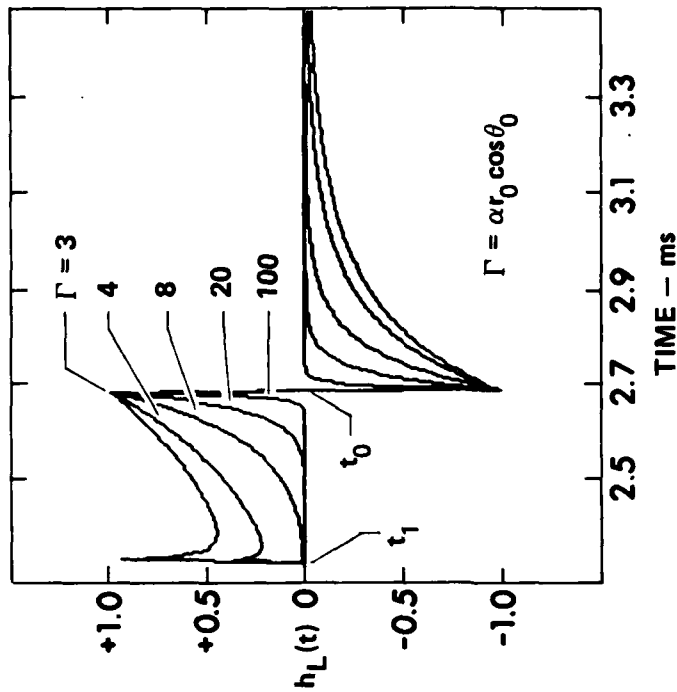
FIGURE 10
IMPULSE RESPONSE $h_L(t)$

$r_0 = 4 \text{ m}$ $\theta_0 = 60°$ $t_1 = r_0 \sin\theta_0/c$

$t_0 = r_0/c$
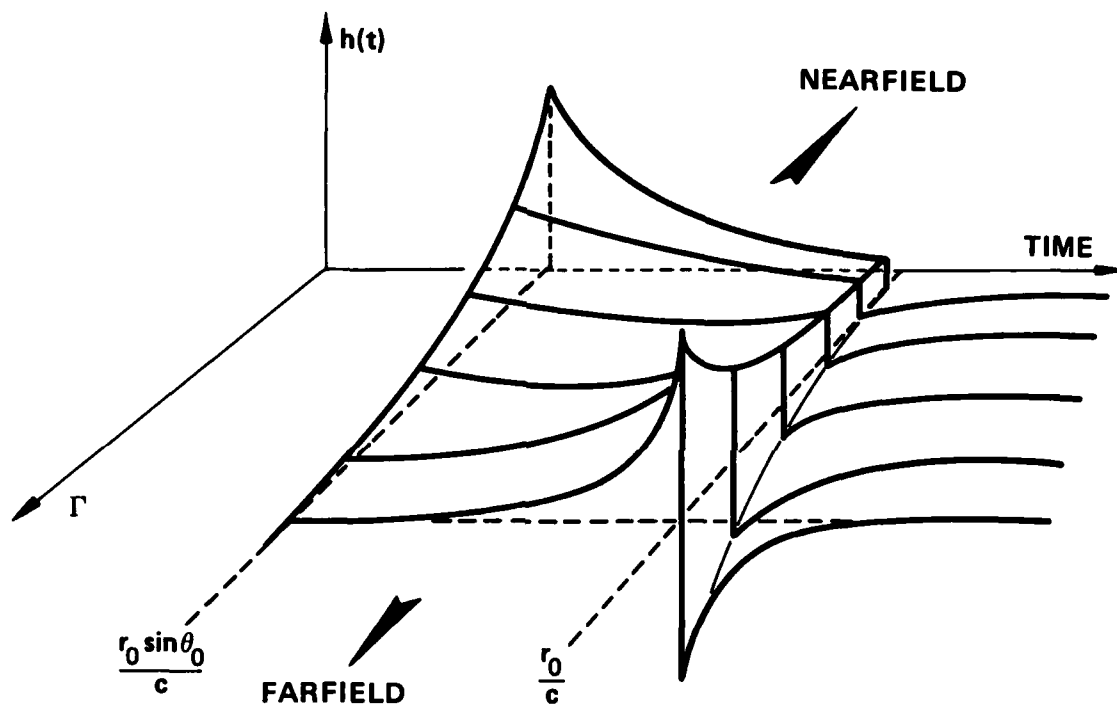
FIGURE 11
IMPULSE RESPONSE AS A FUNCTION OF $\Gamma = \alpha r_0 \cos \theta_0$

Figures 10 and 11 show a curious behavior for $h_L(t)$ when $t_1 < t < t_0$. During this time interval the shape of $h_L(t)$ can change drastically from a monotonically decreasing function having a maximum at time $t_1 = r_0 \sin\theta_0/c$, to a monotonically increasing function having a maximum at time $t_0 = r_0/c$. This can be explained by looking at the two different effects determining the shape of the impulse response: the exponential shading along the axis of the array which is due to the absorption of light in the medium, and the spherical spreading associated with each wavelet radiated by the TS. For simplicity let us assume first that the exponential decay along the depth of the array is much more important than the spherical spreading. This is expected to be the case in the farfield because the distance from each point from the TS to the receiver is almost the same. Also let z_A, z_B, z_C and z_D be the depths of the elementary sources located at points A,B,C and D on the source as shown in Fig. 9. It can be shown that, for any positive α,

$$e^{-\alpha z_A} + e^{-\alpha z_D} < e^{-\alpha z_B} + e^{-\alpha z_C} \qquad (3.16)$$

Therefore the strength of the acoustic disturbance coming from points B and C is always less important than the strength of the disturbance originated from points A and D. Since the latter arrives at the receiver at time t_0, the impulse response $h_L(t)$ is expected to increase gradually from t_1 to t_0.

Let us now assume that the spherical spreading loss associated with each wavelet coming from the array is much more important than the exponential shading along the z-axis of the array. In this case, all of the

elementary sources will have approximately the same strength. This case applies to the nearfield of a TS. The strongest disturbance is therefore the one which suffers the least spherical spreading loss. Consequently it originates from the elementary source on the array which is the closest to the receiver. Since the minimum distance between the source and the receiver is $r_0\sin\theta_0$, the vertical impulse response $h_L(t)$ exhibits a peak at time $t_1=r_0\sin\theta_0/c$ and then decreases gradually until $t_0=r_0/c$.

It is also interesting to note that the impulse response $h_L(t)$ of a stationary thermoacoustic source is very closely related to the half-order derivative operator. This is discussed in Appendix E.

2. Horizontal impulse response $h_\theta(t)$

The horizontal impulse response is obtained by imagining that the optical absorption by the fluid is so high that the laser beam penetrates only a small amount compared to tne beam diameter. Under this condition, the vertical impulse response is set to a delta function : $h_L(t) \rightarrow (K/c)\,\delta(t)$, and the horizontal impulse response may be calculated. Note from Eq. (3 3) that the time derivative operates on the intensity, and from Eq. (3.7), that the mirror image of the source over the interface has already been taken into account in the vertical impulse response, including the constant of proportionality. This means that it would be redundant to again consider these features in $h_\theta(t)$. The horizontal impulse response is thus simply

$$h_\theta(t) = \iint I_N(x,y) \; \delta [t-r(x,y)/c] \, dx \, dy \qquad , \qquad (3.17)$$

where I_N is the normalized laser intensity

$$I_N(x,y) = \frac{S \; I(x,y)}{\displaystyle\iint I(x,y) \, dx \, dy} \qquad . \qquad (3.18)$$

Let us first examine the case of a uniform beam of radius a. In this case $I_N(x,y)$ is equal to unity, and following Morse's analysis[17] of the impulse response of a piston, one finds, if $r_0 \gg a \sin\theta_0$,

$$h_\theta(t) = \int_{-a \sin\theta_0}^{a \sin\theta_0} 2 \sqrt{(a \sin\theta_0)^2 - y^2} \; \delta [t-(r+y)/c] \, dy \quad , \qquad (3.19)$$

or

$$h_\theta(t) = 2 c \sqrt{(a \sin\theta_0)^2 - (r_0 - ct)^2} \qquad (3.20)$$

if $(r_0 - a \sin\theta_0)/c < t < (r_0 + a \sin\theta_0)/c$, and zero otherwise. Similarly, in the case of a Gaussian beam where a denotes the 1/e radius, one would find, provided that $r_0 \gg a \sin\theta_0$,

$$h_\theta(t) = \pi^{1/2} c \, a \sin\theta_0 \; \exp [-\{(r_0 - ct)/(a \sin\theta_0)\}^2] \qquad (3.21)$$

39

if $(r_0 - a \sin\theta_0)/c < t < (r_0 + a \sin\theta_0)/c$, and zero otherwise. It can be verified that

$$\lim_{a \sin\theta_0 / r_0 \to 0} \{ h_a(t) \} = \pi a^2 \, \delta(t - r_0/c) \qquad (3.22)$$

Equations (3.20) and (3.21) provide expressions for the horizontal impulse response in analytical form for either a uniform or a Gaussian intensity shading across the laser beam. The spatial extent of the source induces a frequency filtering which may be found by taking the Fourier transform of $h_a(t)$. For a uniform intensity distribution across a section of the laser beam, the frequency filtering has a Bessel characteristic of the form $2J_1(ka \sin\theta_0)/(ka \sin\theta_0)$ and for the case of the Gaussian distribution, it takes the Gaussian form $\exp[-(ka \sin\theta_0/2)^2]$. The frequency filtering associated with diffraction due to finite laser beamwidth is therefore a low pass filtering, or a smoothing in the time domain.

B. Pressure waveform

In this section we present results obtained using the impulse response technique previously described to predict the pressure waveform radiated by a TS. The double convolution of Eq. (3.4) is evaluated numerically. It is then used to evaluate the case of an unmodulated TS. The results in the farfield limit are compared with analytical predictions

40

derived by Lyamshev and Sedov[18] in their review paper on thermoacoustic sources. The analytical predictions are also compared to experimental results.

Consider a thermoacoustic source of the sort discussed previously. For simplicity we assume that the laser intensity is not amplitude modulated and that the finite beamwidth effects are negligible, i.e., that $h_a(t) \rightarrow S \delta(t)$. To facilitate comparisons with experimental data, we will assume that the laser pulse shape matches the measured pulse shape, which is adequately described by Eq. (2.3). Using Eqs. (3.22) and (3.15) in Eq. (3.4) leads to a straightforward numerical computation of the pressure received at a specified location as a function of time.

Figure 12 shows the evolution of the predicted pressure waveform received in fresh water at the observation point as the nondimensional parameter Γ changes from 200 to 0.2. The position of the receiver is kept constant ($r_0 = 4$ m, $\theta_0 = 60^0$) so that the variation of Γ corresponds in fact to a variation of the effective length $L = \alpha^{-1}$ of the source from 1 cm (short source) to 10 m (long source). The pulse duration was set to 250 μs. The sharp peak in the acoustic response observed in Fig. 12(a) is due to the fact that the laser pulse described by Eq. (3.22) has a discontinuous time derivative at t=0. The negative pressure pulse which appears for all values of Γ in Fig. 12(a)-(f) after the retarded time r_0/c can be explained by the effect of the pressure release interface between air and water. As shown in the figures, the pressure waveform broadens and changes substantially in shape as the source length increases. In the case of a very long source the pressure waveform is seen to begin at time $t_1 = r_0 \sin\theta_0/c$ rather than

41
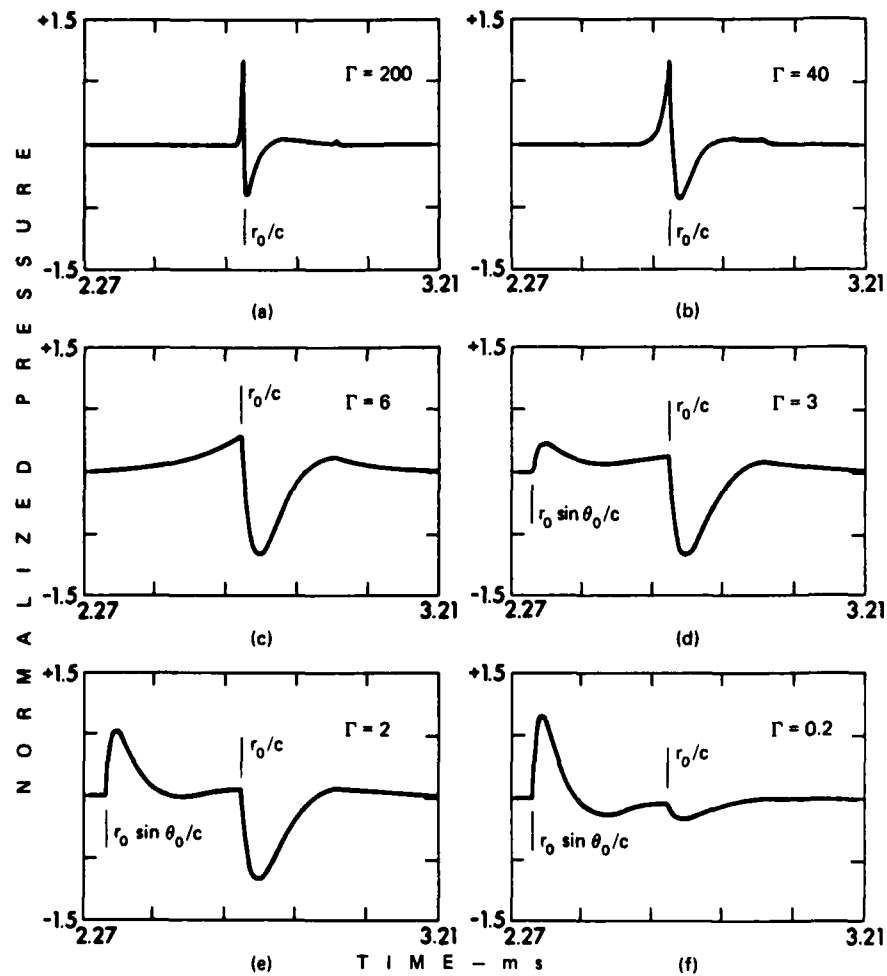
FIGURE 12
PRESSURE WAVEFORM AS A FUNCTION OF $\Gamma = \alpha r_0 \cos \theta_0$
FOR A STATIONARY UNMODULATED LASER PULSE
($r_0 = 4$ m; $\theta_0 = 60°$; $\tau_P = 250 \mu sec$)

the time $t_0 = r_0/c$ as it would in the case of a short source. This result agrees with the analysis presented in Section III.A.1.

Lyamshev and Sedov[18] have shown that in the farfield, the pressure waveform radiated by a TS is proportional to the second time derivative of the laser pulse intensity provided the length of the array is very small compared to a typical acoustic wavelength.[19] The reason the pressure response is proportional to the second time derivative of the laser intensity is explainable in terms of the impulse response approach. As shown by Fig. 10, the impulse response of a very short source tends to behave like the time derivative of a delta function centered at time t_0. The physical cause of this behavior is the pressure release boundary between the air and water. From Eq. (3.3) it then follows that the pressure is proportional to

$$\delta_t (t-r_0/c) * I_t(t) = I_{tt}(t-r_0/c) \qquad . \qquad (3.23)$$

Figure 13(a) shows a comparison between the impulse response approach and Lyamshev and Sedov's predictions for the sound pressure of a short thermoacoustic source. The comparison was made for a modulation frequency of 5 kHz, a laser pulse duration of 1 ms, and for $\Gamma=100$. The laser intensity was described by Eqs. (2.2) and (2.3). As shown in the figure, the numerical and analytical predictions for the short source case are in excellent agreement.

The case of a long and narrow TS has also been studied by Lyamshev and Sedov[18] in the special case of farfield radiation. Their results show

43
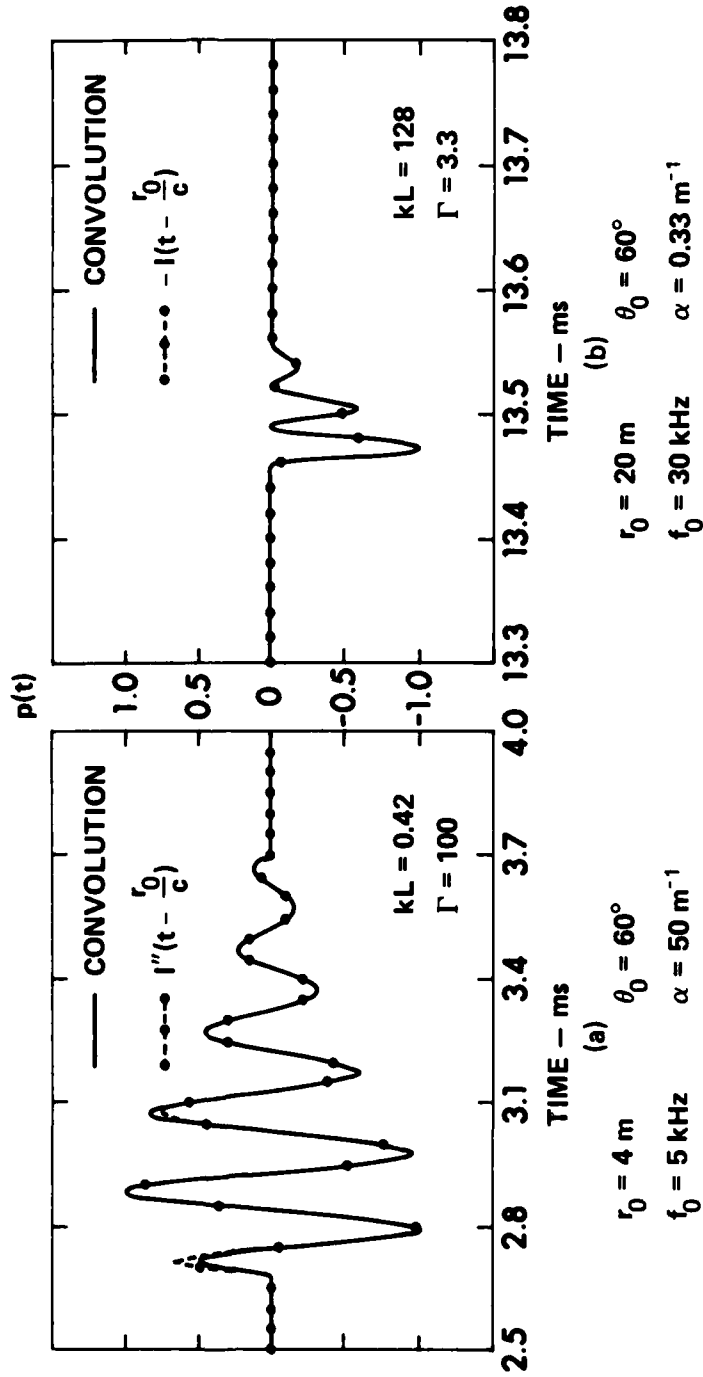
FIGURE 13
FARFIELD COMPARISONS OF PRESSURE WAVEFORMS

44

that under these conditions the pressure waveform appears to be simply proportional to an inverted laser pulse.[20] As indicated by Fig. 13(b), the convolution technique produces, as predicted, a pressure proportional to an inverted laser pulse.

An experimental investigation of thermoacoustic sources was carried out in the fresh water tank at ARL:UT . The lasing element of the optical system was a Neodymium:Glass rod producing infrared light at 1.06 μm in the conventional non-Q-switched mode. At this optical frequency the absorption of light in water was measured to be 13.7 Np/m. Determinations of the optical coefficient of absorption α are reported in Appendix F. More information on the laser apparatus is given in Chapter II.

Figure 14(a) shows a typical acoustic signal recorded on the digital oscilloscope. This waveform was obtained under the following conditions: $r_0 = 0.5$ m ; $\theta_0 = 75^0$; $a = 0.5$ cm ; $\alpha = 13.7$ Np/m ; $f_0 = 35$ kHz ($f_0 = \omega_0/2\pi$); $\tau_p = 1.2$ ms, $\Gamma = 1.77$. Figure 14(b) shows the waveform as predicted by the theory described previously. In the computer prediction, a Gaussian intensity distribution across the laser beam was assumed. The beam radius was very small compared to the main acoustic wavelength $\lambda_0 = c/f_0$, and thus the laser beamwidth had little effect on the resulting pressure waveform. Figure 14 shows that reasonable agreement between the theory and the experiment is obtained. A better fit could easily be obtained by altering the envelope constants for the laser intensity (see Eq. (2.3)). This did not seem appropriate, since these constants have been determined by averaging the envelope over several laser pulses. The discrepancy is attributed to the fact that the laser pulse envelope was not very repeatable. It was also

45
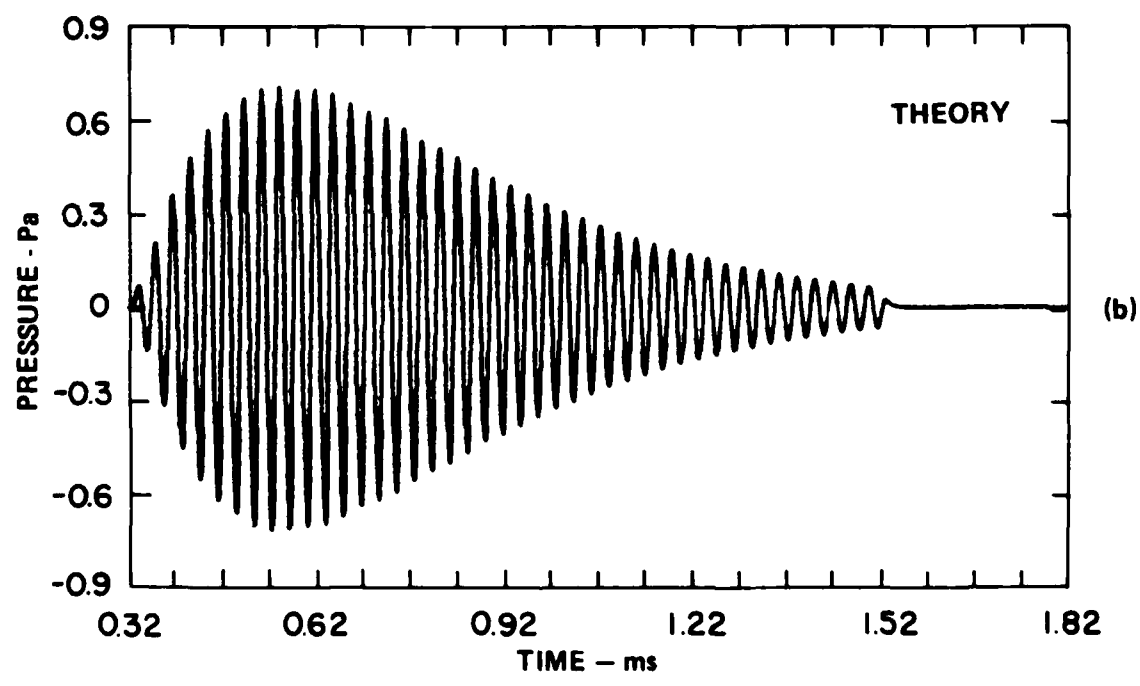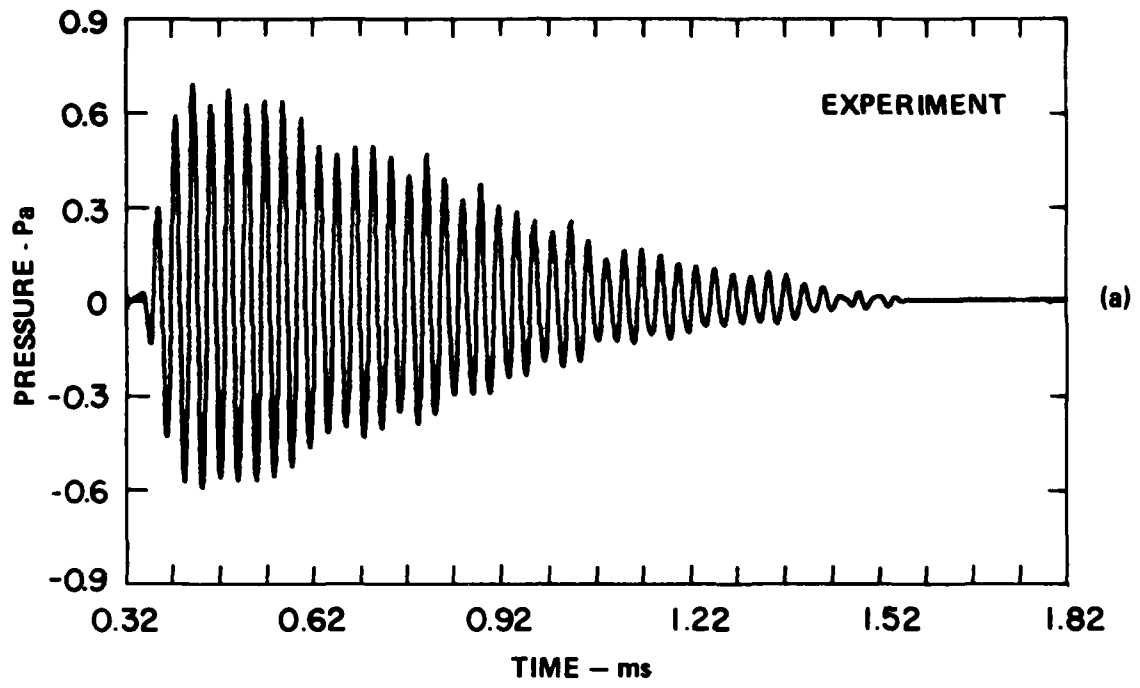
FIGURE 14
EXPERIMENTAL AND THEORETICAL PRESSURE WAVEFORM

ARL:UT
AS-85-205
YHB- GA
2-27-85

noted that the rise-time of the experimental pressure waveform was often shorter than the predicted one. It shows again the inherent non-stationarity of the laser pulse.

The acoustic peak signal shown in Fig. 14(a) was measured to be 122.8 dB re 1 μPa. This level is obtained by taking 20 times the logarithm based 10 of the peak to peak pressure divided by the reference pressure. It also takes into account the directional characteristics of the hydrophone (see Appendix B), the gain of the amplifier, and the loss through the bandpass filter (30-40 kHz). The predicted peak level can be found from Fig. 14(b) to be 123.1 dB re 1 μPa. This remarkable agreement between theory and experiment is certainly fortuitous because it was found that the average difference between experimental levels and theoretical levels is about +4.6 dB. In general, our numerical predictions underestimate the acoustic levels obtained experimentally, but are within a reasonable margin if we consider that the intrinsic properties of the laser pulse, such as its shape, its energy and its duration, vary significantly from pulse to pulse.

C. Directivity patterns

The impulse response described previously provides a means of finding the directivity characteristics of a thermoacoustic source. This is due to the fact that all the directional characteristics of the system are embedded in the impulse response of the system, and therefore one can relate the directivity pattern to the impulse response by a simple Fourier transform. Let us denote by $H(\omega)$ the frequency response of the optoacoustic

47

system. Then, using FT to denote the Fourier transform,

$$H(\omega) = FT [h(t)] = FT [h_\theta(t) * h_L(t)] = H_\theta(\omega) \, H_L(\omega) \quad , \quad (3.24)$$

where $H_\theta(\omega)$ and $H_L(\omega)$ denote, respectively, the Fourier transforms of the horizontal and vertical impulse responses $h_\theta(t)$ and $h_L(t)$. The directivity pattern at a given frequency ω is then simply

$$D(\theta) = 20 \, Log_{10} \frac{\| H(\theta;\omega) \|}{\| H(\theta_N;\omega) \|} \quad , \quad (3.25)$$

where θ_N yields the ...ximum value of $H(\theta)$ at the frequency ω, and the double vertical bars indicate the modulus of a complex quantity. The Fourier transform of $h_\theta(t)$ is obtained directly from Eq. (3.21), and in the case of a Gaussian beam, it gives

$$H_\theta(\omega) = S \, exp [- (ka \sin \theta_0)^2/4] \quad , \quad (3.26)$$

where $k = \omega/c$ is the acoustic wave number. Similarly one can find the Fourier transform of $h_L(t)$ from Eq. (3.15) . It is convenient to use the identity[21]

$$\int_{-\infty}^{t-r/c} f(\theta) [(t-\theta)^2-(r/c)^2]^{-1/2} \, d\theta = \int_{0}^{\infty} f[t-(r \cosh u)/c] \, du \quad . \quad (3.27)$$

By way of Eq. (3.27), the Fourier transform of $h_L(t)$ can be expressed as

48

$$H_L(\omega) = K_1 \int_0^{u_0} \cosh(\gamma \sinh u) \exp(-i\eta \cosh u)\, du$$

$$- K_2 \int_{u_0}^{\infty} \exp(-\gamma \sinh u) \exp(-i\eta \cosh u)\, du \quad , \quad (3.28)$$

where $K_1 = A\beta\alpha\, e^{-\Gamma}/2\pi c_p$,

$K_2 = A\beta\alpha \sinh(\Gamma) / 2\pi c_p$,

$u_0 = \ln[(1+\cos\theta_0)/\sin\theta_0]$,

$\gamma = \alpha r_0 \sin\theta_0$,

$\Gamma = \alpha r_0 \cos\theta_0$,

$\eta = k r_0 \sin\theta$,

and we are considering only angles θ such that $0 \leq \theta \leq \pi/2$. This expression is not easy to integrate analytically but may be easily evaluated numerically. In most practical cases the beam radius is very small compared to an acoustic wavelength so that $h_\theta(t) \rightarrow S\,\delta(t)$ or $H_\theta(\omega) \rightarrow S$ is a good approximation.

Figures 15(a)-(c) show the result of the numerical computation of the directivity pattern of a TS at three radii of observation: r_0 of 1 m , 2 m, and 3 m (i.e., for values of $\Gamma/\cos\theta_0$ of 5, 10, and 15). The modulation frequency was set to 10 kHz and the optical absorption coefficient was 5 Np/m so that the effective length of the array was 20 cm. Figure 15(a) shows that sidelobes exist in the nearfield of a TS. As the receiver moves into the farfield, the sidelobe structure tends to disappear and eventually the computed directivity reduces to the usual farfield analytical form

49
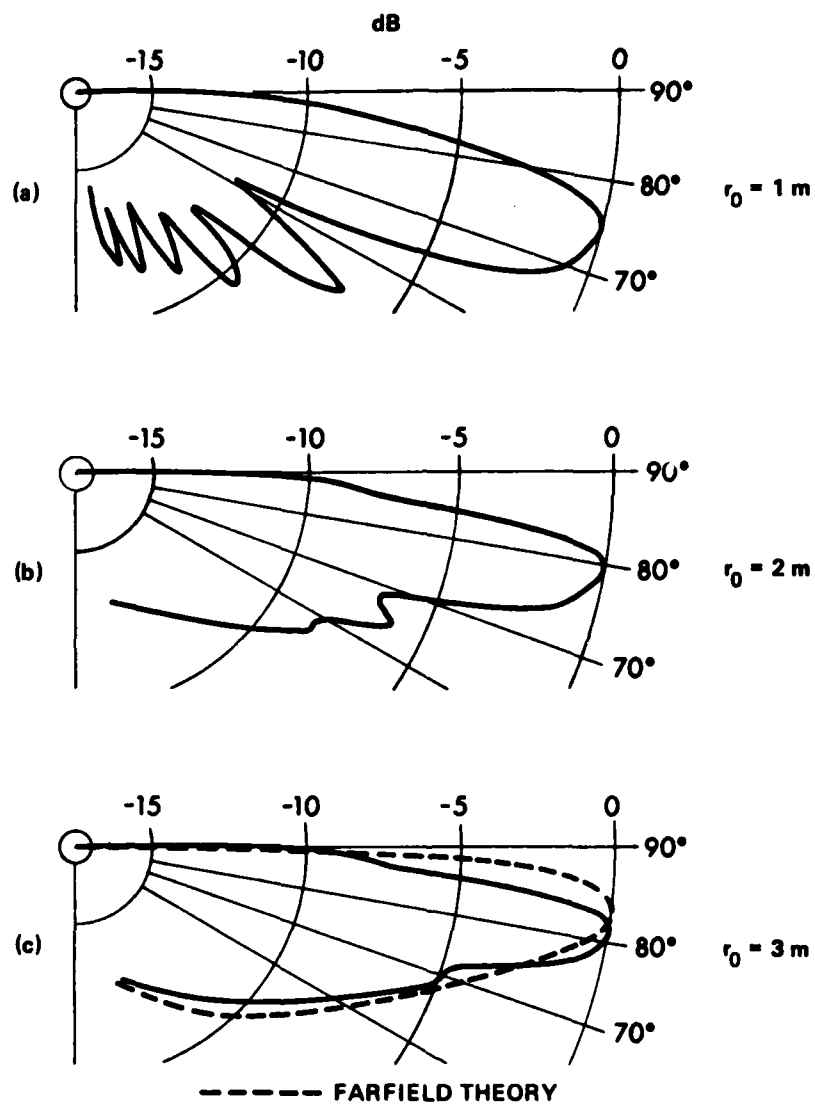
FIGURE 15
DIRECTIVITY OF A STATIONARY THERMOACOUSTIC SOURCE – I

$(f_0 = 10 \text{ kHz}, \alpha = 5 \text{ Np/m}, \sigma = \frac{k}{\alpha} = 8.46)$

described by Lyamshev and Sedov:[18]

$$D(\theta) = \frac{2\,\sigma\,\cos\theta}{1 + \sigma^2\cos^2\theta}\quad,\tag{3.29}$$

where $\sigma = k/\alpha$ is a measure of the length L of the array in terms of an acoustic wavelength λ.

Figure 16 shows the predicted directivity patterns for different wavelengths when the radius of observation and the source length are held constant. The figure shows that by decreasing the number of wavelengths along the length of the source (i.e., for σ decreasing), one decreases the number of sidelobes and increases the angle of tilt of the main lobe away from the interface. Also the half-power beamwidth angle increases drastically so that the end result is a dipole type of directivity as expected from a very small source (relative to a wavelength) radiating on a pressure release interface.

Figure 17 shows the computed directivity when the length of the source varies while the distance of observation r_0 and the modulation frequency f_0 are kept constant. Since we have assumed an exponential law of absorption of light in water, with an optical coefficient of absorption α (see Eq. (3.5)), the quantity $1/\alpha$ represents the depth at which the intensity is attenuated by a factor $1/e$. Again the number of sidelobes and the angle of maximum emission decrease with σ, whereas the half-power beamwidth increases when σ decreases. It is also interesting to note that the nearfield directivity is not simply dictated by the

51
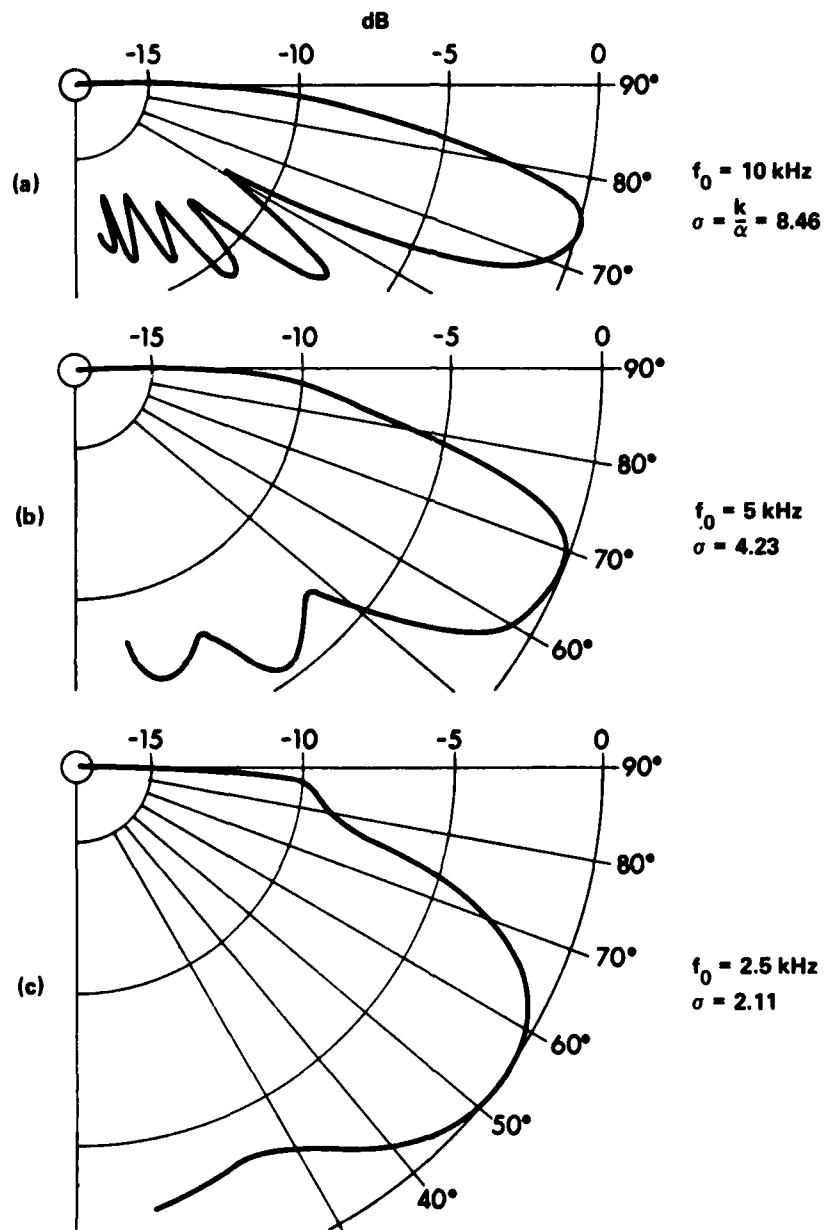
FIGURE 16
DIRECTIVITY OF A STATIONARY THERMOACOUSTIC SOURCE – II
$(r_0 = 1 \text{ m}, \alpha = 5 \text{ Np/m})$
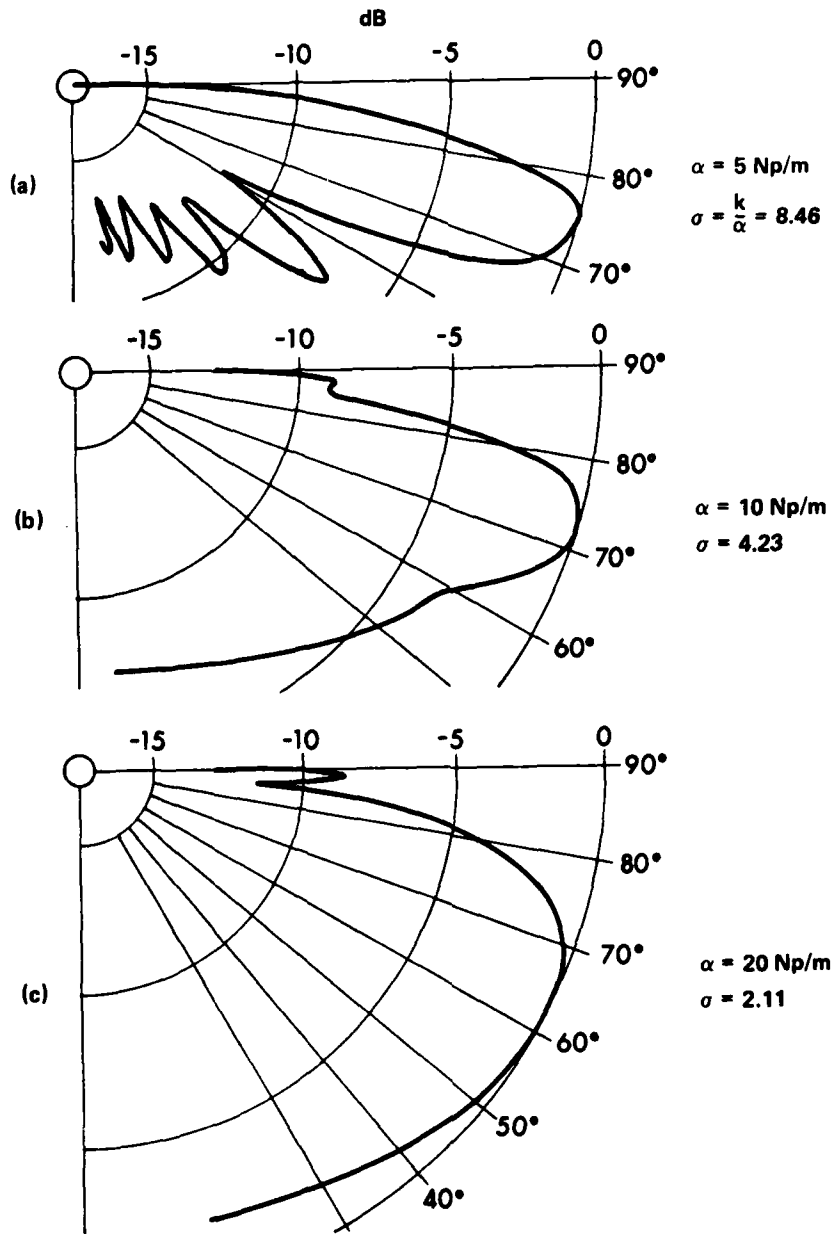
FIGURE 17
DIRECTIVITY OF A STATIONARY THERMOACOUSTIC SOURCE — III

$(r_0 = 1 \text{ m}, f_0 = 10 \text{ kHz})$

53

nondimensional parameter $\delta = k/\alpha$, as in the farfield case, but independently by k and α.

Figure 18 shows the nearfield effects on the half-power beamwidth θ_{HP} as a function of distance r_0 and plotted for several array lengths. As mentioned previously, θ_{HP} decreases with δ. For large values of r_0, θ_{HP} reduces, as expected, to its farfield estimate, which can easily be obtained from Eq. (3.29). In the farfield, θ_{HP} reduces to

$$\theta_{HP} = \cos^{-1}[\,(\sqrt{2}-1)/\delta\,] - \cos^{-1}[\,(\sqrt{2}+1)/\delta\,] \qquad . \qquad (3.30)$$

It is also interesting to note that, for a given source length, θ_{HP} goes through a minimum at a certain distance $r_{0,opt}$. This may be of practical interest for applications where angular resolution is more important than long range propagation.

Figure 19 shows how the nearfield affects the angle of maximum radiation θ_{max}, for different array lengths, as a function of distance. Again, for large values of r_0, θ_{max} reduces to its farfield limit, which can be evaluated from Eq. (3.29) to be

$$\theta_{max} = \cos^{-1}(1/\delta) \qquad . \qquad (3.31)$$

Note that Figures 18 and 19 can be used to define a farfield criterion.

Experimental data were obtained for a modulation frequency of 35 kHz, with $\alpha = 13.7$ Np/m, at a radius of observation of 0.50 m. (Same experiment as the one reported in Fig. 14). Infrared light of optical
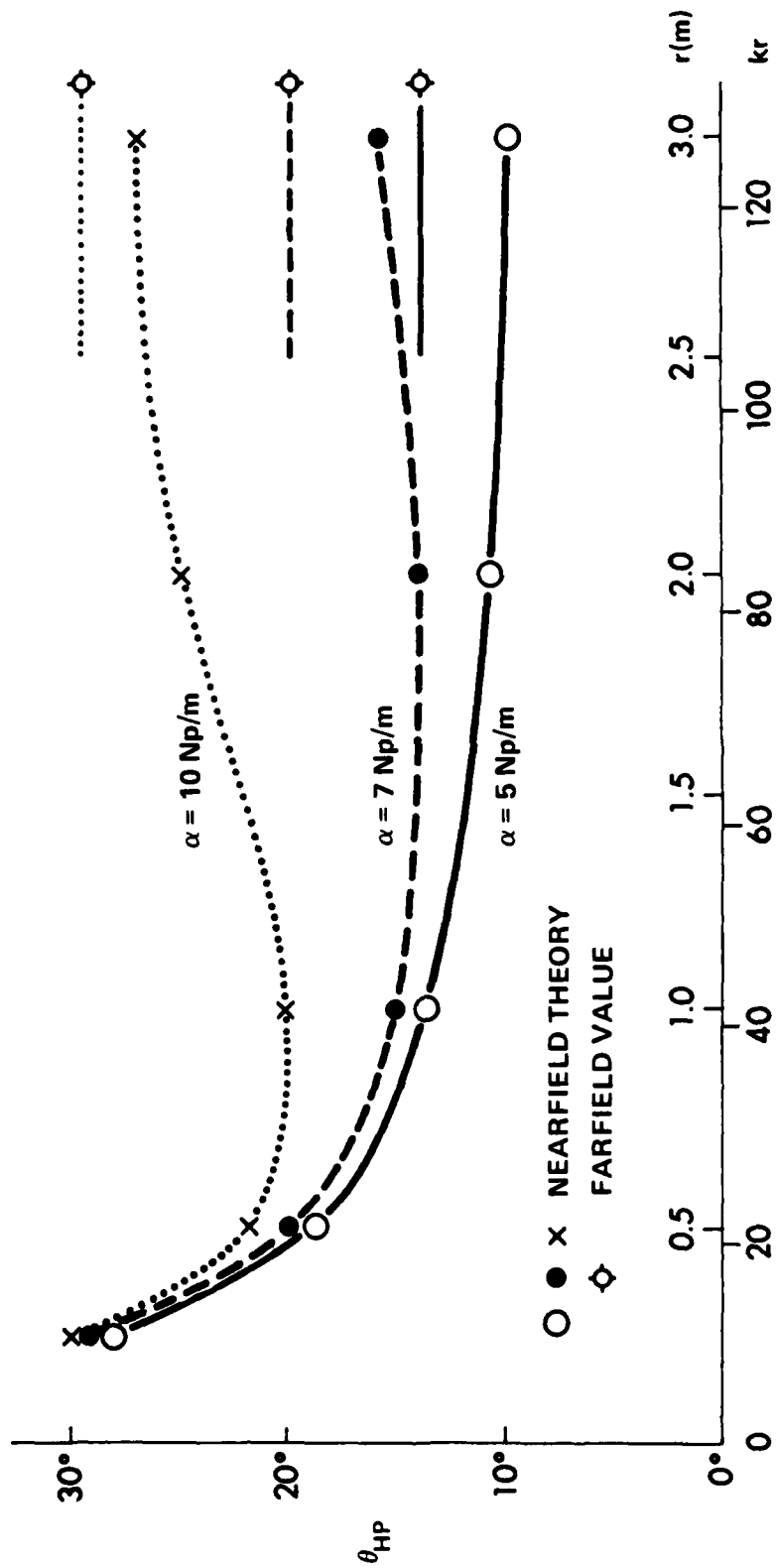
FIGURE 18

NEARFIELD EFFECTS θ_{HP} AS A FUNCTION OF r_0 AND α

55
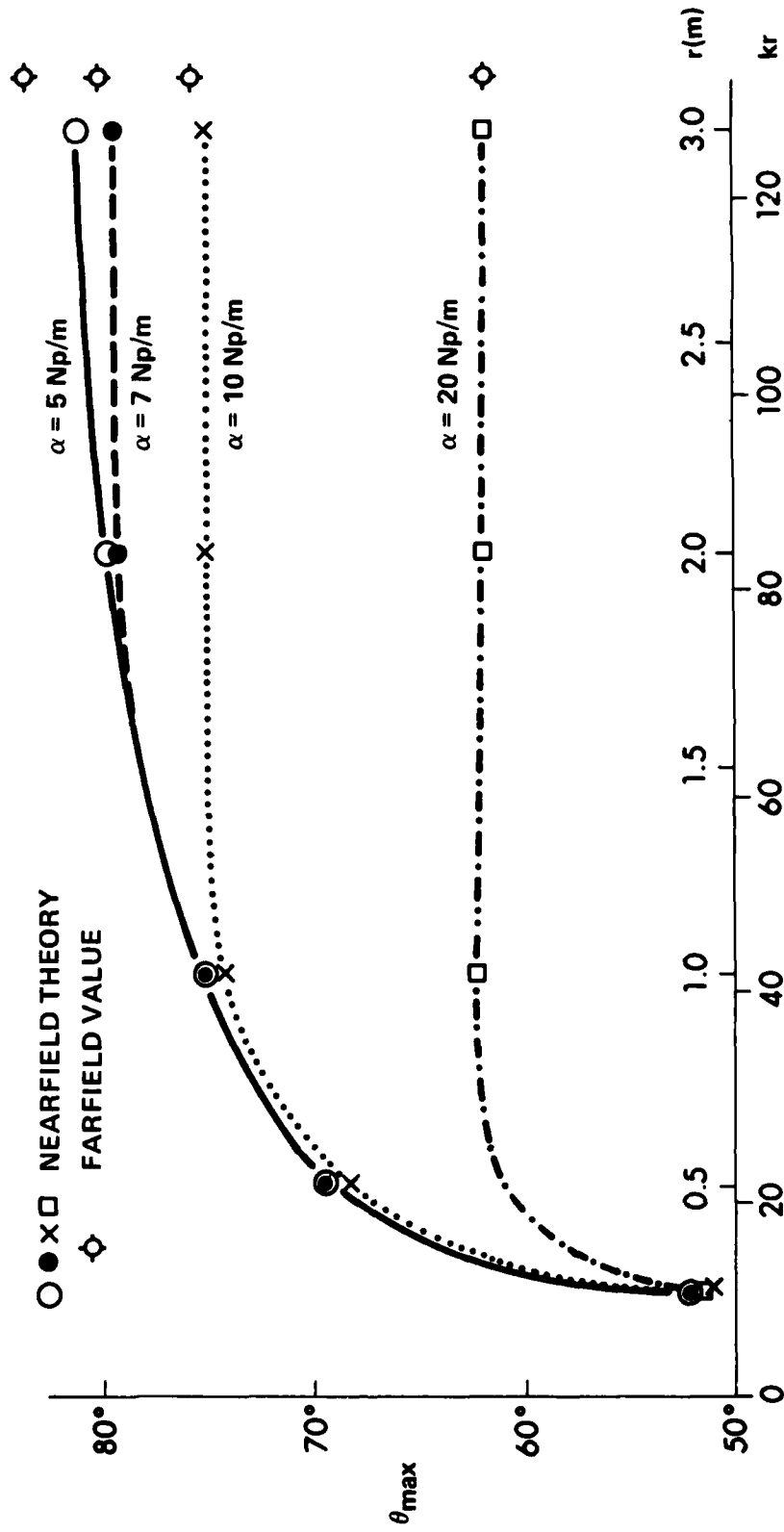
FIGURE 19

NEARFIELD EFFECTS θ_{max} AS A FUNCTION OF r_0 AND α

56

wavelength of 1.06 μm was shined into fresh water (c=1486 m/s). The pulse length was of the order of 1 ms. The receiver was an H-56 hydrophone of sensitivity -171 dB re 1 V/μPa at 35 kHz. The vertical directivity pattern of the transducer H-56 (see Appendix B) was taken into account in the analysis of the directivity of the TS. The signal was amplified and filtered before being stored in a digital oscilloscope. For each waveform, the rms pressure was computed numerically and yielded a value for the sound pressure level in decibels. The rms pressures were averaged over several pulses. The comparison between predictions based on Eqs. (3.24)-(3.28) and experiment is shown in Fig. 20. Good agreement between theory and experiment shows again that the impulse response approach is very well suited for describing the nearfield of a thermoacoustic source.

D. Spreading curves

It is known that, in general, the sound level dependence on distance, or spreading curve, is just a function of the geometrical dimensions of the acoustic source in terms of the acoustic wavelength. Thus, the sound level dependence on distance, denoted by $L_\omega(r)$, can be found at a given frequency ω by taking the Fourier transform of the impulse response of the TS. This can be expressed in a fashion similar to Eq. (3.25),

$$L_\omega(r) = 20 \, Log_{10} \frac{\| H(\omega,r) \|}{\| H(\omega,r) \|_{r=r_{ref}}} \quad , \quad (3.32)$$
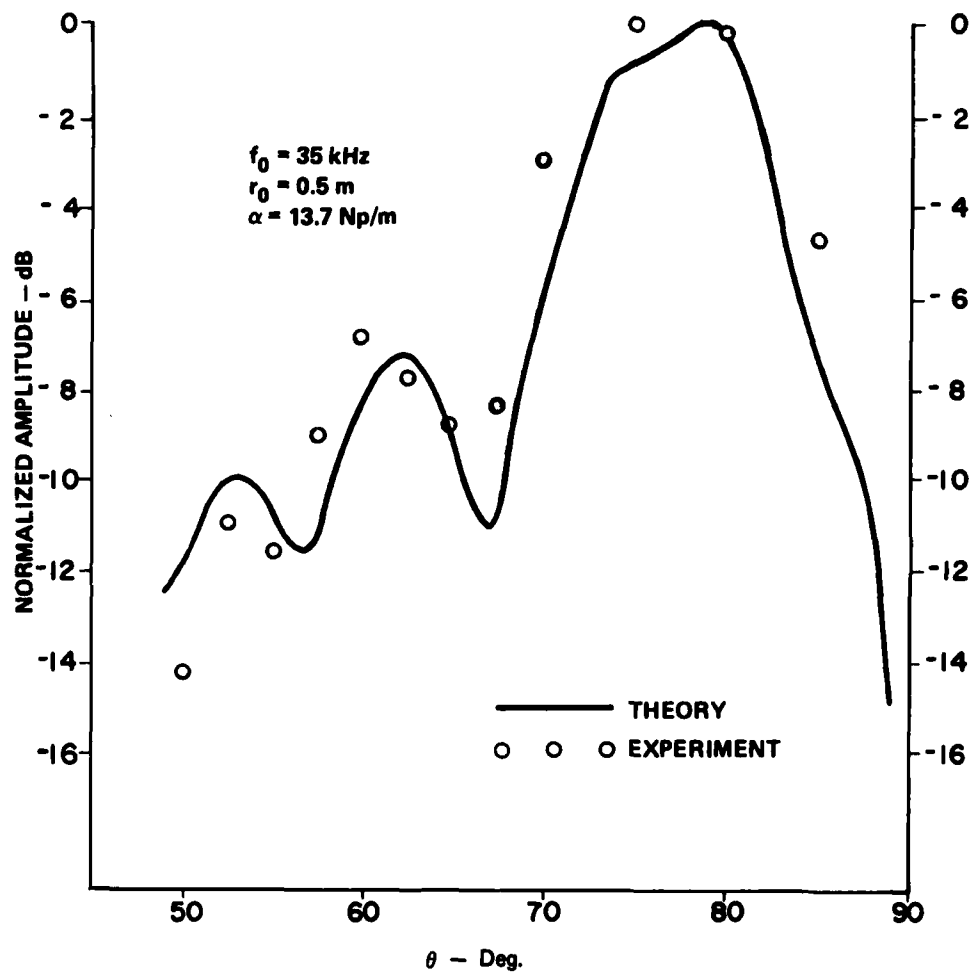
FIGURE 20
NEARFIELD DIRECTIVITY OF A STATIONARY THERMOACOUSTIC SOURCE

where $H(\omega,r)$ is the Fourier transform of $h_L(t)$, which is valid in the nearfield.

The approach for finding $L_\omega(r)$ is thus similar to the one described in the previous section for finding the nearfield directivity $D_\omega(\theta)$. Experimental results presented in Fig. 21 show the spreading characteristic of a stationary thermoacoustic source. The parameters associated with Fig. 21 are $\theta_0 = 84^0$, $f_0 = 35$ kHz, and $\alpha = 13.7$ Np/m. In both theory and experiment, the sound level seems to decrease at a rate of 3 dB per doubling of distance until a range of about 1.5 m, after which the slope increases to a value of 6 dB per doubling of distance. The reason for the change of slope is that, in the nearfield, the TS appears to be essentially a cylindrical source, whereas in the farfield, spherical spreading obviously predominates. The transition between cylindrical and spherical spreading may also be used as a practical estimate of the Rayleigh distance of the thermoacoustic source. Another way to see the transition is to look at the directivity patterns in Fig. 15. As r_0 increases, the major lobe moves toward 84^0. Thus the tendency toward a 6 dB slope is partly neutralized by the progression up the major lobe toward its peak. This argument implies that at same angles the slope might exceed 6 dB in the nearfield.

E. Conclusions

The sound field radiated by a thermoacoustic source has been investigated both theoretically and experimentally. The theory is based on a time domain approach. It shows that the acoustic pressure radiated by the

59
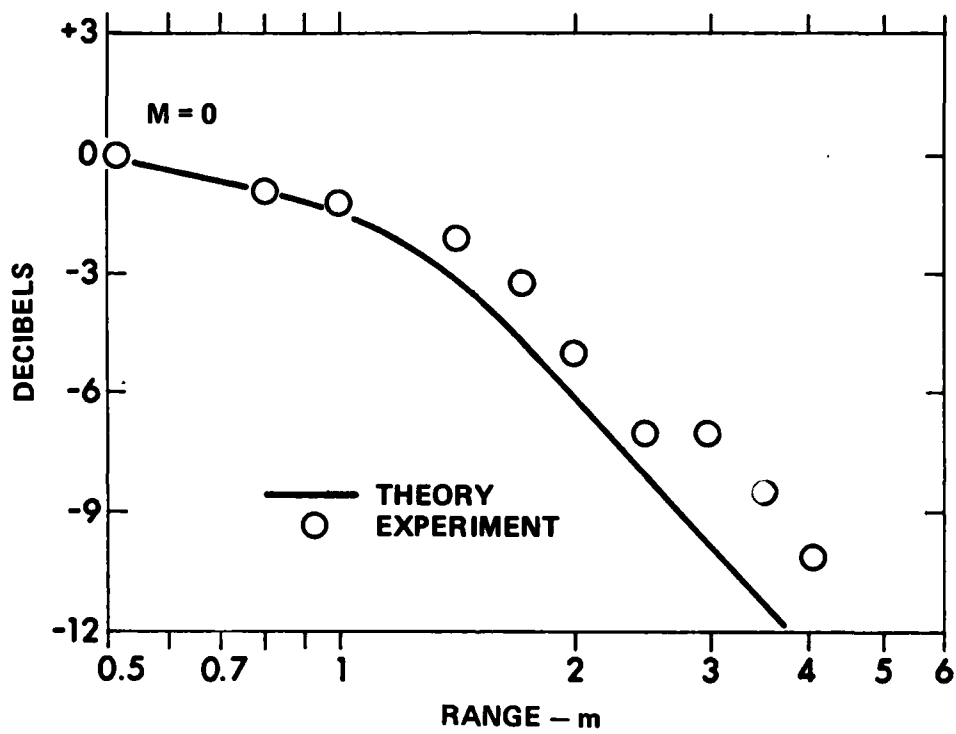
FIGURE 21
SPREADING OF A STATIONARY THERMOACOUSTIC SOURCE

thermal mechanism is a convolution of the impulse response of the system with the thermoacoustic source strength (time derivative of the laser intensity). Although the convolution has to be performed numerically in most practical cases, it offers several advantages: (1) it can be used to investigate the case of a moving thermoacoustic source, (2) it is valid even in the nearfield of the source, (3) although we have restricted our analysis to the most applicable case of a laser beam of Gaussian cross-section intensity distribution with an exponential shading along the beam penetration axis, the model presented here can easily be extended to any laser intensity temporal or spatial profile, and (4) this approach does not require transforms to get time information. Furthermore, the impulse response of a thermoacoustic array may provide insight into several thermoacoustic transient phenomena such as extremely short laser pulses, shock waves induced by a laser source moving at transonic velocity, pressure waveforms radiated by lightning, or even cosmic rays entering the ocean.

The validity of the theoretical model was tested by an experimental investigation of thermoacoustic pressure waveforms and directivity patterns. Results seem to indicate that in the nearfield, the acoustic levels may be quite different from those predicted by a farfield theory, and that sidelobes cannot be neglected in a nearfield directivity pattern. In general, experimental results were in support of the theoretical predictions in both farfield and nearfield cases.

CHAPTER IV

MOVING THERMOACOUSTIC SOURCES[22]

In the previous chapter, we analyzed in detail the acoustic field radiated by a stationary thermoacoustic source. The objective of this chapter is to extend these results to the case of a moving source. As mentioned earlier, the major reason for studying moving thermoacoustic sources (MTS) is that they are expected to produce substantially higher acoustic levels when the source is moving at a velocity close to the speed of sound in water.

In the first section of this chapter, we present the theory that will be used to predict the properties of the acoustic field of an MTS, even in the nearfield of the source. The theory is based on the impulse response described in Section III.A.

Then, in the second section of this chapter, we proceed to analyze successively pressure waveforms, directivity patterns, sound pressure level dependence on source velocity, and spreading curves. Comparisons between theory and experiments are made for subsonic, transonic, and supersonic source velocities.

The last section of this chapter summarizes the main conclusions of this chapter.

A. Theory

1. Pseudo-convolution

The pressure signal radiated by the moving thermoacoustic source (MTS) may be constructed in a three-step procedure as follows. First, the motion of the source is decomposed in time. As in a movie, a "picture" is taken at constant time intervals Δt, showing the laser beam at different positions along its path during the laser pulse duration τ_p. The geometry associated with an MTS is shown in Fig. 22 . Second, for each of these positions (defined by the subscript i in Fig. 22) the impulse response $h_i(t)$ and the corresponding elementary pressure response $p_i(t)$ are evaluated numerically from the analysis presented in Section III.A. Third, the total pressure $p_T(t)$ received at the hydrophone is obtained by adding all the elementary acoustic responses $p_i(t)$ with the suitable time delays corresponding to the motion of the source. Note that this approach is in principle also suitable for a source moving with a nonuniform velocity along its path. However in the following analysis it is assumed for simplicity that the source is moving at a constant velocity v. This model also assumes that the laser beam remains always perpendicular to the water surface. This assumption is discussed in Appendix A.

The first step in the analysis is to discretize in time and space the motion of the source so that the problem can be analyzed numerically. Given that τ_p is the laser pulse duration and Δt the time increment, the motion of the source is represented by N pictures taken

63
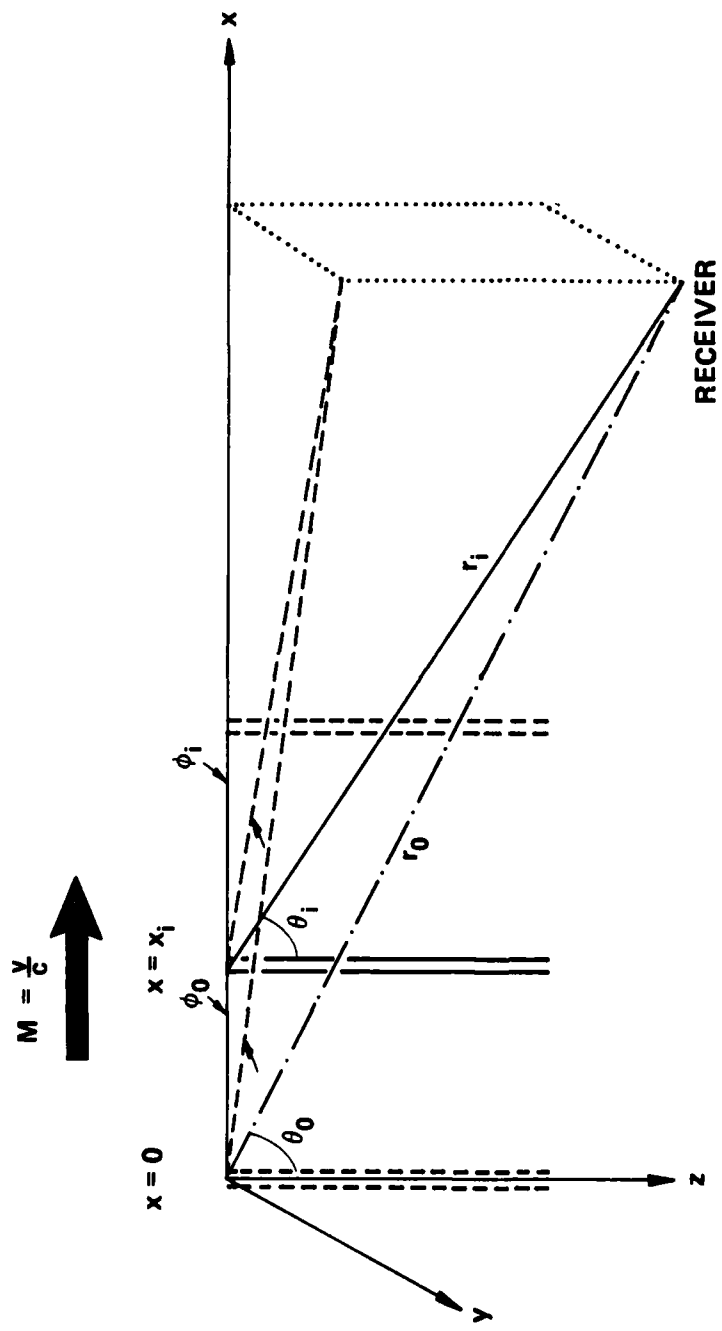
FIGURE 22

MOVING THERMOACOUSTIC SOURCE GEOMETRY

every Δt seconds, such that $N = \tau_p / \Delta t$. For a source moving rectilinearly at constant velocity v, $i \Delta t$ represents the time taken for the laser to move from the origin to the position shown on the i-th picture. The second step is to compute for each of these positions the elementary acoustic pressure radiated by the source when it was at the position shown on the i-th picture, that is to say, after a time delay $i \Delta t$. The laser source intensity at that instant is simply $I(i \Delta t)$ and the impulse response $h_i(t)$ can be evaluated from Eq. (3.15). However it is important to realize that the impulse response is a function of the position of the source because the distance and the angle between the source and the receiver are time dependent in the case of a moving source. Let us denote by r_i and θ_i these coordinates. It can easily be shown that

$$r_i = \left[r_0^2 - 2 r_0 (v i \Delta t) \cos\theta_0 \sin\phi_0 + (v i \Delta t)^2 \right]^{1/2} \qquad (4.1)$$

and

$$\theta_i = \cos^{-1} (r_0 \cos \theta_0 / r_i) \qquad , \qquad (4.2)$$

where r_0, θ_0 and ϕ_0 refer to values at the origin of the motion of the source (t=0). The impulse response $h_i(t)$ is therefore given by Eq. (3.15) where the coordinates r_0 and θ_0 have been replaced by r_i and θ_i using Eqs. (4.1) and (4.2).

The elementary acoustic pressure $p_i(t)$ is then computed as follows. Equation (3 3) shows that the optoacoustic source strength is proportional to the time derivative of the laser intensity. The i-th picture therefore

shows a line source excited by an impulse of strength $I'(i \, \Delta t)$ during a time Δt, and thus the elementary acoustic pressure $p_i(t)$ is given by

$$p_i(t) = I'(i \, \Delta t) \; h_i(t) \; \Delta t \qquad , \qquad (4.3)$$

where the prime denotes a time derivative.

The third step is to add all the elementary acoustic pressures $p_i(t)$ radiated during the motion of the source, taking into account the time delay $i\Delta t$ taken by the source to travel from the origin ($t=0$) to the i-th position. This gives the total acoustic pressure $p_T(t)$ radiated by the thermoacoustic source during its motion:

$$p_T(t) = \sum_{i=0}^{N} p_i(t-i\Delta t) \, \Delta t \qquad (4.4)$$

Combining Eqs.(4.3) and (4.4) gives

$$p_T(t) = \sum_{i=0}^{N} I'(i\Delta t) \; h_i(t-i\Delta t) \, \Delta t \qquad . \qquad (4.5)$$

Equation (4.5) shows that the total pressure received at the observation point is a convolution type summation in the time domain between the "unsteady" (changing shape with time and distance) impulse response $h_i(t)$

66

and the optoacoustic source strength dI/dt. Note that in the case of a stationary source, the shape of the impulse response remains constant and the acoustic pressure $p_T(t)$ is a true convolution between the impulse response and the time derivative of the laser intensity.

In the above results laser beamwidth effects have been neglected. They become, however, very important when the acoustic wavelength is of the order of the laser beam diameter, and this is always the case when the source is moving at velocities close to transonic. In order to have a model valid for any source velocity, it is therefore necessary to take into account laser beamwidth effects. This is the object of the next section.

2. Laser beamwidth effects

It was shown in Chapter III (see Eq. (3.4)) that laser beamwidth effects can be accounted for by a convolution involving the impulse response $h_a(t)$ of a cross section of the laser beam. This impulse response is defined as the time response at the receiver to an impulse of heat applied at a specified depth and over an area corresponding to the laser beamwidth. If $r_0 \gg a$, where a is the laser beam radius, then

$$h_a(t) = \pi^{1/2} c a \sin\theta_0 \exp\left\{ -[(r_0 - ct)/(a \sin\theta_0)]^2 \right\} \quad , \quad (3.21)$$

where we have assumed that the intensity distribution across a section of the laser beam is Gaussian. This last equation has been derived previously in Chapter III. The effect of the finite beamwidth of the laser may be

thought of as introducing many infinitesimally thin line sources into each "picture" of the source at time t_i. This effect may be included mathematically by convolving the cross-section impulse response with $p_T(t)$. The result is an induced smoothing of the pressure waveform that is a low-pass filtering in the frequency domain. The frequency filtering $H_\theta(\omega)$ associated with laser beamwidth effects may be obtained by taking the Fourier transform of $h_\theta(t)$. It is necessary to note, however, that in order to account for the motion of the source, the main wave number $k_0=\omega_0/c$ of the acoustic radiation must be replaced by its Doppler shifted version $k_d = k_0/D = k_0/|1-M\sin\theta_0\cos\phi_0|$, where D is known as the Doppler factor. (The $\sin\theta_0\cos\phi_0$ term in the Doppler shift correction is due to the fact that the receiver sees an apparent velocity that is different from the actual velocity of the source which has Mach number M=v/c. This was first noticed by Doppler[23] in 1842). The result is

$$H_\theta(\omega) = \pi\, a^2 \sin^2\theta_0 \exp\left[-(k_d\, a\, \sin\theta_0/2) \right. \qquad (4.6)$$

It should be understood that in the case of a moving source, the coordinates of the source r_0 and θ_0 are time dependent, so that in fact Eq. (4.6) is an approximation to the real frequency filtering associated with finite laser beamwidth effects. Since these effects are usually small, it seems unnecessary to get an exact and much more complicated expression for $H_\theta(\omega)$, and therefore Eq. (4.6) is expected to yield good results provided that finite laser beamwidth effects are relatively small. When the source is moving at velocities close to the speed of sound in the fluid, the Doppler

shifted wavelength characteristic of the acoustic radiation shrinks to a value very small compared to the beam radius a , thus generating very significant diffraction effects. In this case the approximation that diffraction effects are small breaks down. The finite beamwidth effects near transonic velocity will be discussed later in more detail.

The time domain approach used to predict the pressure waveform radiated by an MTS is perfectly suitable for a numerical computation and the theoretical predictions obtained with this model will be discussed in the next section.

3. Numerical predictions

Some typical predicted pressure waveforms radiated by a moving thermoacoustic source are presented in Fig. 23. These waveforms were obtained by computer simulation, using the impulse response approach described above. The computer program used for these simulations is given in Appendix G. These predictions were made for some realistic values of the important parameters: $r_0 = 4$ m , $\theta_0 = 75^0$, $\phi_0 = 0^0$, $\alpha = 13.7$ Np/m (Nd:Glass lasing wavelength of 1.06 μm in fresh water), a=0.5 cm, f_0=7 kHz, τ_p=1 ms, and c = 1486 m/s. The Mach number of the source M = v/c was varied from 0 to 1.5.

Figure 23(a) shows the pressure waveform observed at the receiver when the source is stationary. There is a periodic nature to the response due to the modulation of the intensity of the laser pulse and a roughly exponential decay in the amplitude due to the decay in the laser intensity.

69
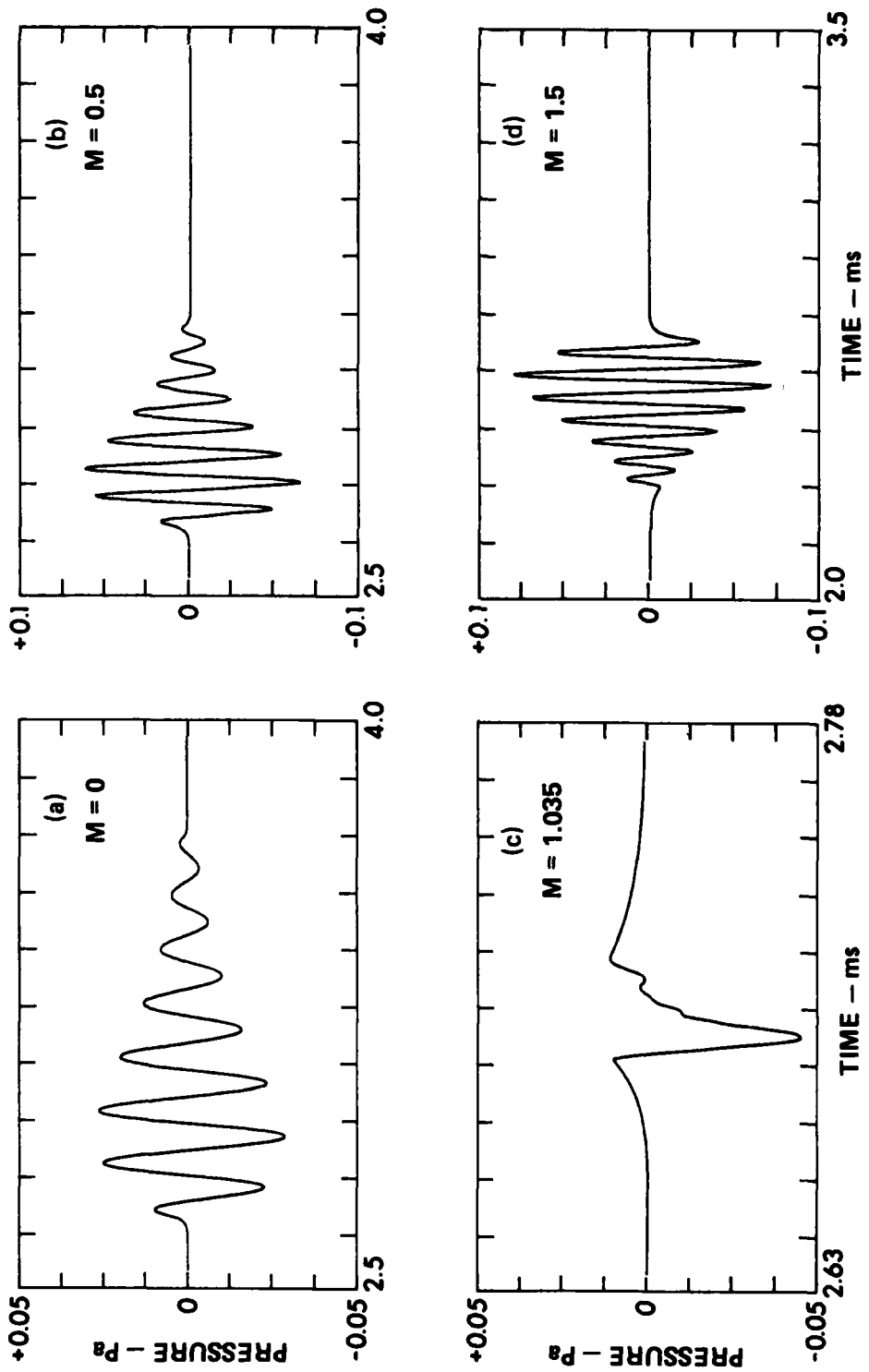
FIGURE 23

NUMERICAL PREDICTIONS OF MTS PRESSURE WAVEFORMS

$r_0 = 4\ m,\ \theta_0 = 75^\circ,\ \phi_0 = 0^\circ,\ \alpha = 13.7\ Np/m,\ f_0 = 7\ kHz$

Figure 23(b) shows the acoustic response when the source is moving at M=0.5. Clearly there is a time compression of the acoustic signal observed at the receiver, i.e., an increase in amplitude and frequency. This is a typical effect of the Doppler shift which occurs for moving sources. One important advantage of the time domain approach used in the numerical computation of the pressure waveform is that the Doppler shift is implicitly taken into account by the time delays of the pseudo-convolution (see Eq. (45)); therefore the Doppler shift appears naturally and it is valid even if the source is moving at transonic velocity. A detailed analysis of the Doppler shift associated with a moving source of finite length may be found in reference 24. To a first approximation the Doppler factor D seen by the receiver in Fig. 23(b) is $(1-M\sin\theta_0\cos\phi_0) = 0.517$ so that the Doppler shifted frequency in Fig. 23(b) is about $f_d = f_0/D = 13.5$ kHz. This is in good agreement with the Doppler shifted frequency of 13.6 kHz measured from Fig. 23(b).

Figure 23(c) shows the pressure waveform observed at the receiver when the source is moving at a velocity such that $M\sin\theta_0\cos\phi_0 = 1$, i.e., so that the receiver perceives the source to be moving at Mach one. In this case, the Doppler factor D goes to zero and subsequently the Doppler shifted frequency goes to infinity so that the Doppler shifted wavelength goes to zero. This means that in the transonic regime, diffraction effects due to the finite width of the laser beam will be important. Fig. 23(c) shows that the received pulse is extremely short (of the order of the transit time $2a/c$ across the laser beam diameter) and there is therefore no periodic structure in the pressure waveform but only a strong inverted

71

pulse whose shape depends mainly on the intensity distribution across a section of the laser beam. This is discussed in more detail in Appendix H. Note also that, as predicted by Eq. (4.6), laser beamwidth effects limit the amplitude of the pressure response when the source is moving at transonic velocity. Previously reported results which describe the pressure field of an MTS in terms of the pressure field of a stationary source compensated by a Doppler shift $D = (1-M\sin\theta_0\cos\phi_0)$ predict an infinite amplitude for a source moving at Mach one because they have not included the fact that the angle from the source to the receiver is location dependent, and hence have used a poor approximation to the Doppler factor.

Finally it is interesting to note in Fig. 23(d) that the time axis seems to be inverted. This effect is sometimes referred to as time inversion and it occurs when a source moves toward the receiver faster than the disturbances it generates. In such an event, the first sound wavelets to be observed by the receiver will be those excited last. This effect has been known for more than a century. Rayleigh[25], for instance, explains how a musical piece played at Mach two, can be heard "in tune, but played backwards". Note also that the predicted Doppler shifted frequency in Fig. 23(d) is 16.0 kHz which is in good agreement with the Doppler shifted frequency predicted by $f_d = f_0/D = 15.6$ kHz.

B. Experimental results

The experimental results presented in this section are grouped into four categories: pressure waveforms, directivity patterns, sound level

72

dependence on source velocity, and spreading curves. The experimental procedure was described in Chapter II.

1. Pressure waveforms

The pressure waveform radiated by a thermoacoustic source moving at Mach 1.6 is shown in Fig. 24. In both cases the pressures are normalized to one at their peak values. The values of the parameters relevant to Fig. 24 are : $r_0 = 4$ m , $\theta_0 = 80^0$, $\phi_0 = 0^0$, $f_0 = 35$ kHz , and $\tau_p = 0.8$ ms. There is fairly good agreement between the theory (Fig. 24(a)) and the experiment (Fig. 24(b)). Note that time inversion does occur at such a supersonic source velocity, and it is very clearly observed experimentally. The slight discrepancy (93 μs) between the predicted and experimental values of the arrival time of the acoustic pulse at the receiver is attributed to the fact that the time delay between the discharge of the laser flashlamp and the actual lasing of the rod (about 180 μs) was not perfectly constant so that the initial coordinates r_0 and θ_0 of the thermoacoustic source were known within only a certain accuracy.

Next we turn our attention to the pressure waveform when the source velocity is such that $M \sin\theta_0 \cos\phi_0 = 1$. Figure 25(a) shows the results of three different theoretical prediction schemes. The solid line in Fig. 25(a) represents the prediction obtained from the numerical analysis presented in the first section of this chapter. The long dashed line in the same figure was obtained by using a simplified approach which is described in Appendix H . In this approach, the pressure waveform can be

73
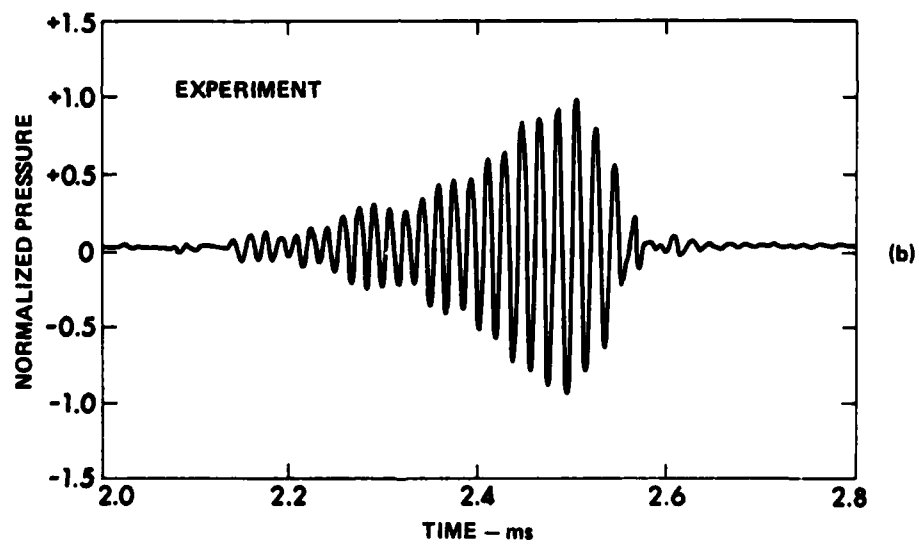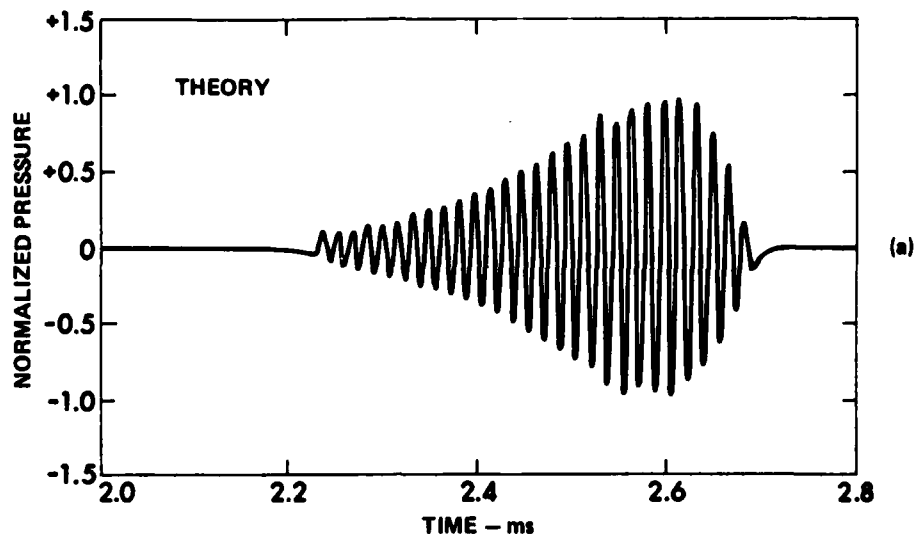
FIGURE 24
PRESSURE WAVEFORMS
$r_0 = 4 \, m, \theta_0 = 80°, \phi_0 = 0°, f_0 = 35 \, kHz$
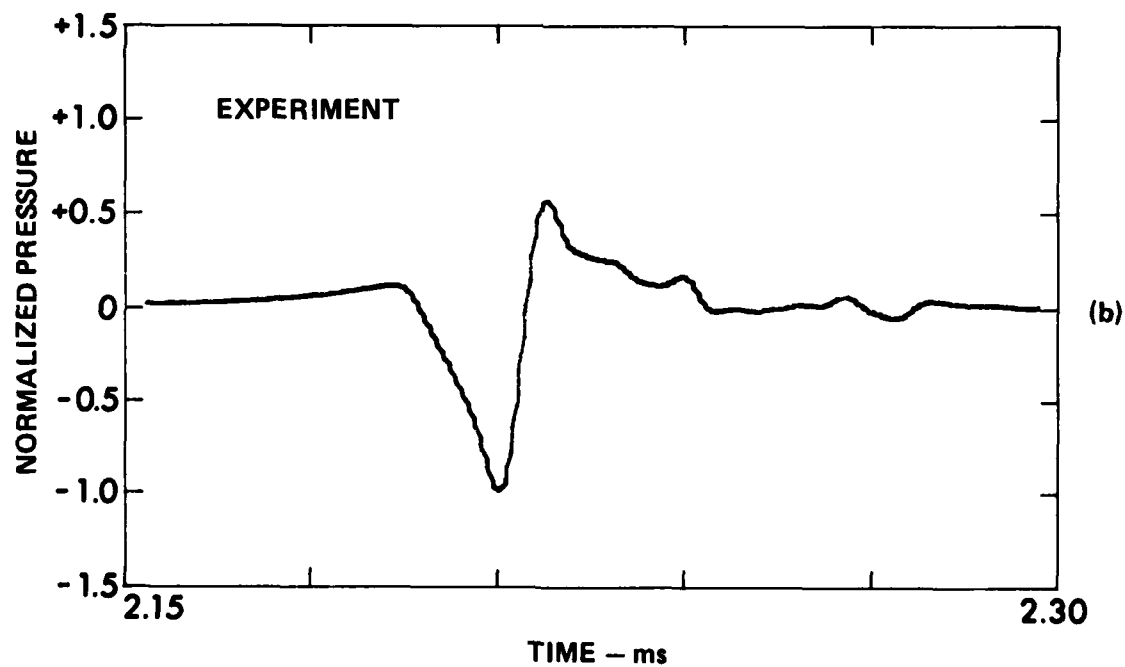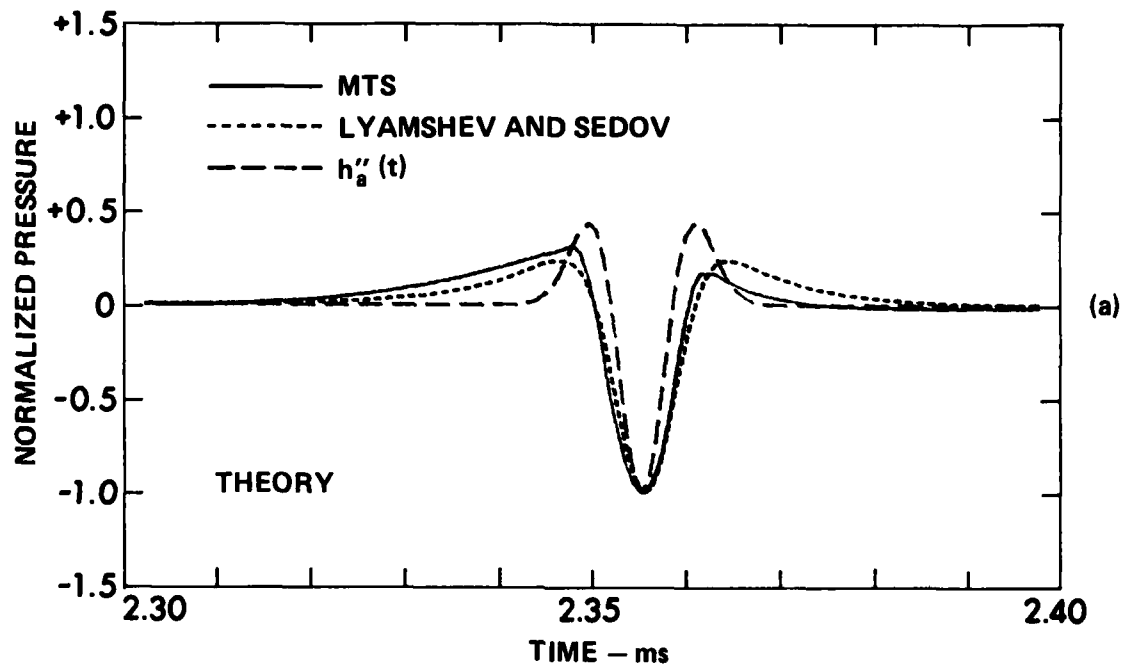
**FIGURE 25
LASER-INDUCED MACH WAVE**

$r_0 = 3.50 \text{ m}, \theta_0 = 80°, \phi_0 = 0°, f_0 = 20 \text{ kHz}$

approximated by the second time derivative of the impulse response of a cross section of the laser beam. The third curve (short dashed line) in Fig. 25(a) represents the analytical prediction of Lyamshev and Sedov given by Eq. (5) in Ref. 26. The values of the parameters relevant to Fig. 25 are $r_0 = 3.50$ m , $\theta_0 = 80^0$, $\phi_0 = 0^0$, $M = 1.03$, $f_0 = 20$ KHz , and $\tau_p = 0.8$ ms.

The three curves in Fig. 25 have the same main features: an exponential growth, followed by a strong inverted pulse and an exponential decay. The exponential growth is characteristic of the arrival at the receiver of wavelets coming successively from a depth $z_0 = r_0 \cos\theta_0$ to a zero depth at the air-water boundary. The inverted nature of the strong pulse is characteristic of a pressure release boundary condition at the air-water interface. The exponential decay is the result of the exponential law of absorption of light in water. The last wavelets arriving at the receiver come from the furthest points on the column of water being illuminated by the laser and therefore they have very low intensity.

Figure 25(b) shows an acoustic pulse recorded experimentally in a Mach wave. There is an overall agreement with the theoretical predictions given in Fig. 25(a) although the result shown in Fig. 25(b) has a higher peak after the inverted pulse and shows more high frequency content. The pulse was recorded by an H-23 hydrophone, amplified by 40.5 dB and filtered between 1 and 200 kHz. The beam radius on the surface of the water was about 7 mm, and the corresponding peak sound level was measured to be about 142 dB re 1 μPa at 3.50 m from the source. The asymmetry in the experimental waveform is attributed to nonlinear effects. It has been shown[27] that nonlinear effects associated with the temperature

76

dependence of the thermodynamic coefficients (β,c_p) cause an increase in the tail of the received signal. This is due to the fact that the heating of the medium being illuminated increases the coefficient of thermal expansion and, consequently, the efficiency of the conversion of electromagnetic energy into acoustic energy.

2. Directivity patterns

Next consider the directivity pattern of an MTS in the x-z plane. It is important to note that the motion of the MTS induces a variation of the angle of observation between the source and the receiver, and hence a variation of the Doppler shifted frequency, so that the received frequency is in fact a function of source location. The directivity pattern of an MTS is not therefore given at a single frequency but rather in a frequency interval. The smaller the ratio $Mc\tau_p/r_0$, the smaller the frequency interval. It is therefore necessary to define the concept of directivity for a moving source. In our study a directivity pattern is a plot of the sound pressure level as a function of the angle of observation between the source and the receiver, at the origin (time t=0) of the laser pulse. In other words, all the parameters such as modulation frequency, laser pulse duration, and initial distance of observation, are kept constant in a directivity pattern. The only parameter allowed to change is the initial angle of observation θ_0 , in the case of a directivity pattern in the vertical plane, and ϕ_0 in the case of a directivity pattern in the horizontal plane. The frequency content of the received signal is therefore allowed to change (sometimes drastically) in

the same directivity pattern. The sound pressure level is obtained by taking 20 times the logarithm based 10 of the ratio of the peak-to-peak pressure signal received at the hydrophone to a reference value of 1 μPa. It should be noted that the shape of the directivity patterns does not change significantly when rms pressures are used instead of peak-to-peak pressures. A directivity pattern defined in such a way is very practical from an experimental standpoint, since it gives an estimate of the sound pressure level versus angle under the same operating conditions of the laser.

The vertical directivity of thermoacoustic source is shown in Fig. 26. The theoretical curves were obtained by running the numerical program described previously, over several values of the angle θ_0. The other parameters were $r_0 = 3$ m , $\phi_0 = 0^0$, $\alpha = 13.7$ Np/m, and $\tau_p = 0.8$ ms. The circles represent experimental measurements. The left-hand directivity pattern in Fig. 26 was obtained with a stationary source modulated at 35 kHz while the right-hand one was obtained for a source moving at Mach 1.6 and a modulation frequency of 25 kHz. The experiment confirms that even though the modulation frequency was lower for the moving source, its directivity turns out to be sharper than that of the stationary source, because the received Doppler shifted frequency is greater than f_0 by the Doppler factor. The half-power beamwidth was measured to be 11^0 for the stationary source and 7^0 for the moving source. This agrees well with the predicted respective values of 11^0 and 6^0. Although the source appears at first glance to be a broadside array whose main lobe should be at $\theta_0 = 90^0$, the presence of the air-water interface produces a tilt in the lobe so that

78
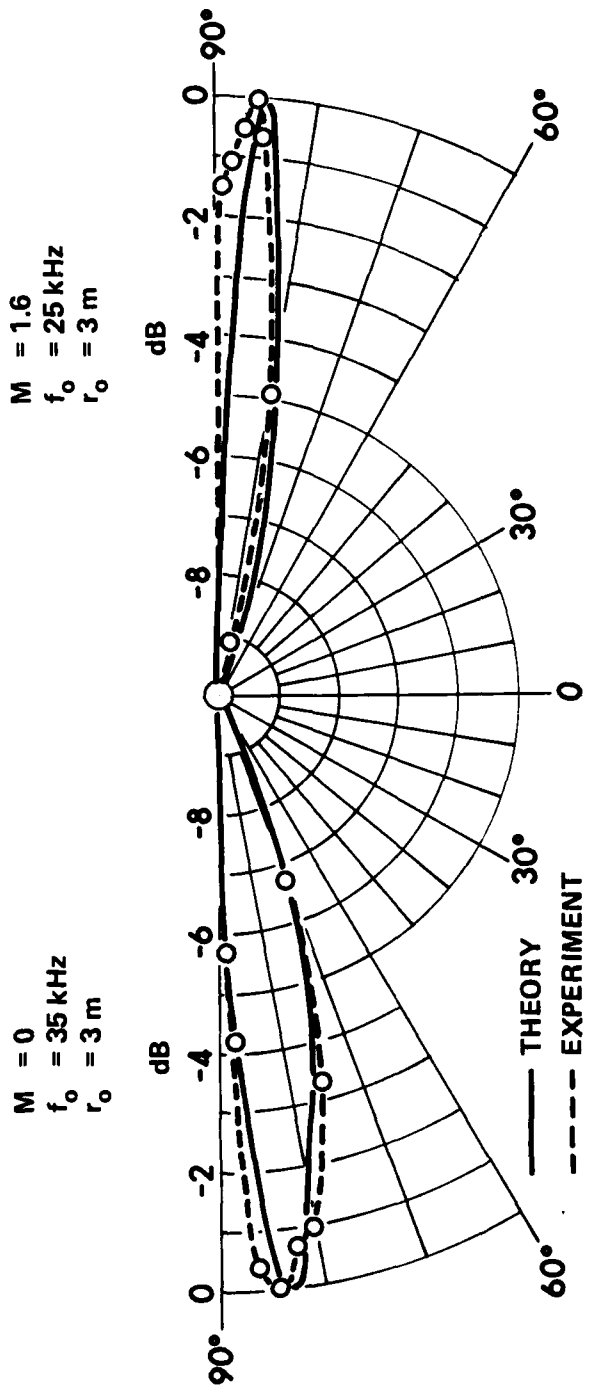
FIGURE 26
VERTICAL DIRECTIVITY OF AN MTS

there is no pressure at the boundary. The tilt angle for the main lobe was measured to be 84^0 for the stationary source and 86^0 for the supersonic source. Again this confirms the validity of the model which predicts 83^0 in the first case and 85^0 in the second.

Two experimental directivity patterns in the vertical x-z plane of an MTS moving at Mach one are shown in Fig. 27. The laser intensity was modulated at 25 kHz and 35 kHz respectively for the two directivity patterns, and in both cases the initial coordinates of the MTS were $r_0 = 4$ m and $\phi_0 = 0^0$. The two curves are very similar which confirms the fact that the modulation frequency does not play an important role in the directivity pattern of an MTS moving at transonic velocity. Theoretical curves are not shown in Fig. 27 because the numerical codes seem to yield unstable results near Mach one. The reason for this discrepancy has not been determined yet. It should be emphasized that experimental results for a source moving at Mach 1 are highly dependent upon the frequency response of the receiving hardware (hydrophone-amplifier-filter) which should optimally have a very large bandwith. However, the H-56 hydrophone used in this experiment has an upper frequency limit of about 70 kHz (see calibration curves in Appendix B). Moreover, the correction for the vertical sensitivity of the hydrophone is very difficult to assess when the received signal is broadband. Thus quantitative measurements around Mach 1 are to be taken cautiously.

The directivity pattern in a plane parallel to the interface between air and water (x-y plane) will be referred to as a horizontal directivity pattern. Figure 28 shows the horizontal directivity pattern of an MTS for

80
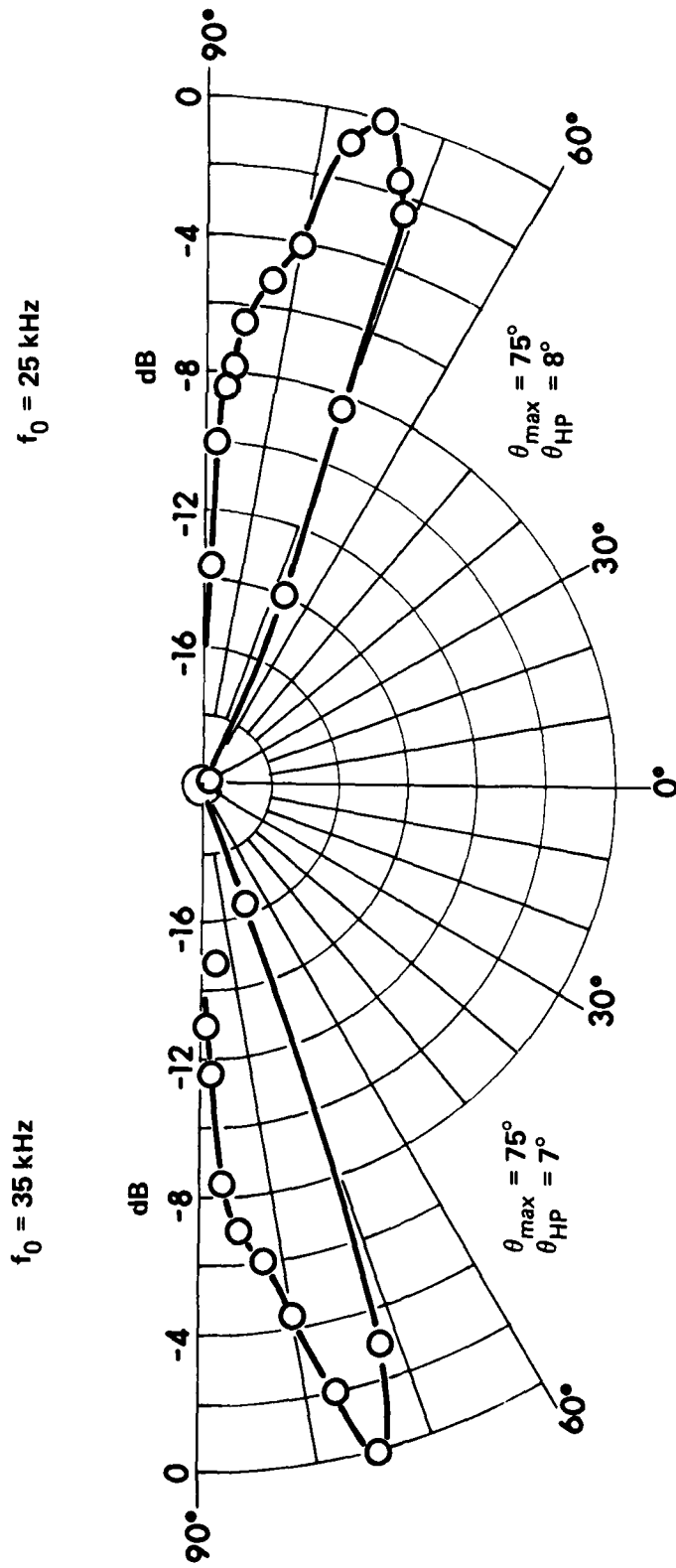
FIGURE 27
VERTICAL DIRECTIVITY OF A TRANSONIC MTS

81
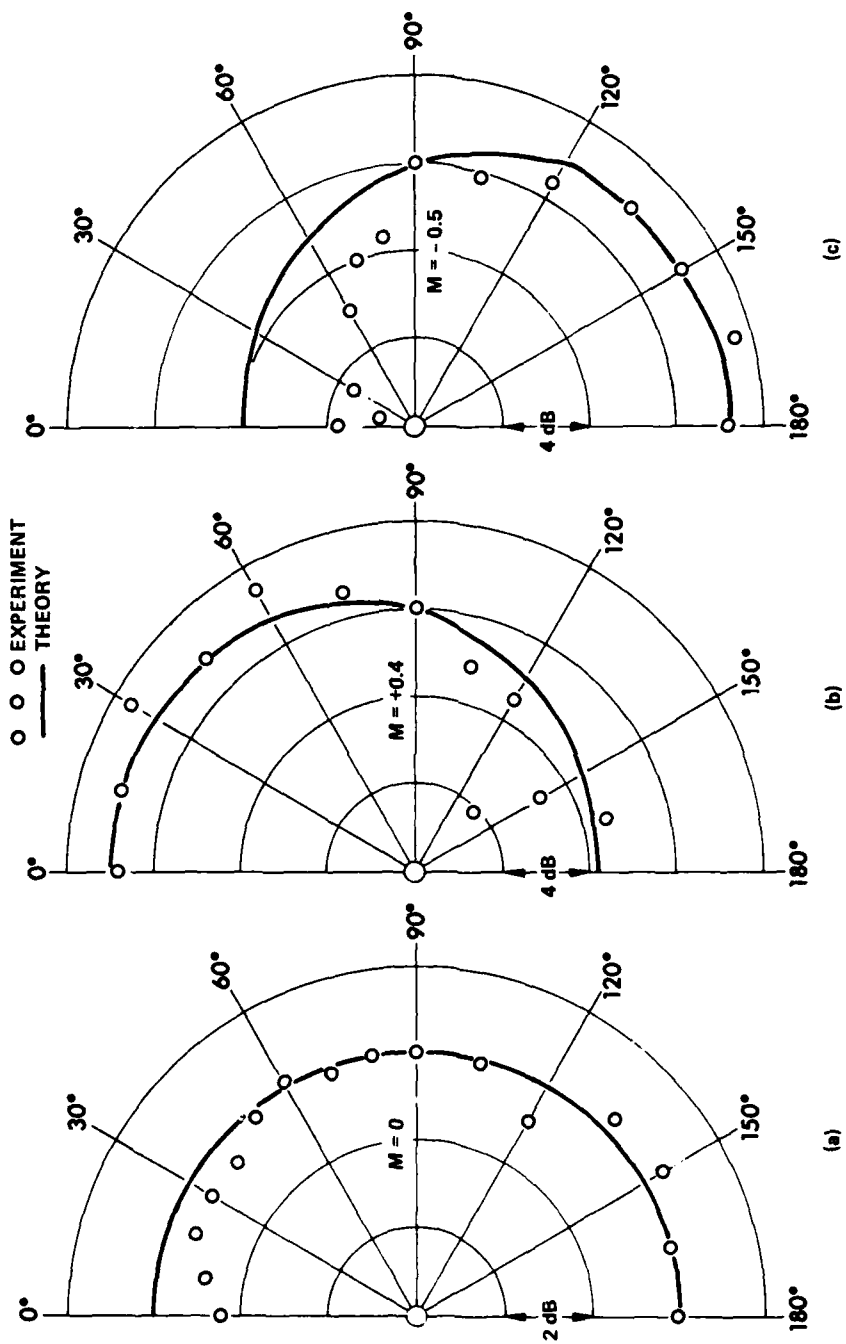
FIGURE 28
HORIZONTAL DIRECTIVITY OF AN MTS
$r_0 = 2 \, m, \theta_0 = 80°, f_0 = 25 \, kHz$

82
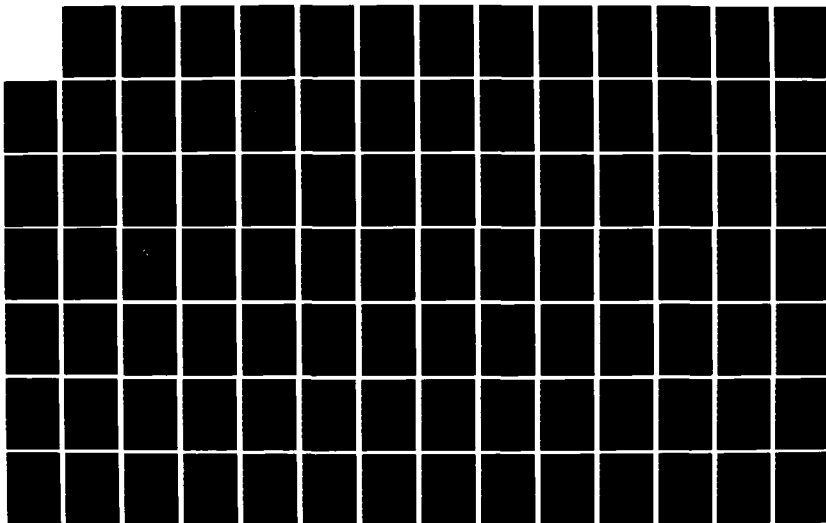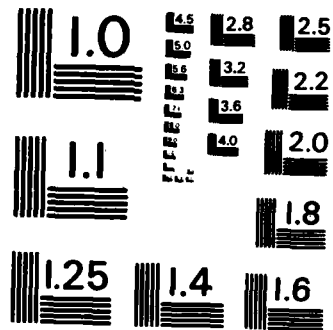
MICROCOPY RESOLUTION TEST CHART

NATIONAL BUREAU OF STANDARDS – 1963 – A

three different source velocities, but under similar conditions: $r_0 = 2 \, m$, $f_0 = 25kHz$ and $\theta_0 = 80^0$. When the source is stationary, the measured acoustic radiation is fairly omnidirectional, as predicted by the theory given by the solid line in Fig. 28(a). The results are normalized by the pressure signal received at $\phi_0 = 90^0$. The theoretical curves were obtained by running the numerical program described previously, over several values of the angle ϕ_0. Fig. 28(b), whose scale differs from that of Fig. 28(a), shows the horizontal directivity pattern of an MTS moving at $M = 0.4$ towards the receiver, and Fig. 28(c) applies to the case of an MTS moving at $M = 0.5$ away from the receiver. In both cases there is reasonable agreement between theory and experiment and the results show that indeed acoustic radiation is stronger in the direction of motion of the source. The theoretical model seems, however, to overestimate the acoustic level in the direction opposite to the motion of the source and this discrepancy is not fully understood.

The horizontal directivity pattern of a transonic TS was investigated experimentally and the result is given in Fig. 29. It shows that more than 30 dB in acoustic amplitude can be gained in the Mach cone where a very strong broadband signal is emitted by the moving source, as indicated by the upper time waveform in Fig. 29. Both time waveforms in Fig. 29 are normalized to unity. When the Doppler shifted wavelength $\lambda_d = \lambda_0 |1 - M\sin\theta_0\cos\phi_0|$ is of the order of the laser beam diameter, diffraction effects are obviously important and a strong diffraction loss is expected to reduce the sound level. This happens when
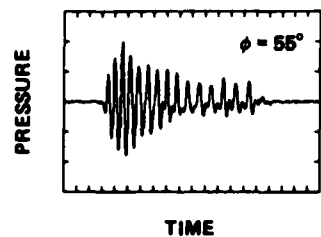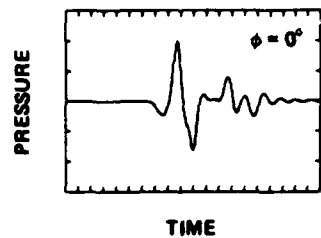
M = 1
f_0 = 25 kHz
r_0 = 2.0 m
θ_0 = 80°
α = 13.7 Np/m
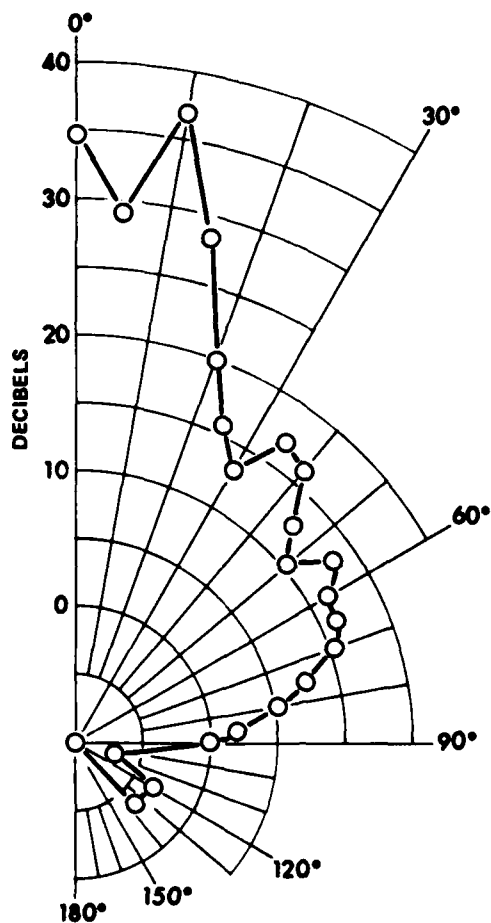
FIGURE 29
HORIZONTAL DIRECTIVITY OF A TRANSONIC MTS

84

$$\cos \phi_{lim} = (1 - 2a/\lambda_0) / M \sin \theta_0 \qquad , \qquad (4.7)$$

that is to say, when $\phi_{lim} = 32^0$, and this may be an explanation for the sudden drop in level around $\phi_0 = 30^0$. The second waveform shown in Fig. 29 indicates that for angles $\phi_0 > \phi_{lim}$ (i.e., well outside the Mach cone), the received pressure waveform is not a strong transient but rather a waveform modulated at its Doppler shifted frequency. Hence there are two angular regions associated with transonic source motion. In one region the waveform is a Mach wave and in the other region the laser modulation waveform is dominant.

Directivity patterns were also obtained for the case of a long and narrow thermoacoustic source created by illuminating the water with the ruby laser ($\alpha=1.5$ Np/m). Experimental data are given in Appendix I.

3. Sound level versus Mach number

In another set of measurements we investigated the dependence of the sound pressure level on the source velocity. The results are shown in Fig. 30, where the dashed line represents the theoretical predictions obtained by numerical analysis of the pressure waveforms computed for several values of the Mach number as seen by the receiver, $M = M \sin \theta_0 \cos \phi_0$. The general shape of the predicted curve follows the trend of the experimental data with, however, an unexplained discrepancy in the amplitude of the sharp peak which occurs around $M=1$. It is possible that in the transonic regime, some nonlinear effects, which have not been included

85
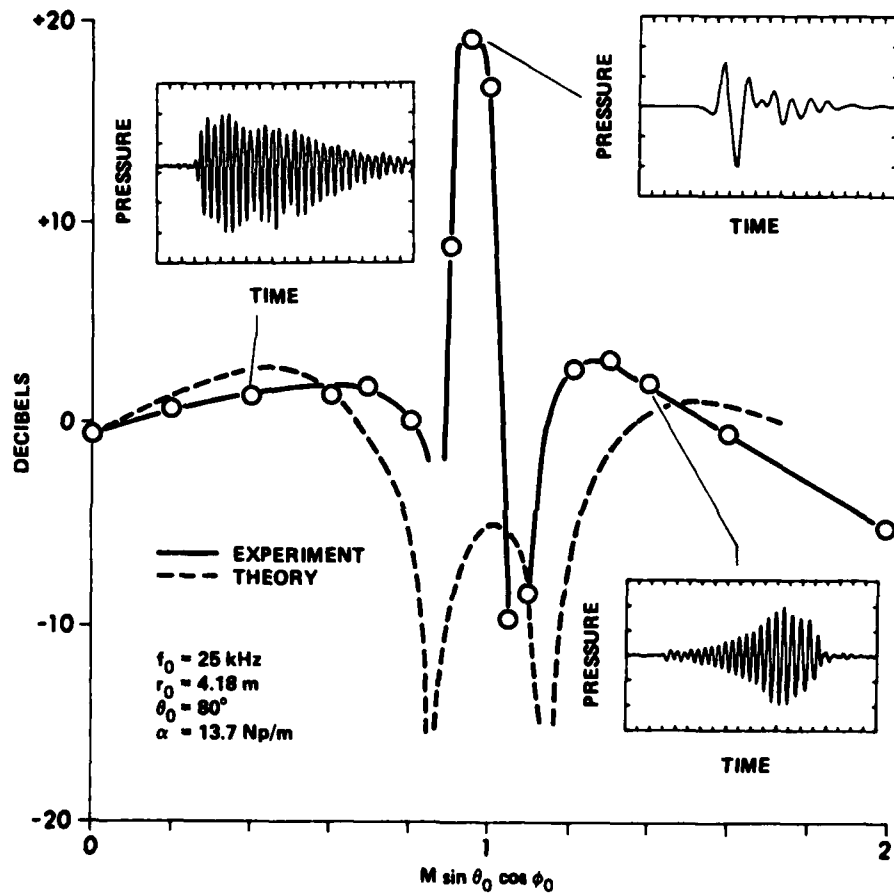
FIGURE 30
RELATIVE SOUND PRESSURE LEVEL versus MACH NUMBER

in the present model, become of significant importance. The results shown in Fig. 30 are normalized so that both theory and experiment have a value of 0 dB at M=0 .In fact the absolute level measured experimentally at M=0 was of 116.7 dB, whereas the theory predicts a level of 109.4 dB. This significant difference is so far unexplained.

The physical interpretation of the two symmetric dips around M = 1 is that diffraction effects due to the finite width of the laser beam become important and tend to lower significantly the acoustic radiation. In the case of monochromatic radiation we have seen that the frequency filtering associated with finite beamwidth effects is given by Eq. (4.6) which shows that a diffraction loss of 3 dB is expected to occur when

$$(k_d \, a \, sin\theta_0 /2)^2 = Ln (10^{3/20}) \qquad , \qquad (4.8)$$

that is to say , when $M = 1 \pm 5.35 \, \Omega$, where $\Omega = f_0 / (c/a \, sin\theta_0)$ is a nondimensional frequency. In our experiments Ω is 0.0828 so that the 3 dB points are expected to occur around M = 0.6 and M = 1.4 . As indicated by Fig. 30, this is confirmed experimentally. When M approaches unity, the acoustic signal becomes so short that the monochromatic assumption is not valid any more and thus Eq. (4.6) cannot be used to predict the diffraction loss. In fact at M = 1, all of the acoustic disturbances emitted during the motion of the source seem to add coherently , so that a strong transient is observed at the receiver. A gain of more than 25 dB has been observed over the amplitude of a stationary laser source of similar characteristics.

The three normalized waveforms shown in the windows of Fig. 30

indicate the typical behavior of the pressure waveform for the three regions of the curve. In the first region the thermoacoustic signal is modulated at its Doppler frequency. When M is further increased, diffraction effects reduce the acoustic level until the monochromatic assumption does not hold and a very strong transient is generated as indicated in the second region. In the third region, when diffraction effects become negligible, one can observe time-inverted thermoacoustic signals.

4. Spreading curves

The spreading curves shown in Fig. 31 show the sound level dependence on the distance r_0 between the thermoacoustic source and the receiver. These curves are plotted for three different source velocities: M=0 , M=1 , and M=1.5. The other parameters of interest are f_0=35 kHz , θ_0=84^0 , and ϕ_0=0^0 . The predicted spreading curves, indicated by a solid line in Fig. 31 , were obtained as follows.

In the case of a TS, the predicted spreading curve was obtained from Eq. (3.32). For the case of an MTS, Eq. (3.32) does not apply because the received frequency is actually time dependent. In Fig. 31, the theoretical predictions for transonic and supersonic regimes are based on the assumption that the Doppler shifted wavelength characteristic of the acoustic radiation is small compared to the distance of observation, so that spherical spreading (6 dB per doubling distance) dominates over cylindrical spreading (3 dB per doubling distance). Experimental data support this assumption very well, as indicated by Fig. 31.

88
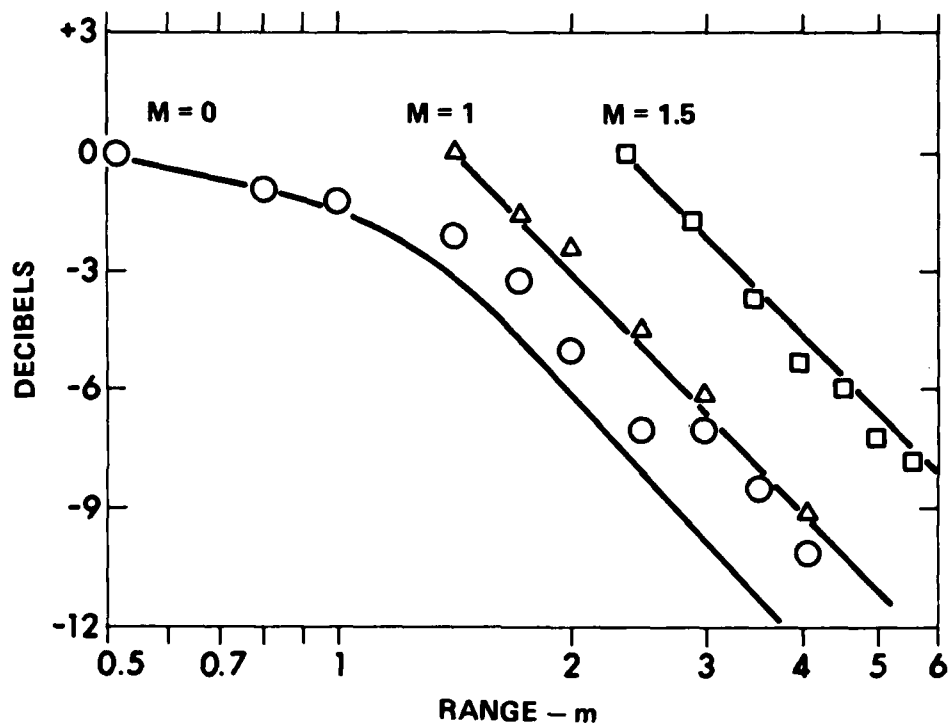
FIGURE 31
SPREADING CURVES FOR AN MTS
$f_0 = 35\,\text{kHz}, \theta_0 = 84^\circ, \phi_0 = 0^\circ$

C. Conclusions

The acoustic characteristics of a moving thermoacoustic source created by moving a modulated laser across a fluid-air boundary have been examined by imagining the source to consist of many line sources each of which are excited at successive times corresponding to the motion of the laser source along its path. In this manner it is possible to construct the acoustic pressure received by a hydrophone by adding the sound contribution of each line source with the appropriate delay. The result is a pseudo-convolution between the impulse response of the system and the acoustic source strength. This analysis lends itself well to numerical simulation. It is valid in the nearfield of the thermoacoustic source and, in principle, for any source velocities. In the case of a stationary source, the impulse response of the system is fixed in time, so the pressure calculation reduces to a true convolution. Further, it is possible to include the effect of the finite beamwidth of the laser beam by convolving the pressure calculated assuming an infinitesimal beam with the impulse response of the system to laser heat applied across the beam at a fixed depth in the fluid. Although this impulse response is a function of the location and velocity of the source, the corrections produced by the nonstationarity of the source are small and may be ignored.

Experimental results have been presented which indicate excellent agreement between the measured and predicted waveforms including the subsonic, transonic, and supersonic cases. It has been shown that the waveforms in these three velocity regions differ markedly from one another.

90

In the subsonic region the waveform consists of a modulated signal with an envelope that first grows rapidly and then decays slowly. As the source velocity increases, the amplitude and frequency of the waveform increase and the total time of duration decreases. In the supersonic region, the pressure waveform is very similar to that for the subsonic region, but the signal is time inverted. This time inversion phenomenon is caused by moving the source toward the receiver at a speed faster than the speed of sound. In the transonic region the waveform shows almost no frequency modulation, but is a very fast negative pulse with smaller leading and lagging positive exponential tails. Previous analyses[18,26] in which the pressure field radiated by an MTS is replaced by the pressure field of an equivalent stationary array, corrected by a Doppler shift, have failed at transonic source velocities because of neglecting the fact that the Mach number of the source as seen by the receiver depends on angle and hence location of the source.

Experimental measurements and theoretical predictions for the directivity patterns produced by a moving laser source were shown to be in good agreement. These results were presented for both the horizontal and vertical planes. The results also show that near transonic source velocity the modulation frequency of the laser is not a significant determinant of the directivity pattern. Below and above transonic source velocity, the modulation frequency has a direct effect on the directivity pattern; a narrower beam is produced as the modulation frequency increases.

Experimental results and theoretical predictions were also presented for the sound pressure level as a function of the source velocity as seen by a

hydrophone at a fixed position. These results show the largest discrepancy of all of the theory and experiment comparisons. Although the curves have a similar shape there is a notable and large disagreement near Mach one. Experimentally, large acoustic signals were observed near transonic source velocity, with amplification of almost 20 dB above the levels in the subsonic and supersonic region, and more than 30 dB in the horizontal directivity pattern in the direction of motion of the source. Theoretically, the predicted amplification at transonic velocity is much smaller than the one measured experimentally. This suggests that there may be nonlinear mechanisms which become important near Mach one and which have not been included in the physical model. More work is necessary to explain the exact nature of this discrepancy.

Finally, experimental results for the spreading of the moving and stationary laser source were compared to theoretical predictions. It was shown that in the nearfield, the laser source exhibits cylindrical spreading, then switches over to spherical spreading in the farfield. These results agree well with physical intuition.

CHAPTER V

THE DOPPLER SHIFT OF AN ACOUSTIC SOURCE MOVING
AT TRANSONIC VELOCITY[24]

In order to improve the intrinsically low efficiency of the conversion by thermal expansion, of light into sound, Soviet ph sicists have studied[28-32] vei'y closely the sound field radiated by a thermoacoustic source moving at transonic velocity. They have shown experimentally that indeed a substantial gain in sound level occurs when the source is moving transonically. This has also been confirmed experimentally in the previous chapter. It is a striking fact, however, that most theories which rely on the Doppler shift to account for the motion of the source break down at transonic source velocity. The reason for this is that, according to classical theory, the Doppler shift associated with an acoustic source moving at constant velocity induces a straining of the time coordinate, as perceived at the receiver. This time straining is described by

$$t' = t (1 - M \cos \Theta) \qquad , \qquad (5 \cdot 1)$$

where t' denotes the time coordinate in the fixed frame of reference (receiver), t is the time coordinate in the moving frame of reference (source), M is the Mach number of the source, and Θ is the angle between the direction of motion of the source and the direction of observation. At

93

transonic velocities, t' can assume a value of zero, in which case all the acoustic energy emitted by the source is received in an infinitesimal increment of time. This implies an infinite instantaneous power which is not physically realizable. The object of this chapter is to use the method of characteristics to find the exact Doppler shift of a transonic source. Two cases are considered: a point source and a line source of finite length, both moving rectilinearly towards or away from a point receiver.

A. Point source

1. Characteristics

Consider a point source moving at constant velocity in a straight line, as shown in Fig. 32. Let us assume that the source is emitting a rectangular pulse of duration τ_p. This simplification is justified by the fact that we are primarily concerned with time scales and not wave shapes. The present analysis is not, however, restricted to transient sources. It is understood that τ_p is just a characteristic time of the acoustic emission. The Doppler factor D may then be described as the ratio of the pulse duration $\tau_{\mathbf{p}}$ recorded at the receiver to the pulse duration τ_p emitted by the source.

$$D = \tau_{\mathbf{p}} / \tau_p \qquad (5.2)$$

Note that $\tau_{\mathbf{p}}$, and therefore D, are allowed to take on negative values which

94
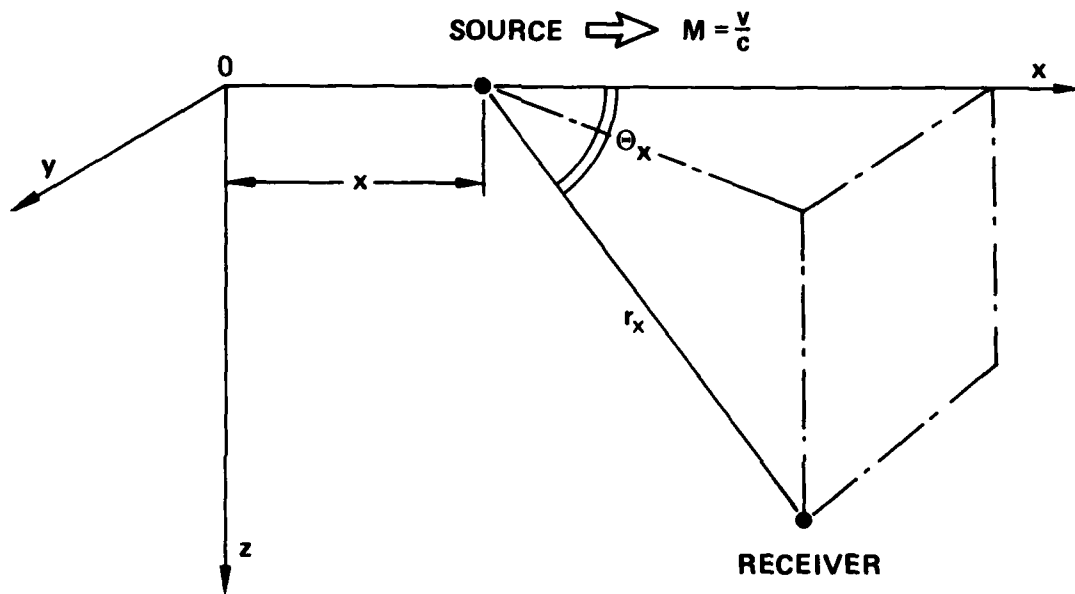
FIGURE 32
MOVING POINT SOURCE GEOMETRY

is what will happen at supersonic source velocities. It is an effect of the time reversal phenemenon which occurs when a source is moving faster than the disturbances it generates.

Another quantity relevant to the motion of an acoustic source is the Doppler gain G, defined by

$$G = |1 / D| \qquad . \qquad (5.3)$$

The gain can be explained in terms of conservation of energy. The motion of the source induces a change in the time scales, but the net energy flux at the receiver is unchanged. The average power in the received signal must change accordingly then. Reducing the received pulse duration therefore increases the average received power by the factor G. It is important to note that, if the source is directional, the motion of the source induces a redistribution of energy as a function of angle of observation, and thus the gain G is not just the gain in amplitude of the acoustic pressure. This dependence of the source directivity properties as seen by the receiver, on source motion, makes the problem much more complicated and it is beyond the scope of the analysis presented in this chapter. Time inversion has no effect on the gain G, since only its amplitude has a significant meaning. This is why an absolute value was introduced in Eq. (5.3).

The problem is therefore to find the pulse duration τ_p recorded at the receiver. A convenient approach for solving this problem is to use the method of characteristics which consists of finding the time of arrival of each wavelet coming from the source during its motion along the x-axis.

96

The results are plotted in the x-t plane.

Let us define $t_R(x)$ as the time of arrival at the receiver of a wavelet emitted when the source was at a distance x from the origin. The zero of time is chosen for convenience to coincide with the zero of space, i.e., t=0 when the source is at x=0. Then $t_R(x)$ can be expressed as follows:

$$t_R(x) = (x/v) + (r_x/c) \qquad , \qquad (5.4)$$

where c is the sound speed in the medium and r_x is the distance between the source and the receiver when the source is at a distance x from the origin. It can easily be shown that

$$t_R(x;M) = (x/Mc) + c^{-1} [r_0^2 - 2r_0 x \cos\Theta_0 + x^2]^{1/2} \quad , \qquad (5.5)$$

where the subscript o refers to an initial value (x=0; t=0), and M=v/c is the Mach number of the source. Note that $\cos\Theta_0$ corresponds to $\sin\theta_0 \cos\phi_0$ in the notation of Chapter IV. The slope of the characteristics $t_R(x;M)$ in the x-t plane may be found by differentiating Eq. (5.5) with respect to x. It is found that

$$d/dx [t_R(x)] = (1 - M \cos\Theta_x)/v \qquad , \qquad (5.6)$$

where Θ_x indicates that the angle of observation Θ depends on the source location x. If M is a constant along the source path, $M \cos\Theta_x$ is a nonlinear function of the spatial coordinate x. This means that, in general, the

97

characteristics are curved.

Subsonic, transonic, and supersonic regimes may be defined from the slopes of the characteristics. Equation (5.6) shows that a negative slope can occur only if $M > 1/\cos\Theta_x$, i.e., only at supersonic velocities. If the source is moving at supersonic velocity, but has already passed over the receiver and is moving away from it, $\cos\Theta_x$ is negative and therefore the slope is positive. The transonic regime occurs only for $M = 1/\cos\Theta_x$, i.e., when the slope is zero. In the Soviet literature, $\cos\Theta = 1/M$ is sometimes referred to as the Cerenkov direction. The subsonic regime occurs for positive slopes of the characteristics. The characteristics $t_R(x;M)$ are plotted in Fig. 33 for various values of the Mach number M.

In the limit of $x \gg r_0$, Θ_x approaches π , and from Eq. (5.6), the slope of the characteristics goes to a maximum value of $(1/v + 1/c)$. The interpretation of this result is that both subsonically and supersonically moving point sources do not induce time-inversion on the receiver waveform, once they are moving away from the receiver. Regardless of the source speed, supersonic or subsonic, wavelets emitted at a given time will arrive at the receiver before those emitted a short time later. For supersonically moving sources, the time gap between the two wavelets is accentuated because the later wavelet has so much farther to travel.

It therefore seems appropriate to make a distinction between a supersonic source and a source that is seen as supersonic by the receiver. In the first case, the Mach number of the source is such that $M \cos\Theta_0 > 1$, whereas in the second case, time inversion occurs and the slope of the
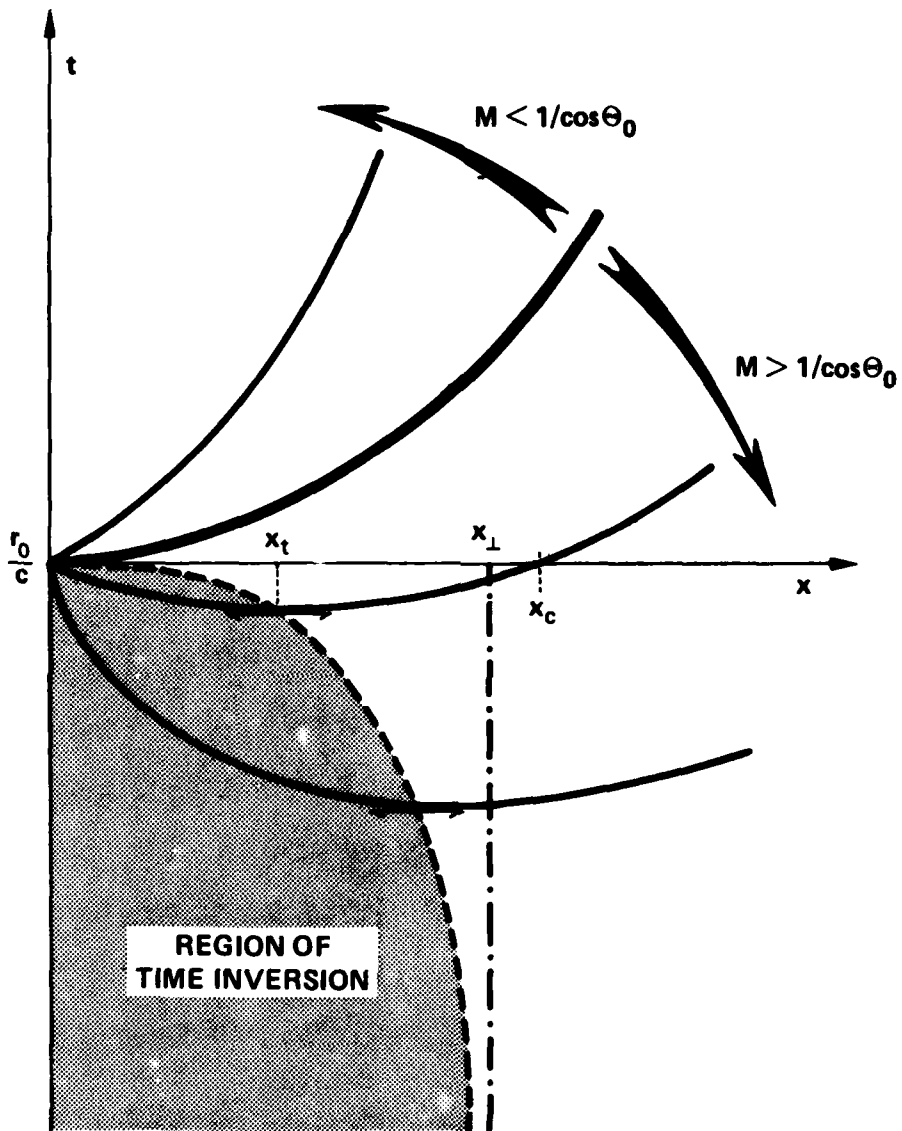
FIGURE 33
CHARACTERISTICS FOR A MOVING POINT SOURCE

characteristic is negative. This distinction is emphasized in Fig. 33 by indicating the region of time inversion.

Also of interest is the locus of the points of zero slope in the characteristics, i.e., the transonic region. From Eq. (5.5), we can set d/dx $[t_R(x)] = 0$, and obtain the following equation for the points of zero slope:

$$x_t = r_0 \cos\theta_0 \left[1 - \sqrt{(\cos^{-2}\theta_0 - 1)/(M^2 - 1)} \right] \qquad . \qquad (5.7)$$

The transonic region is indicated by the dashed line on Fig. 33.

Another interesting parameter is the distance x_c at which the characteristics cross the line $t_R = r_0/c$. Wavelets emitted from this location will arrive at the receiver simultaneously with those emitted at $x = 0$, $t = 0$. Clearly, x_c exists only for a source moving at supersonic speed, and x_c is always greater than x_t. It is possible to solve for x_c by setting $t_R(x_c) = r_0/c$ in Eq. (5.5). It is found that, provided $M > 1/\cos\theta_0$,

$$x_c = 2 r_0 M \left[(M \cos\theta_0 - 1)/(M^2 - 1) \right] \qquad . \qquad (5.8)$$

2. Pulse duration

The x-t plane is a convenient way to find the received pulse duration and therefore the corresponding Doppler shift. First let us define x_N as the distance traveled by the source during the pulse duration, $x_N = v \, \tau_p$. Since

100

$t_R(x)$ is the time of arrival of a wavelet coming from x, the set of all $t_R(x)$ for $0 \leq x \leq x_N$, written as $t_R(0 \leq x \leq x_N)$, subsequently represents the time gap between the arrivals of all wavelets emitted during the motion of the source. The recorded pulse duration τ_p is the difference between the maximum and the minimum values of the set. In other words, τ_p is the projection on the time axis of the characteristic for a given Mach number, over all x, such that $0 \leq x \leq x_N$.

$$\tau_p = \text{Proj}_t [t_R(0 \leq x \leq x_N)] \qquad . \qquad (5.9)$$

From Eqs. (5.2) and (5.3), it is clear that in order for the Doppler gain to be infinite, it is necessary for τ_p to be zero. This requires all of the wavelets emitted by the source to be received simultaneously, i.e., that the characteristic be a straight line at $t_R = r_0/c$. From Eq. (5.6), we see that the characteristic cannot be a horizontal line unless $M \cos\theta_x$ is equal to unity. For a source moving at uniform Mach number, this requires θ_x to be a constant, and the only geometry which permits θ_x to be constant places the receiver directly on the path of the source. If the source is not constrained to move at a constant Mach number, other geometries which permit τ_p to be zero are possible, but this would violate the assumption of a source moving at constant velocity, and the preceding analysis would be invalid. Hence, unless the receiver is directly on the path line of the source, τ_p and the Doppler gain are always finite. If the receiver is on the source path line, it is necessary to include diffraction effects induced by the finite dimension of any real physical source, in order to prove that, in reality, the received

101

pulse duration cannot be less than the transit time across the source and, hence, that the Doppler gain is still bounded.

If we restrict the analysis to the case of a source moving at constant velocity, it is straightforward to find an analytical expression for the received pulse duration and the corresponding Doppler factor.

First, consider subsonic motion of the point source. As mentioned earlier, when $M < 1/\cos\Theta_0$, the slope of the characteristic is always positive. This means that the order of arrival of the wavelets at the receiver remains unchanged as compared to their order of emission. In this case, the "projection operator" defined by Eq. (5.9) is simply

$$\tau_p = t_R(x_N) - t_R(0) \qquad , \qquad (5.10)$$

where

$$x_N = M c \tau_p \qquad . \qquad (5.11)$$

Combining with Eq. (5.5) yields

$$\tau_p = (x_N/v) + c^{-1} \sqrt{r_0^2 - 2 r_0 x_N \cos\Theta_0 + x_N^2} - (r_0/c) \quad . \qquad (5.12)$$

Substituting Eq. (5.12) into Eq. (5.2) yields an expression for the Doppler factor:

$$D = 1 + (M/x_N)\sqrt{r_0^2 - 2 r_0 x_N \cos\Theta_0 + x_N^2} - (r_0/c\tau_p) \quad . \qquad (5.13)$$

Defining a nondimensional distance $R_0 = r_0/c\tau_p$ (this quantity can also be

102

regarded as an inverse nondimensional pulse duration, or a nondimensional frequency), we finally rewrite the Doppler factor in the form

$$D = 1 - R_0 \left[1 - \sqrt{1 - 2(M/R_0)\cos\theta_0 + (M/R_0)^2} \right] . \qquad (5.14)$$

Equation (5.14) gives a practical estimate of the Doppler factor of a moving source, when one wants to take into account the change in angle of observation as the source is moving. As an example, the received pulse duration was measured in the study of moving thermoacoustic sources, and it was compared with the predicted value of $D \, \tau_p$ (see Eq. (5.2)). The Doppler shift D was computed first assuming that the angle of observation θ was constant during the motion of the source, and second, in the more accurate way described by Eq. (5.14). Figure 34 shows that Eq. (5.14) fits the data better than the simple estimate $D = 1 - M \cos\theta_0$. The experimental data were obtained from the study of the horizontal directivity described in Section IV.B. The Mach number of the source was 0.4, the radius of observation was 2 m, the depth of the receiver was 0.35 m ($\theta_0 = 80^0$), and the modulation frequency was 25 kHz. This simple experiment shows that Eq. (5.14) is useful in some practical cases.

Next, consider supersonic motion of the source. In this case, the problem is more complicated since the slope of the characteristics is negative until $x = x_t$; then it becomes positive (see Fig. 33). Therefore the projection operation defined by Eq. (5.9) can be expressed analytically as follows.
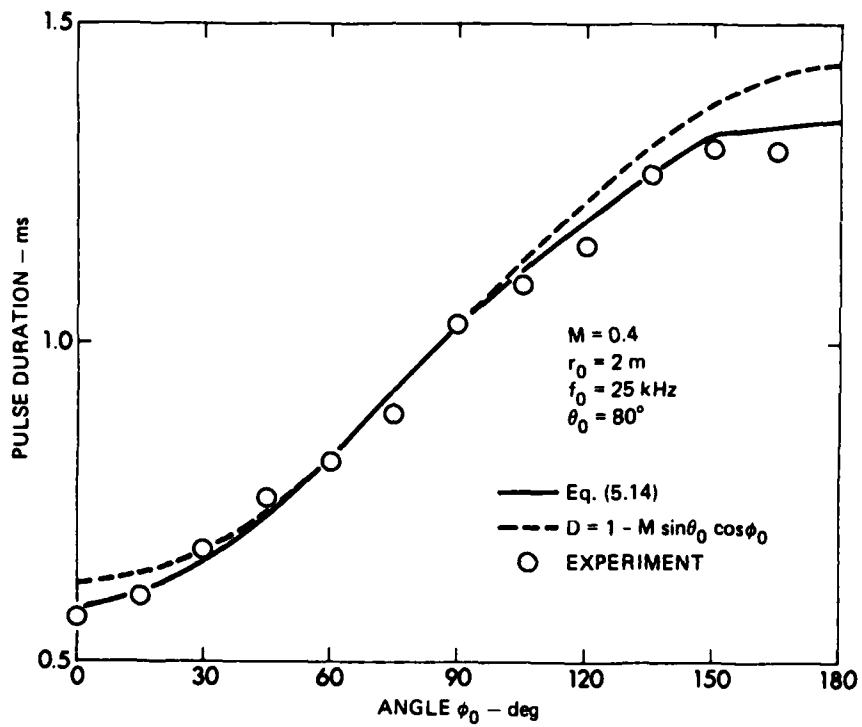
FIGURE 34
DOPPLER SHIFTED PULSE DURATION

If $x_N \leq x_t$, $\tau_p = t_R(x_N) - t_R(0)$ (5.15a)

If $x_t \leq x \leq x_c$, $\tau_p = t_R(x_t) - t_R(0)$ (5.15b)

If $x_N > x_c$, $\tau_p = t_R(x_N) - t_R(x_t)$,   (5.15c)

where x_N, x_t, and x_c are defined by Eqs. (5.11), (5.7), and (5.8). The Doppler shift can be expressed explicitly by making use of Eqs. (5.5) and (5.7). The results are summarized below in nondimensional form.

For $x_N \leq x_t$,

$$D_0 = 1 - R_0 \left[1 - \sqrt{1 - 2(M/R_0) \cos\theta_0 + (M/R_0)^2} \right]$$ (5.16a)

For $x_t < x_N \leq x_c$

$$D_1 = R_0 \left[(\cos\theta_0/M) - (\sin\theta_0/M\sqrt{M^2-1}) - 1 + \sin\theta_0 \sqrt{M^2/M^2-1} \right]$$

(5.16b)

For $x_N > x_c$

$$D_2 = D_0 - D_1$$ (5.16c)

Notice that Eq. (5.14) and Eq.(5.16a) are identical. By examining the farfield limit of the solutions given in Eqs. (5.14) and (5.16), it is possible to compare the results above to the classical solution. It is necessary to take the farfield limit because there is an implicit assumption in the classical

105

solution that the angle of observation Θ is independent of source location. This assumption is only valid if $r_0 \gg c\, \tau_p$, i.e., in the farfield. In the farfield limit, Eq. (5.16a) applies and hence Eq. (5.14) describes the Doppler shift for any Mach number and any source location.

Expanding the square root in Eq. (5.14) in terms of the small parameter (M/R_0) and retaining only first order terms, yields

$$D = 1 - M \cos \Theta_0 \quad , \quad (5.17)$$

which is the standard form for the Doppler factor. Note that, for $M = 1/\cos\Theta_0$, the gain becomes infinite. With the exception of the previously discussed case of a source moving at Mach 1 on a straight line towards the receiver, the infinite gain disappears when higher order terms are retained in Eq. (5.14). Hence, in the farfield, the analysis presented here recovers the standard form but, with only one exception, the analysis guarantees finite Doppler gain.

It is also interesting to note that, at least for subsonic velocities,[33] the received pulse duration can be expressed in the following manner:

$$\tau_p = \int_0^{x_N} (dt_R/dx)\, dx \quad . \quad (5.18)$$

Substituting Eq. (5.6) yields

$$D = 1 - (x_N)^{-1} \int_0^{x_N} M \cos \Theta_x\, dx \quad , \quad (5.19)$$

106

which clearly shows that the global Doppler shift (over the whole path of the source) is an average of the Doppler shifts for each position of the source along its path. The integral in Eq. (5.19) can be evaluated by expressing $\cos\Theta_X$ in terms of x. It can easily be shown from the geometry that

$$\cos\Theta_X = \frac{r_0 \cos\Theta_0 - x}{\sqrt{r_0^2 - 2 x r_0 \cos\Theta_0 + x^2}} \qquad (5.20)$$

Note that when the source has passed over the receiver, $\cos\Theta_0 < 0$ so that Eq. (5.20) still applies. Combining Eqs. (5.19) and (5.20) leads as expected to Eq. (5.14), which in turn reduces to the standard form of the Doppler factor, Eq. (5.17), provided that $r_0 \gg c\tau_p$.

Equations (5.2), (5.14), and (5.15) have been used together with Eqs. (5.5), (5.7), (5.8), and (5.11) to compute the Doppler factor and therefore the gain of a moving point source. Figure 35 shows a three-dimensional plot of the gain G versus Mach number and nondimensional pulse duration $T_0 = c\tau_p/r_0 = (R_0)^{-1}$. The initial angle Θ_0 was set to 45^0. It can be seen from Fig. 35 that for any Mach number, the acoustic response observed at the receiver is always finite. Also of interest is the fact that the maximum gain in Fig. 35 occurs at a Mach number which depends on the

107
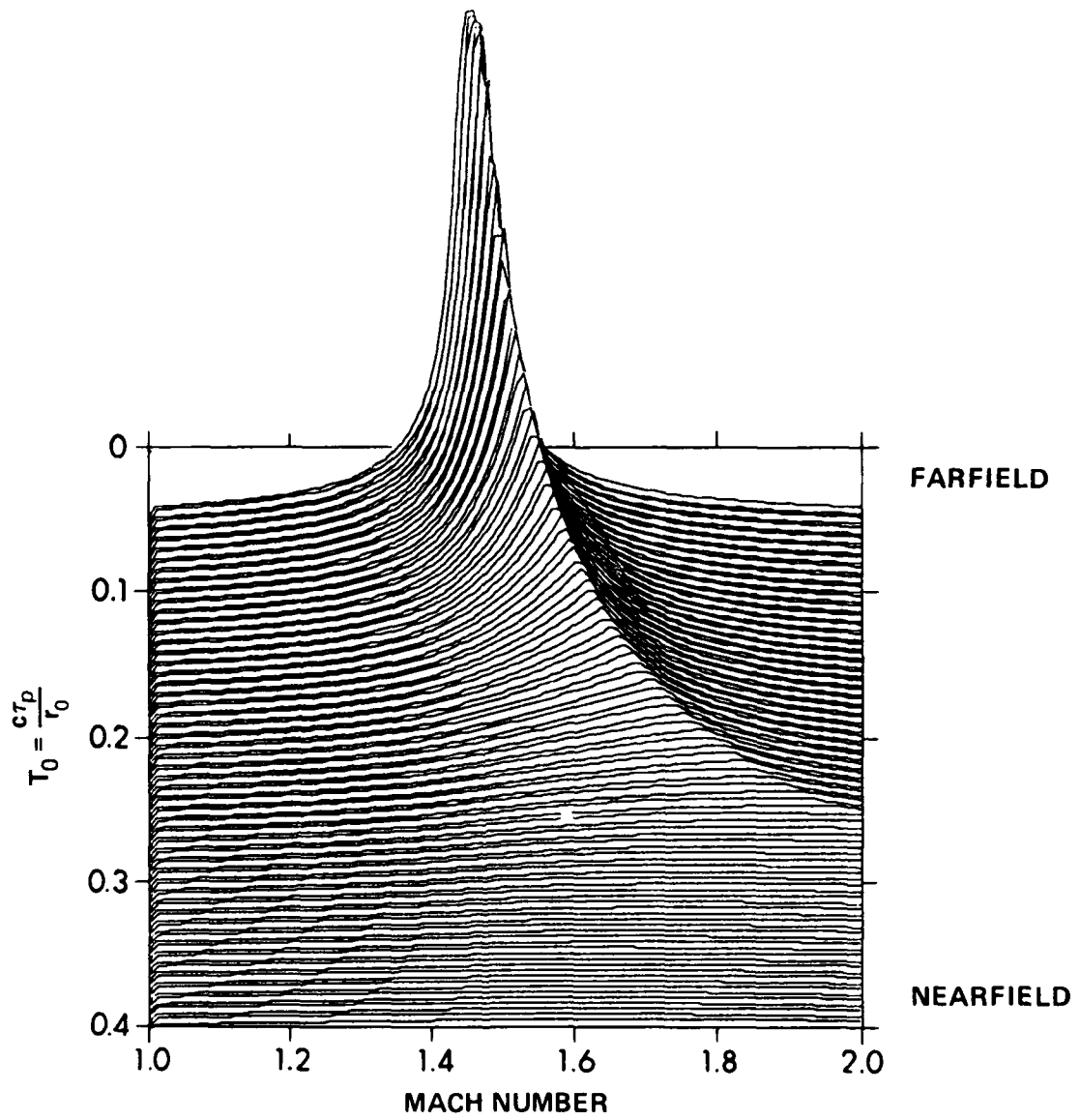
FIGURE 35
GAIN OF A MOVING POINT SOURCE

108

nondimensional parameter R_0, whereas one would have expected from the classical theory an infinite response occuring always at $M = 1/\cos\Theta_0$. The object of the next paragraph is to find, for a given value of R_0, the Mach number which will minimize the Doppler factor, or maximize the Doppler gain.

3. Maximum gain and optimum Mach number

It has been shown previously that the gain of a point source moving at any constant velocity is always bounded, except for $\Theta=0$. This result leads to questions about whether it is possible to predict the value of the maximum gain and the value of Mach number at which the peak occurs. These answers are easily found numerically, but in this paragraph, we instead develop an analytical scheme for prediction purposes.

First, consider the case of a source moving at a subsonic velocity. The maximum gain G* may be found by differentiating Eq. (5.14) with respect to M, to find a value of the Mach number M*, which minimizes the Doppler factor to a value D*. From Eq. (5.14) it is shown that

$$M^* = R_0 \cos \Theta_0 \qquad (5.21)$$

Substituting M* into Eq. (5.14) yields

$$D^* = 1 - R_0 \left(1 - \sin \Theta_0 \right) \qquad , \qquad (5.22)$$

109

and

$$G^* = \left| \ [\,1 - R_0\,(\,1 - \sin \alpha_0\,)\,]^{-1} \ \right| \quad . \qquad (5.23)$$

Note that the assumption $M < 1/\cos\Theta_0$ can be combined with Eq. (5.23) to show that this estimation scheme is valid only if

$$R_0 < 1/\cos^2\Theta_0 \qquad . \qquad (5.24)$$

Next, consider the case of a source moving at $M > 1/\cos\Theta_0$. In this case, the differentiation procedure discussed above is not analytically simple and it seems more appropriate to apply some physical insight. From Eqs. (5.2) and (5.3) the maximum gain occurs when the received pulse duration is minimum. The received pulse duration is minimized if $x_N < x_t$, but then this implies that the source at no time appears to the receiver to be moving transonically. Since we expect the gain to be maximized close to the transonic region, we therefore require $x_N > x_t$. Given this constraint, τ_p is minimized at a constant value , provided x_N is between x_t and x_c. Although τ_p does not vary if x_N is in the range $x_t \leq x_N \leq x_c$, the pulse duration in the frame of the source, τ_p , increases as x_N increases. Because we wish to minimize the Doppler factor, Eq. (5.2) suggests that we want to maximize τ_p within the range that produces the minimum acceptable τ_p. We therefore choose $x_N = x_c$. By recalling that $x_N = Mc\,\tau_p$, and using Eq. (5.8), we get

$$M^* = R_0 \cos\Theta_0 \pm \sqrt{(R_0\cos\Theta_0)^2 - 2R_0 + 1} \qquad . \qquad (5.25)$$

The negative root in Eq. (5.25) has to be discarded because Eq. (5.8) indicates that, for any Mach number, $x_c > 2 r_0 \cos\Theta_0$, so M^* must be larger than $R_0 \cos\Theta_0$. By substituting Eq. (5.25) into Eq. (5.15b), it is found that D^* is given by

$$D^* = R_0 [(\cos\Theta_0/M^*) - (\sin\Theta_0/M^*\sqrt{M^{*2}-1}) - 1 + (M^*\sin\Theta_0/\sqrt{M^{*2}-1})] .$$
$$(5.26)$$

The maximum gain G^* is given by $1 / |D^*|$. Equation (5.25) can be applied only if the argument of the square root is greater or equal to zero. It can be shown that this implies

$$R_0 \geq (1 + \sin\Theta_0)/\cos^2\Theta_0 \qquad . \qquad (5.27)$$

If inequality (5.27) is not satisfied, one has to use a different prediction scheme.

Table III shows a comparison between the estimated values of G^* and M^* supplied by Eq. (5.25) and the inverse of D^* in Eq. (5.26), and numerically determined values. For values of R_0 such that

$$1/\cos^2\Theta_0 \leq R_0 \leq (1+\sin\Theta_0)/\cos^2\Theta_0 \qquad , \qquad (5.28)$$

111

TABLE III

OPTIMUM MACH NUMBER AND GAIN AS A FUNCTION
OF NONDIMENSIONAL PULSE DURATION

$\Theta_0 = 15^0$		Mach number		Gain (dB) (*)	
T_0	R_0	estimated	computed	estimated	computed
.3	3.33	1.05	1.06	23.2	22.9
.5	2.0	1.08	1.08	18.6	18.5
.7	1.43	1.16	1.15	12.7	12.8
.9	1.11	1.07	1.04	7.5	7.5
1.0	1.0	0.97	0.97	5.9	5.9
1.5	0.67	0.64	0.65	3.0	3.0
2.0	0.5	0.48	0.49	2.0	2.0
3.0	0.33	0.32	0.33	1.2	1.2

(*) : Gain (dB) = $10 \log_{10} (G)$

$R_0 = c \, \tau_p \, / \, r_0$

$T_0 = (R_0)^{-1}$

we have used the prediction scheme based on Eqs. (5.21) to (5.23). Although Eq. (5.24) is violated for the range of values of R_0 (1.07 ≤ R_0 ≤ 1.35), this method still yields a reasonable estimate for the optimum gain and Mach number of a moving source. This is due to the fact that M^* is a slowly varying function of R_0. As indicated in Table III, good agreement exists for a wide range of nondimensional pulse durations. Hence it is possible to estimate the maximum gain of a moving point source , based on a pulse duration analysis.

B. Line source

The analysis of the Doppler shift of a point source may be extended to the more realistic case of an acoustic array of finite length L moving at constant velocity v = Mc in the +x direction. The approach is similar to the one used above. The method of characteristics is used to study the pulse duration recorded at the fixed point receiver and consequently, the Doppler shift and the Doppler gain induced by the motion of the source.

1. Characteristics

Consider a line source of length L which moves at constant velocity perpendicular to its axis past a fixed point receiver as shown in Fig. 36. For the sake of simplicity, it is assumed as in Section V.A that the source is emitting a rectangular pulse of duration τ_p. It is convenient to define the leading edge (first wavelet) and the trailing edge (last wavelet) of the

113
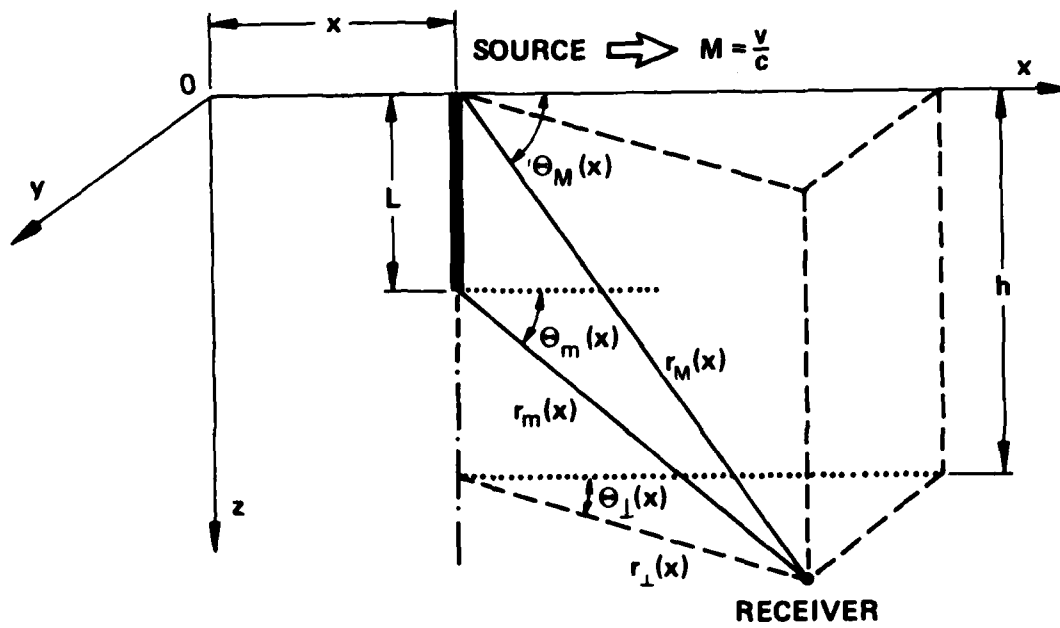
**FIGURE 36
MOVING LINE SOURCE GEOMETRY**

pulse being received at the observation point. Let $t_m(x)$ be the time of arrival of the first wavelet emitted by the source when it was at a distance x from the origin; and similarly let $t_M(x)$ be the time of arrival of the last wavelet emitted when the source was at location x. Again we choose the origin of time to coincide with the origin of the source emission at $x = 0$. The first wavelet emanates from the source location which is closest to the receiver. Let us denote by $r_m(x)$ the corresponding minimum distance. Similarly the last wavelet comes from the point on the line source farthest from the receiver. The corresponding distance will be denoted $r_M(x)$. Both $r_m(x)$ and $r_M(x)$ are shown in Fig. 36. Using the definitions of $r_m(x)$ and $r_M(x)$, we have

$$t_m(x) = (x/v) + [\, r_m(x)/c\,] \qquad , \qquad (5.29)$$

and

$$t_M(x) = (x/v) + [\, r_M(x)/c\,] \qquad . \qquad (5.30)$$

Let us define the time $\tau(x)$ as a characteristic time of the "vertical diffraction" across the line source:

$$\tau(x) = t_M(x) - t_m(x) \qquad . \qquad (5.31)$$

Combining Eq. (5.31) with Eqs. (5.29) and (5.30) yields

$$\tau(x) = [\, r_M(x) - r_m(x) \,] \,/\, c \qquad . \qquad (5.32)$$

This vertical diffraction time represents the time gap between the arrivals of the wavelets coming from the closest and farthest points of the line source, when it is at a distance x from the origin. From elementary geometrical considerations, it can be seen that $\tau(x)$ increases as the source nears the receiver, and decreases as the source moves away from the receiver. Note that a minimum pulse duration that can be observed at the receiver is always greater than zero, whether the source moves or is stationary. This implies that the Doppler gain will always be finite, even if the receiver is in the path of motion of the source.

If the line source is viewed as an array of an infinite number of point sources, then the received pulse duration may be considered as having two contributing factors: the pulse duration associated with a moving point source, and the vertical diffraction time. The time coordinate straining due to the motion of a point source was discussed in Section V.A. It remains then to use these results to determine the characteristics of a line source. The line source geometry may be divided into three cases, each of which is treated separately below: the short array, the array of length comparable to the receiver depth, and the long array.

First consider a short source as defined by L/h < 1 , where h is the depth of the receiver. By referring to Fig. 36, one can see that the nearest point to the receiver is the point at the deep end of the source, and that the farthest point from the receiver is the point located at $z = 0$. If $\Theta_m(x)$ and $\Theta_M(x)$ are the angles formed between the direction of motion and the

116

vectors to the receiver from the nearest and farthest points on the source, respectively, when it is located at position x, then

$$d/dx \, [r_m(x)] = - \cos \Theta_m(x) \quad , \tag{5.33}$$

and

$$d/dx \, [r_M(x)] = - \cos \Theta_M(x) \quad . \tag{5.34}$$

Equations (5.33) and (5.34) are valid even if the source has passed over the receiver. Combining Eqs. (5.33) and (5.34) with Eqs. (5.29) and (5.30) yields

$$d/dx(t_m) = [\, 1 - M \cos \Theta_m(x) \,] \, / \, v \quad , \tag{5.35}$$

and

$$d/dx \, (t_M) = [\, 1 - M \cos \Theta_M(x) \,] \, / \, v \quad . \tag{5.36}$$

From Eqs. (5.35) and (5.36), the characteristics of a short array may be drawn. As in the point source case, the characteristics are in general curved.

Next, consider an array whose length is comparable to the depth of the receiver. Such a source is defined by $1 \le L/h < 2$. In this case, the shortest distance between the array and the receiver is the distance from the array point located at the same depth as the receiver. Let us denote this distance by $r_\perp(x)$ and the angle to the receiver as $\Theta_\perp(x)$. Then

117

$$r_m(x) = r_\perp(x) \qquad . \qquad (5.37)$$

Under these conditions,

$$d/dx \, (r_m) = - \cos \Theta_\perp(x) \qquad , \qquad (5.38)$$

and

$$d/dx \, (r_M) = - \cos \Theta_M(x) \qquad . \qquad (5.39)$$

This leads to the following slopes for the characteristics:

$$d/dt \, (t_m) = [\, 1 - M \cos \Theta_\perp(x) \,] \, / \, v \qquad , \qquad (5.40)$$

and

$$d/dx \, (t_M) = [\, 1 - M \cos \Theta_M(x) \,] \, / \, v \qquad . \qquad (5.41)$$

Note that Eqs. (5.40) and (5.41) are identical to Eqs. (5.35) and (5.36) with the transformation $\Theta_m \rightarrow \Theta_\perp$.

Finally consider the case of a long line source (L/h $\gtrsim$ 2) . Now the shortest distance to the receiver is that from the source point located at the same depth, and the longest distance is from the deepest source point. Retaining the definition of Θ_M as the angle associated with the vector from

118

the farthest source point to the receiver, Eqs. (5.40) and (5.41) are still valid.

Figure 37 shows the characteristics of a line source by showing the characteristics associated with motion of the nearest and farthest points from the receiver. The characteristics for each point resemble Fig. 33 closely, and it is possible for each source location on the line source to define x_l and x_c. For a given Mach number, the time separation between the two characteristics corresponding to the two location is $\tau(x)$.

An interesting phenomenon occurs when $1/\cos\Theta_m < M < 1/\cos\Theta_M$. In this case, time reversal occurs on wavelets coming from the point source closest to the receiver (i.e., the slope of $t_m(x)$ is negative), while no time reversal affects the wavelets coming from the farthest point of the line source (i.e., the slope of $t_M(x)$ is still positive). This "partial time inversion" region is the smooth transition from apparently subsonic to apparently supersonic behavior, as seen by the receiver. It is therefore the transonic region. This phenomenon can also be understood as a phase inversion affecting only wavelets coming from a certain part of the line source. This suggests the possibility of reshuffling the wavelets between the source and the receiver. If a source is emitting a signal which varies with its depth, for example, the sequence A, B, C, D, E, then it seems possible to receive the sequence A, D, C, B, E. This may possibly have some applications in signal encryption.

119
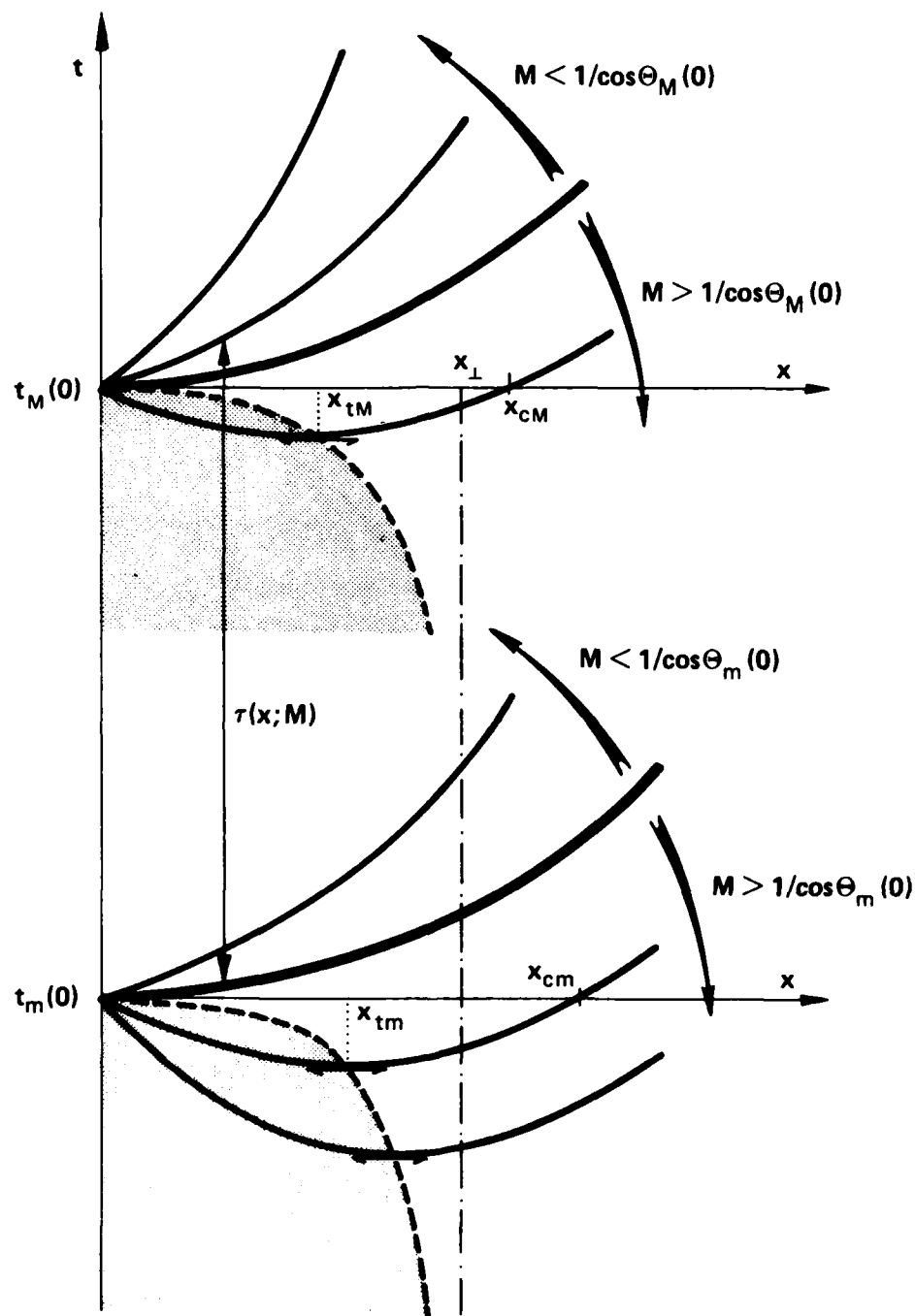
FIGURE 37
CHARACTERISTICS FOR A MOVING LINE SOURCE

120

2. Pulse duration

As discussed in the case of a point source, it is convenient to describe the emission at the source as a rectangular pulse of duration τ_p during which the source travels a distance $x_N = v \tau_p$. Since $\tau(x)$ has been defined as the time duration of the disturbance generated by the source when it was at a distance x from the origin, $\tau(0 \le x < x_N)$ subsequently represents the time gap between the arrivals of all wavelets emitted during the motion of the source. Therefore the received pulse duration τ_p is the projection on the time axis of $\tau(0 \le x \le xN)$. As usual, the Doppler factor is the straining of the time coordinate due to the motion of the source. It is given by

$$ D = \frac{\tau_p}{\tau_p + \tau(0)} \quad , \tag{5.42} $$

where $\tau(0)$ is the vertical diffraction time at the origin. Note that Eq. (5.42) differs from Eq. (5.2) for the point source because the finite extent of the line source will cause the received pulse to spread in time.

The received pulse duration can be expressed in analytical form by examining the characteristics to determine their projection on the time axis. As in the point source case, a distinction must be made between a line source which appears to the receiver to be moving subsonically and a line source which seems to be moving supersonically.

If $M < 1/\cos\Theta_m(0)$ then the entire line source appears to the receiver

121

to be moving subsonically. Another way of stating this is to say that the characteristic for each point on the line source has a positive slope. For a moving line source of this type, the earliest arrival of sound comes from the first wavelet emitted by the point source nearest to the receiver. The latest sound comes from the last wavelet emitted by the point source farthest from the receiver. Hence

$$\tau_p = t_M(x_N) - t_m(0) \qquad . \qquad (5.43)$$

If $1/\cos\theta_m(0) < M < 1/\cos\theta_M(0)$, the characteristic $t_M(x)$ has always a positive slope, whereas the slope of $t_m(x)$ is negative for $x < x_{tm}$ and positive for $x > x_{tm}$. Here x_{tm} denotes the location at which the nearest point source appears to be moving at transonic velocity. It may be found from Eq. (5.7). It is therefore necessary to consider two cases in order to evaluate the received pulse duration τ_p. The cases depend on the distance x_N traveled by the source. If $x_N < x_{tm}$, the first wavelet that reaches the receiver arrives at time $t_m(x_N)$ (see Fig. 37). Similarly, the last wavelet that reaches the receiver arrives at time $t_M(x_N)$. However, if $x_N \geq x_{tm}$, the time of arrival of the first wavelet is $t_m(x_{tm})$ and the last wavelet still reaches the receiver at $t_M(x_N)$. The received pulse duration is therefore given by Eqs. (5.44) and (5.45).

If $x_N < x_{tm}$,

$$\tau_p = t_M(x_N) - t_m(x_N) \qquad . \qquad (5.44)$$

122

If $x_N \geq x_{tm}$,

$$\tau_p = t_M(x_N) - t_m(x_{tm}) \qquad . \qquad (5.45)$$

If $M > 1/\cos\Theta_M(0)$, then the entire line source appears to the receiver to be moving supersonically at time t=0. This implies that the characteristic of each point source starts out with a negative slope. Two different cases depending on x_N, must be investigated. As shown in Fig. 37, if $x_N < x_{tm}$, the time of arrival at the receiver of the first wavelet is given by $t_m(x_N)$, whereas the time of arrival of the last wavelet is $t_M(0)$. However, if $x_N \geq x_{tm}$, Fig. 37 shows that the times of arrival of the first and last wavelets are, respectively, $t_m(x_{tm})$ and $t_M(x_N)$. The received pulse duration is therefore given by Eqs. (5.46) and (5.47).

If $x_N < x_{tm}$,

$$\tau_p = t_M(0) - t_m(x_N) \qquad . \qquad (5.46)$$

If $x_N \geq x_{tm}$,

$$\tau_p = t_M(x_N) - t_m(x_{tm}) \qquad . \qquad (5.47)$$

Note that in all of these cases, subsonic and supersonic, the received pulse duration is greater than the vertical diffraction time at the origin, $\tau(0)$. From Eq. (5.42) and the definition of the Doppler gain, Eq. (5.3), we may determine an upper bound for the gain of

$$G < 1 + [\tau_p / \tau(0)] \qquad (5.48)$$

Hence, a line source moving at any Mach number will always produce a finite gain at the receiver. For a point source $\tau(0) = 0$, and we recover the result that $G < \infty$, i.e., that the Doppler gain is finite.

A computer program has been written to evaluate the gain associated with an acoustic line source of finite length moving at constant velocity. Figures 38(a) and 38(b) are three dimensional plots showing the Doppler gain as a function of both Mach number and pulse duration. The length of the array was set to $L = 0.01$ m in Fig. 38(a), and $L = 0.1$ m in Fig. 38(b). In each case, the receiver's coordinates were $x = 4$ m, $y = 0$ m, and $z = 4$ m, (see Fig. 36.). The pulse duration varied between $\tau_p = 0.02$ ms and $\tau_p = 2$ ms; in nondimensional form, this means that $T_0 = c\tau_p/r_0$ varied from 0.005 to 0.525.

As expected from the previous discussion, the gain associated with the motion of the source is always finite. It is also interesting to note that the finite length of the array introduces some "damping" into the response. Figure 38(a) shows a noticeably sharper peak in the gain than Fig. 38(b) which is at the same scale. This can be explained by noticing that the longer the source, the longer its "vertical diffraction time", and therefore the more time spreading in the response, and the lower the gain.

124
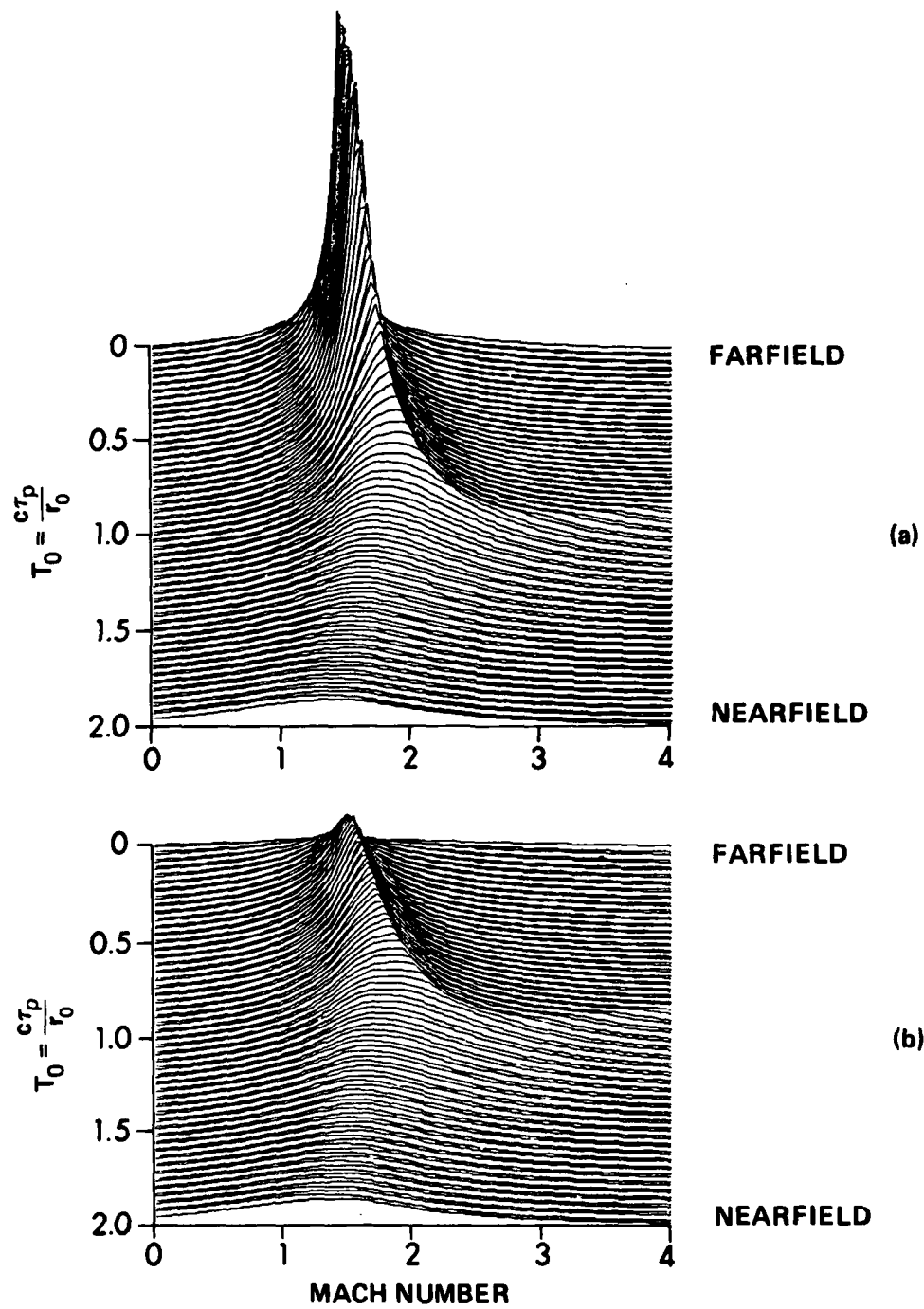
FIGURE 38
GAIN FOR A MOVING LINE SOURCE

C. Conclusions

It has been shown that the Doppler gain associated with a point source moving at constant velocity in a line past a point receiver is always finite, even when the source is moving at transonic velocity. The only exception is when the source is moving straight at the receiver. In this case, it is necessary to include the diffraction effects induced by the finite dimensions of any real source, in order to argue that the Doppler gain is still bounded.

A simple analytical prediction scheme has been used to find the maximum gain and the optimum Mach number for a moving point source. The results are valid for the case of a source passing over the receiver. In addition, simple expressions have been developed by examining the source characteristics for the Doppler shifts associated with a source moving at constant velocity.

The results for a moving point source were extended to include the case of a moving line source. The analysis of the Doppler shift for a line source of finite length, moving at constant velocity in a straight line, are very much like those of a point source. The Doppler gain is finite for all Mach numbers, including transonic, and the Mach number which produces the maximum gain is a function of the nondimensional distance $R_0 = r_0/c\tau_p$. It was also shown that the Doppler gain of an acoustic array moving at constant velocity decreases with the array length. Finally, it was shown that even in the case of a line source moving at transonic velocity directly toward a point receiver, the Doppler gain is always finite.

Although the present analysis is carried out for the case of a transient pulse emission of finite duration at the source, the results can easily be extended to the case of any arbitrary source function. In the analysis, the pulse duration plays the role of a characteristic time, such as the period for the case of monochromatic signals.

CHAPTER VI

CONCLUSIONS AND SUGGESTIONS

The thermoacoustic mechanism of sound generation by a laser pulse beamed into water has been investigated, both theoretically and experimentally, for both stationary and moving sources. The theoretical model is based on the linear Westervelt-Larson equation[8] describing thermoacoustic sound generation for an inviscid medium containing a heat source such as a laser beam in water. A time domain analysis is developed in order to find the pressure field radiated by the thermoacoustic source. The acoustic pressure is expressed as a convolution type summation between the impulse response of the system and the thermoacoustic source strength (time derivative of the laser intensity). Although this approach requires in most cases the use of a computer, it offers several advantages: (1) It is valid in the nearfield of the source and this has been verified experimentally. (2) It is also valid for any source velocities, because the Doppler shift associated with the motion of the source appears naturally within the "pseudo-convolution". (3) Although the analysis presented here is restricted to the common case of a laser beam with a Gaussian cross section intensity distribution, with an exponential shading along the beam penetration axis, the model can be extended to any laser intensity profile. (4) The impulse response of a thermoacoustic source is a useful tool in analyzing the acoustic response to thermoacoustic transient phenomena such as extremely short laser pulses or Mach waves produced by a laser

128

beam moving at high velocity. It turns out that these transient signals are among the most promising ways to generate reasonably high thermoacoustic levels.

Experimental results were obtained with a laser system providing up to 5 joules of energy over a pulse duration of approximately 1 ms, during which the intensity was modulated at a single frequency between 5 and 80 kHz. Most of the experimental results were obtained with a Neodymium-Glass laser (optical wavelength 1.06 µm), so that the thermoacoustic source length in water was fairly short (~0.1m). Some experimental results are also given for the case of a long (~1m) thermoacoustic source which was obtained by using a ruby laser (optical wavelength 0.6943 µm).

The main experimental results can be grouped into four categories: pressure waveforms, directivity patterns, sound level dependence on source velocity, and spreading curves. Source velocities up to Mach 2 were investigated with special attention to the case of transonic velocity. In general, the experimental results are in good agreement with theoretical predictions, and this confirms the validity of the Westervelt-Larson model even for supersonic velocities.

Finally, the Doppler shift of an acoustic source moving at transonic velocity was analyzed theoretically by taking into account the time dependence of the angle of observation between the source and the receiver. It was shown that this time dependence removes the singularity which occurs in the standard theory, when the source is moving at transonic velocity. It was also shown that, in the case of a line source, the transition

129

between subsonic and supersonic regimes is a region where only wavelets coming from a certain part of the source are time-inverted, whereas the rest of the wavelets are not. This partial time inversion suggests the possibility of reshuffling the wavelets in a signal and this may have some applications in signal encryption. Future work on this topic should also include diffraction effects due to the finite size of the source, and non-rectilinear motion of the source to analyze path curvature, source acceleration, caustics and focusing effects.

The results reported in this study show that, in general, the experimental results are in good agreement with the theoretical predictions. The major discrepancy was found to be that the theoretical model underestimates by a significant amount the measured acoustic level when the source is moving at transonic velocity. However, the predicted waveform is in reasonable agreement with the measured waveform. It was found experimentally that by moving the source at transonic velocity, a gain of about 20 dB could be expected, and a very strong broadband pressure transient was generated. A sound pressure level of 152 dB re 1 μPa at 1 m was measured for such a Mach wave. This high level shows that the low frequency components of the broadband signal can propagate at fairly large ranges before being absorbed. The theoretical model predicts that in the vicinity of Mach one, diffraction effects become predominant and actually tend to ruin the efficiency of the process. Although diffraction effects were clearly observed around Mach one, it is not fully understood why the theoretical model underestimates the measured level. A possible explanation[27] is that nonlinear effects, such as the temperature

130

dependence of the thermodynamic coefficient β, become important and cannot be neglected.

The surprisingly high thermoacoustic levels measured at transonic source velocity indicate that, at least for sonar applications, future work should focus on laser induced Mach waves. It has been suggested[12,26,34] that the acoustic disturbance generated by a transonic thermoacoustic source is identical to the one generated by a stationary source of the same optical energy but delivered over an extremely short period of time. Although this is approximately true for an observer very far from the source, there is still a major advantage in using a moving source instead of a stationary source: The region of the medium which absorbs the heat produced by the laser beam is spread over the laser path length whereas in the case of a stationary source it is localized to the laser beam cross section. This means that the maximum energy density acceptable before surface evaporation or explosive boiling occurs in the medium is much higher in the case of a moving source than for a stationary source. In fact it is increased by a factor $v\tau_p/2a$, where v is the source velocity, τ_p the laser pulse duration, and $2a$ the beam diameter.

There are several reasons for choosing the thermoacoustic mechanism of laser sound generation over other mechanisms such as surface evaporation, explosive boiling, or optical breakdown. Although these other mechanisms are intrinsically more efficient than the thermoacoustic mechanism,[2,35,36,37] they cannot produce narrow directional sound beams. Moreover these energy conversion mechanisms are still not very well understood. It seems therefore safer to use the

131

thermoacoustic process and to push its upper limit by scanning the laser beam at high velocities. The strongest acoustic signal that can be generated by a moving thermoacoustic source occurs when the laser beam is moving at transonic velocity. However it should be emphasized that in this case the recorded acoustic signal has a very short duration so that the information content in the signal is limited. Also the high frequencies of such a pulse are attenuated very quickly in the water as the signal propagates. This problem can be overcome by finding judicious ways of depositing the heat source in the medium.

A possible design which has been investigated in detail both theoretically and experimentally by Soviet physicists,[38] consists of using a stationary laser source delivering a periodic train of very short laser pulses, separated in time by an arbitrary delay T_0. This is achieved for instance by Q-switching the laser source. In this design, a strong and directional acoustic disturbance of main frequency component $1/T_0$, is expected to propagate at long distances under water. As shown in reference 38, this design increases by a factor of about four the thermoacoustic intensity over that of a standard monochromatic modulation system. However the upper limit of the energy density acceptable to stay within the range of the thermal mechanism of sound generation is limited by the fact that the source is stationary.

A more sophisticated design has recently been suggested by Pierce and Hsieh.[39] It consists of splitting the laser beam into several beams, separated by an arbitrary distance λ_0 on the surface of the water, and all moving at a slightly supersonic velocity. The theoretical analysis, which is

based on a very general acoustic pumping principle,[40] predicts that this configuration allows a very strong quasi-plane wave of main frequency component c/λ_0 , to propagate very far under water in a very collimated beam. The motion of the source would allow very high electromagnetic energy levels to be deposited into the water, within the range of the thermoacoustic sound generation mechanism, and without surface evaporation or explosive boiling deteriorating the directional properties of the sound beam. At sufficiently high energy levels, which would produce other mechanisms if the source were stationary, nonlinear effects due to the temperature dependence of the thermodynamic parameters (β, c_p) could even enhance the thermoacoustic conversion efficiency.[27] The experimental investigation of such a design seems to be the logical extension of the work on laser thermoacoustic sources. If experimental results confirm the usefulness of this design, it would certainly place thermoacoustics within the range of some sonar applications.

Laser performances are of course a determinant factor in the capabilities of a thermoacoustic sonar. Fortunately, laser technology has improved considerably over the last two decades, and it is expected to do so in the near future. It is now possible to find pulsed solid state lasers that emit a single pulse of several hundred joules over several milliseconds.

Another type of laser that may be suitable for some underwater applications of thermoacoustics, is the fairly new excimer laser.[41] This laser delivers very short pulses (4-50 ns) in the ultraviolet spectrum (0.18 to 0.3 μm) at a very high repetition rate so that high mean powers are

133

achievable. The optical frequency can be downshifted to wavelengths suitable for thermoacoustic purposes (0.5 to 1 μm) by a very efficient method known as the stimulated Raman scattering. Moreover these lasers are reliable, easy to operate, very pure and they can produce a very small beam diameter so that very high energy densities can be produced fairly easily. However, the pulse duration is too short to take advantage of any motion of the source.

Infrared lasers such as the CO_2 laser, or the NH_3 laser, are among the most efficient CW-lasers. In certain applications, the CO_2 laser can deliver up to 500 kW continuous.[42] Unfortunately the spectral region of these lasers is too far away from the region of interest for thermoacoustic applications. (Stimulated Raman scattering may be used only to increase the lasing wavelength, not to decrease it.)

However recent developments on chemically pumped lasers seem to indicate[43] that a continuous high-power laser of wavelength 1.3 μm could be developed , and this laser would certainly be perfectly suitable for underwater applications of thermoacoustics.

In summary, it seems that the laser technology is improving so rapidly that in a not too distant future, one could conceivably design a laser-induced sonar based on the principles of thermoacoustic generation of sound.

APPENDIX A

NONUNIFORMITY OF THE LASER SCANNING VELOCITY
AND OBLIQUE INCIDENCE OF THE LASER BEAM

In this study, it is assumed that the laser beam remains perpendicular to the surface of the water during the laser pulse duration. This is just an approximation to the real physical situation encountered in the experiment, because, as indicated in Fig. 1, the rotating mirror imposes during the laser pulse duration a deflection angle $\psi(t)$ which is in general not zero. This has two consequences: first, the laser scanning velocity v will not be rigorously constant in time; and second, the laser beam will be refracted as it enters the water because the speed of light is different in air and water. The objective of this appendix is to quantify the importance of these two effects.

It can be shown from elementary geometrical considerations that the velocity v of the laser spot on the water surface, is given by

$$v(t) = \frac{h \, \Omega}{\cos^2 \psi(t)} \quad , \qquad (A1)$$

where h is the distance between the rotating mirror and the water surface, Ω is the angular velocity of the rotating mirror, and $\psi(t)$ is the angle between the laser beam and the vertical axis as indicated in Fig. 1. The relative error $\Delta v/v$ can therefore be written as

$$\Delta v / v = 1 - \cos^{-2} \psi(t) \qquad , \qquad (A2)$$

which shows that the maximum error occurs when $\psi(t)$ is maximum. If we assume that the laser beam is perpendicular to the water surface at the mid-point in the laser pulse duration τ_p, so that $\psi(o) = \psi(\tau_p)$, then it can be shown that $\psi(t)$ is maximum at $t=0$, and it takes the value

$$\psi(o) = \tan^{-1} (M c \tau_p / 2h) \qquad , \qquad (A3)$$

where $M=v/c$ is the Mach number of the thermoacoustic source, and c is the sound speed in water. Equations (A2) and (A3) can be combined to find the maximum relative error in the nonuniformity of the laser spot on the surface of the water.

The second effect induced by the non-perpendicularity of the laser beam on the water surface is a refraction of the beam as it penetrates into the water. This refraction effect is described by Snell's law:

$$\sin \psi(t) / c_{air} = \sin \Psi(t) / c_{water} \qquad , \qquad (A4)$$

where $\Psi(t)$ is the refracted angle between the laser beam and the vertical, in the water; $\psi(t)$ is the incident angle of the laser beam on the water surface; and c_{water} and c_{air} are, respectively, the speed of light in water and in air. The index of refraction n, defined as the ratio of c_{air} over

c_{water}, is 1.33 for both optical wavelengths (0.6943 μm and 1.06 μm) used in the experiment. Therefore the tilt angle $\Psi(t)$ of the laser beam in water is given by

$$\sin \Psi(t) = 0.75 \sin \psi(t) \quad , \quad (A5)$$

and the maximum tilt angle occurs when $\psi(t)$ is maximum, i.e., at t=0. Combining Eqs. (A3) and (A5) gives an estimate of the maximum tilt angle of the thermoacoustic source, as a function of Mach number:

$$\Psi(0) = \sin^{-1}\left\{ 0.75 \sin\left[\tan^{-1}\left(M c \, \tau_p / 2 h \right) \right] \right\} \quad . \quad (A6)$$

The following table gives some numerical estimates of $\psi(0)$, $\Psi(0)$, in degrees, and $\Delta v/v$ as a function of Mach number of the laser spot on the surface of the water. It is assumed that the speed of sound in water is c = 1486 m/s , the height between the rotating mirror and the water surface is h = 4.06 m , and that the laser pulse duration is τ_p = 1 ms.

TABLE IV

ERRORS ASSOCIATED WITH THE NONUNIFORMITY
OF THE LASER SCANNING VELOCITY

M	$\psi(0)$	$\dot{\psi}(0)$	$\Delta v/v$ (%)
0	0	0	0
0.5	5.2	3.9	0.8
1	10.4	7.8	3.3
1.5	15.4	11.5	7.5
2	20.1	14.9	13.4
2.5	24.6	18.2	20.9

APPENDIX B

FREQUENCY RESPONSE AND BEAM PATTERNS OF THE HYDROPHONE

The hydrophone used in the study of thermoacoustic sources was, in most cases, the USRD type H-56 hydrophone (serial number 114). This hydrophone is a high sensitivity and low self-noise device, so that weak acoustic signals can be detected. The most important electroacoustic characteristics of the H-56 can be found in reference 44.

Figure 39 shows the sensitivity of the H-56 as a function of frequency, from 10 kHz to 90 kHz. Figure 40 (a)-(g) represents the sensitivity of the H-56 as a function of angle in the x-z plane (see Fig. 22), for several frequencies: 10 kHz, 20 kHz, 30 kHz, 40 kHz, 50 kHz, 75 kHz, and 100 kHz.

The sensitivity of the receiving hydrophone as a function of (received) frequency and angle was taken into account in the experimental analysis of thermoacoustic sources.

139

ACOUSTIC   CALIBRATION

CHART: H-56 S/N 114 CAL   DATE: JAN 30

PROJECTOR: TR 225   HYDROPHONES:

RANGE FT: 15   DRIVE VOLTS: 20   STD: H23-325   REC. GATE MSEC: .4

DEPTH FT: 5   XMIT WIDTH MSEC: .5   TEST: H56-114   FILTER: 5-200K
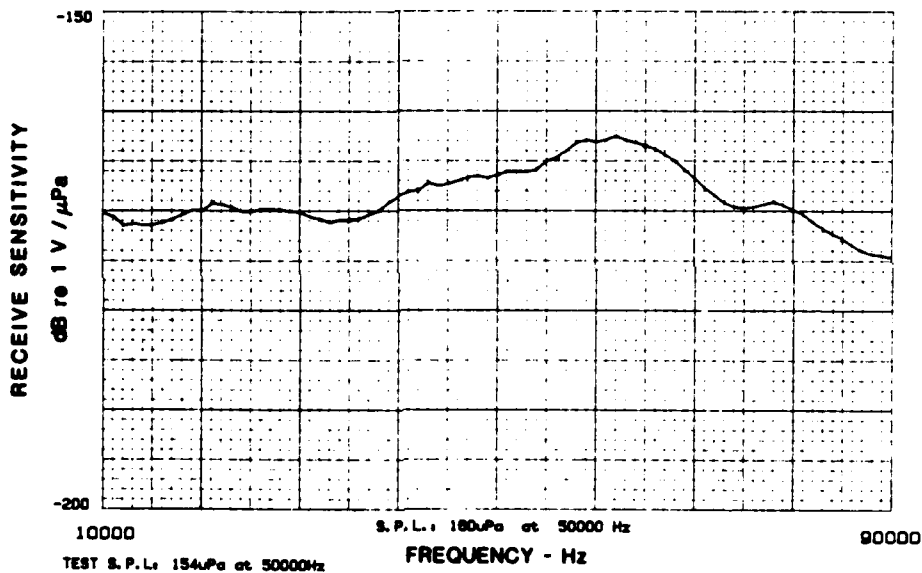
FIGURE 39
SENSITIVITY OF THE HYDROPHONE

140

DIRECTIVITY PATTERN

FOR: HYDROPHONE

PATTERN AXIS: VERTICAL   DATE: JAN 29

PROJ: TR 225   HYDR: H56-114
FREQ. Hz: .10000   SENS:
XMIT GATE MSEC: .5   REC GATE MSEC: .4
DRIVE: FILTER: 5-100K
E (Vrms): .10.0
I (mA): .

RANGE FT: .15.0
DEPTH FT: .5.0
TEMP C: 21
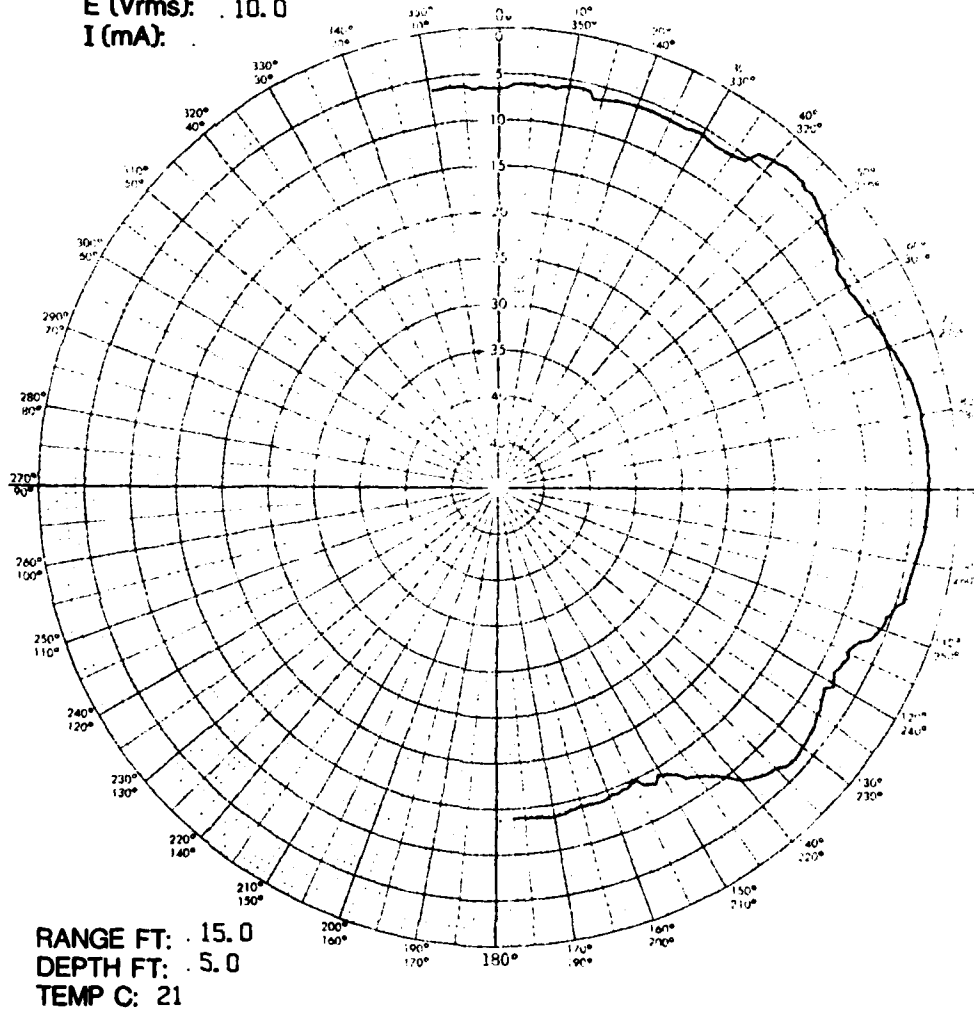
FIGURE 40 (a)

DIRECTIVITY PATTERN

FOR: HYDROPHONE

PATTERN AXIS: VERTICAL   DATE: JAN 29

PROJ: TR 225   HYDR: H56-114

FREQ. Hz: 20000   SENS:

XMIT GATE MSEC: .5   REC GATE MSEC: .4

DRIVE: FILTER: 5-100K

E (Vrms): 10.0

I (mA):
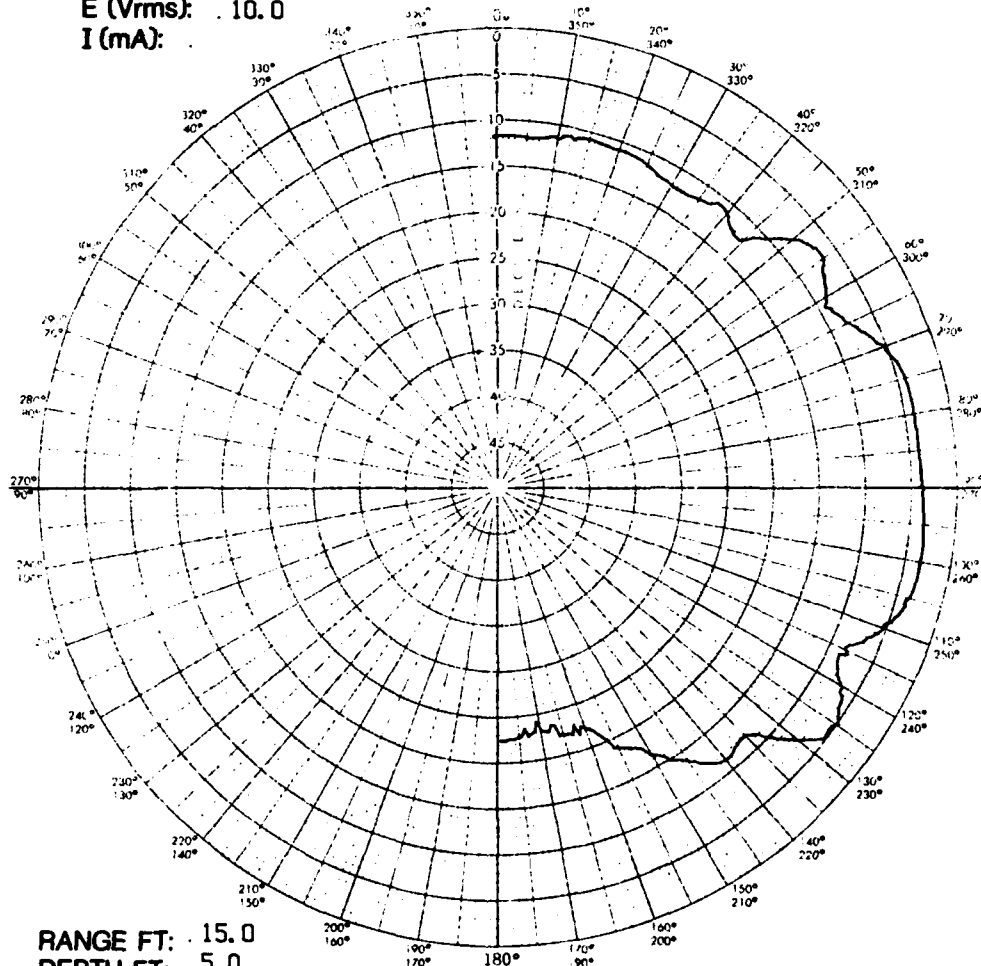
RANGE FT: 15.0

DEPTH FT: 5.0

TEMP C: 21

FIGURE 40 (b)

DIRECTIVITY PATTERN

FOR: HYDROPHONE

PATTERN AXIS: VERTICAL   DATE: JAN 29

PROJ: TR 225   HYDR: H56-114
FREQ. Hz: .30000   SENS:
XMIT GATE MSEC: .5   REC GATE MSEC: .4
DRIVE: FILTER: 5-100K
E (Vrms): 10.0
I (mA):
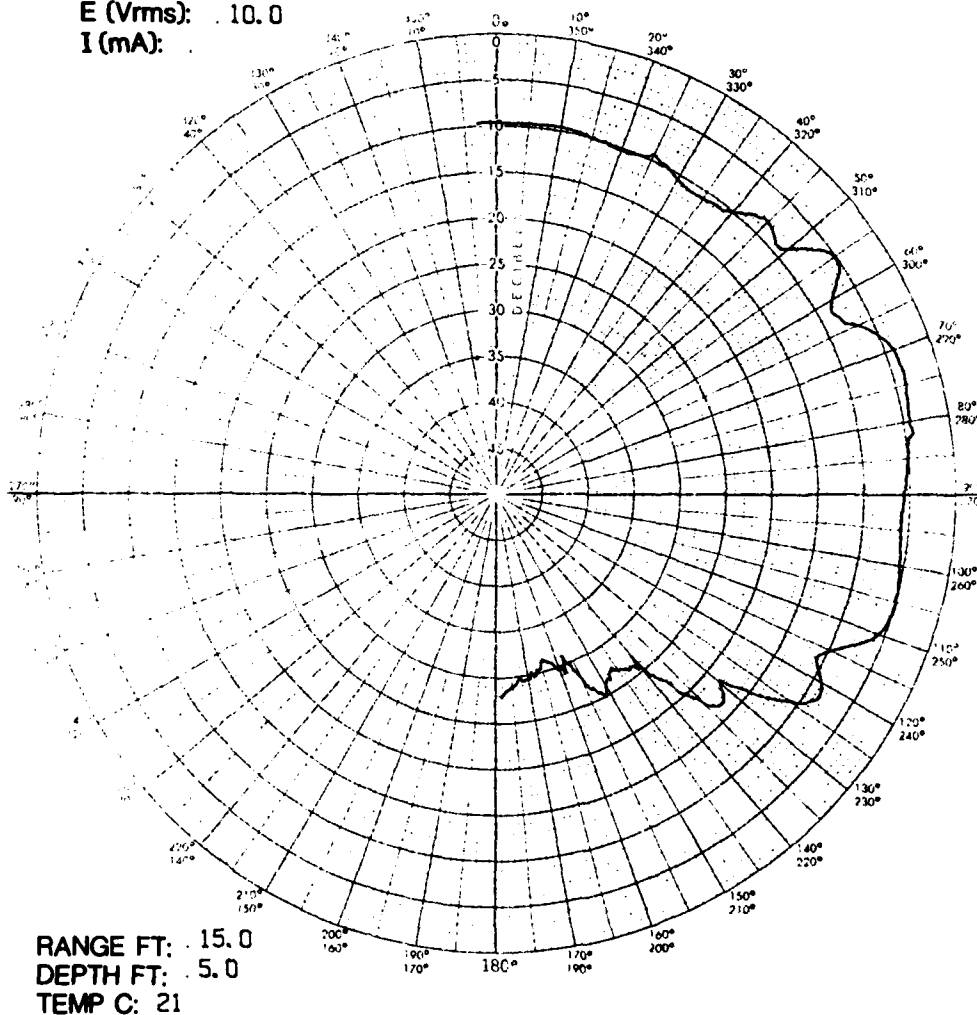
RANGE FT: 15.0
DEPTH FT: 5.0
TEMP C: 21

FIGURE 40 (c)

143

DIRECTIVITY PATTERN

FOR: HYDROPHONE

PATTERN AXIS: VERTICAL   DATE: JAN 29

PROJ: TR 225

FREQ. Hz: .40000

XMIT GATE MSEC: .5

DRIVE:

E (Vrms): .10.0

I (mA):

HYDR: H56-114

SENS:

REC GATE MSEC: .4

FILTER: 5-100K

RANGE FT: 15.0

DEPTH FT: 5.0

TEMP C: 21
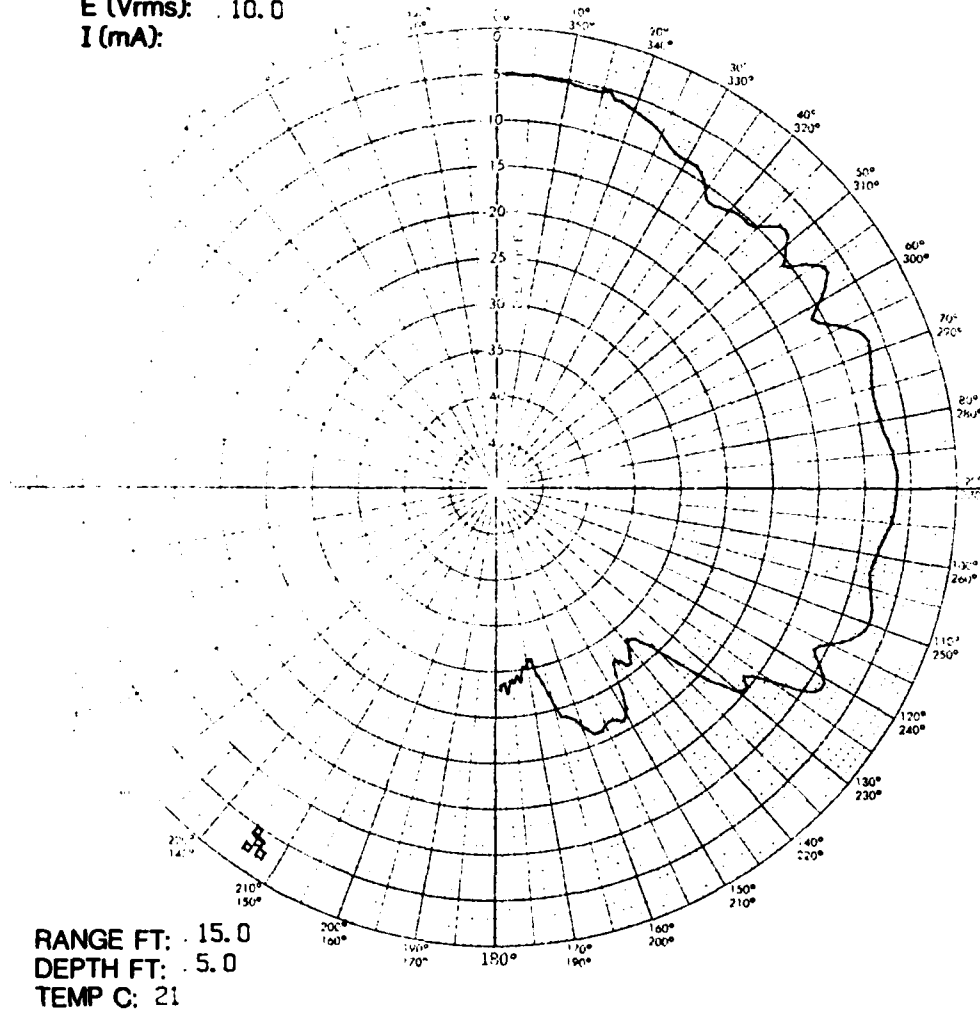
FIGURE 40 (d)

DIRECTIVITY PATTERN

FOR: HYDROPHONE

PATTERN AXIS: VERTICAL   DATE: JAN 29

PROJ: TR 225   HYDR: H56-114

FREQ. Hz: .50000   SENS:

XMIT GATE MSEC: .5   REC GATE MSEC: .4

DRIVE: FILTER: 5-100K

E (Vrms): .10.0

I (mA): .

RANGE FT: .15.0
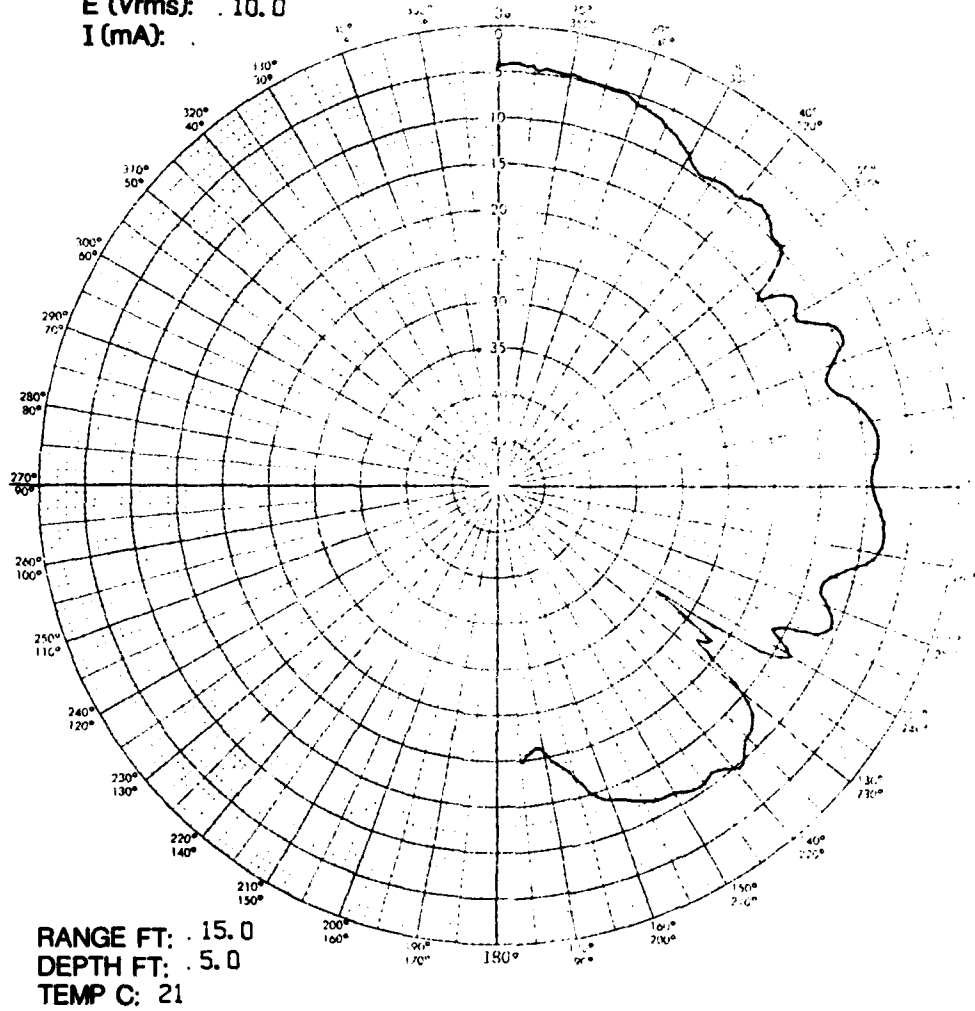
DEPTH FT: .5.0

TEMP C: 21

FIGURE 40 (e)

DIRECTIVITY PATTERN

FOR: HYDROPHONE

PATTERN AXIS: VERTICAL   DATE: JAN 29

PROJ: TR 225   HYDR: H56-114
FREQ. Hz: .75000   SENS:
XMIT GATE MSEC: .5   REC GATE MSEC: .4
DRIVE: FILTER: 5-100K
E (Vrms): .10.0
I (mA): .
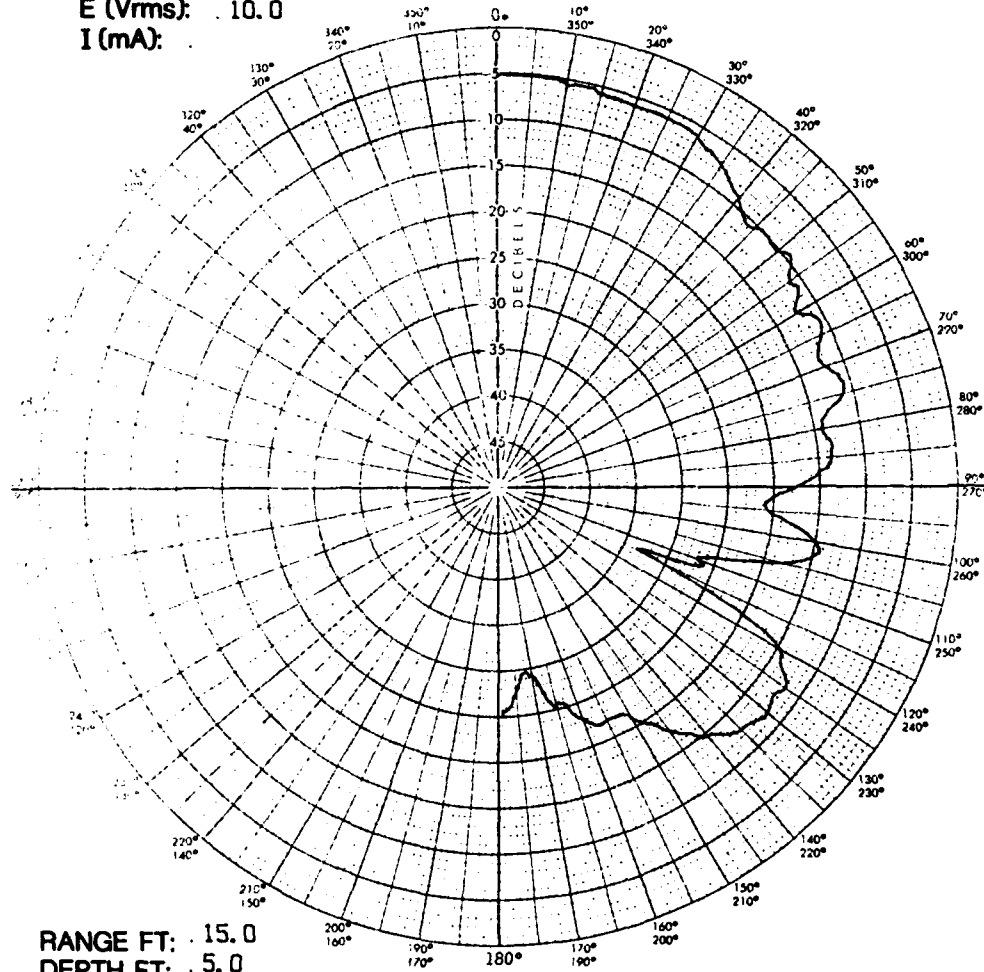
RANGE FT: .15.0
DEPTH FT: .5.0
TEMP C: 21

FIGURE 40 (f)

DIRECTIVITY PATTERN

FOR: HYDROPHONE
PATTERN AXIS: VERTICAL   DATE: JAN 29

PROJ: TR 225   HYDR: H56-114
FREQ. Hz: .100000   SENS:
XMIT GATE MSEC: .5   REC GATE MSEC: .4
DRIVE: FILTER: 5-100K
E (Vrms): .10.0
I (mA):

RANGE FT: 15.0
DEPTH FT: 5.0
TEMP C: 21
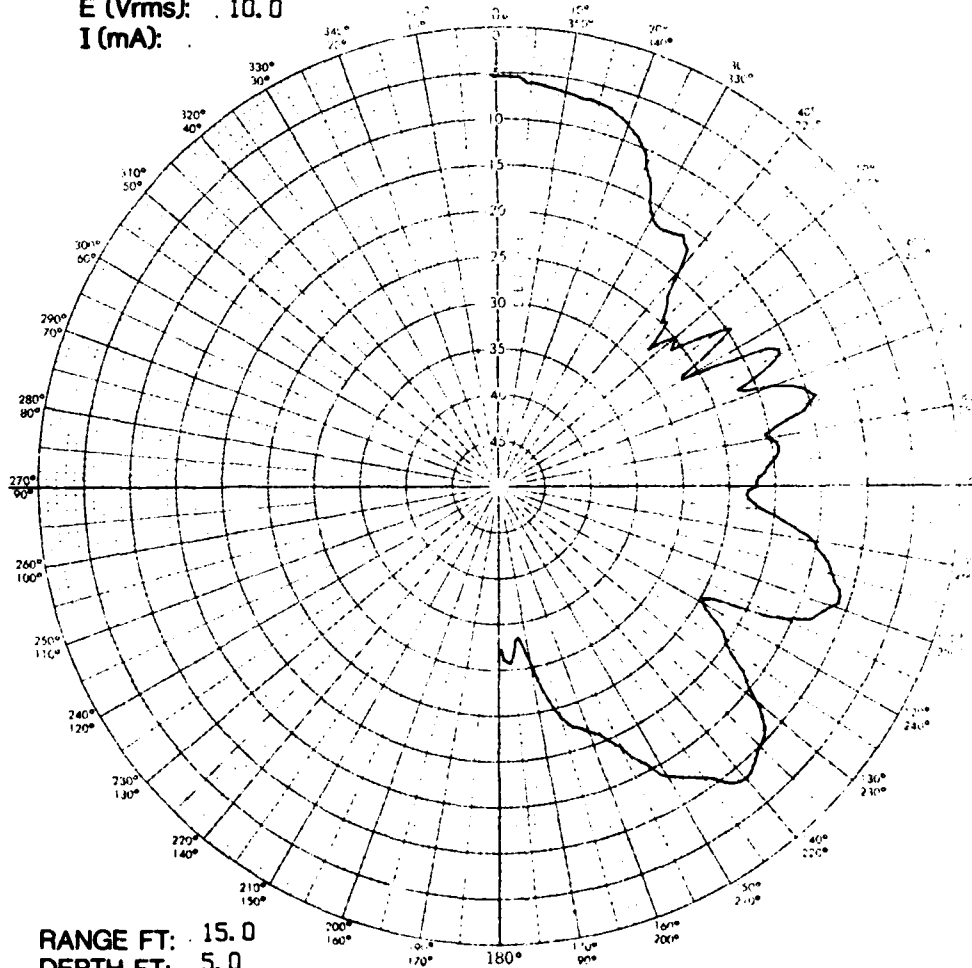
FIGURE 40 (g)

APPENDIX C

INTERFACE BETWEEN THE OSCILLOSCOPE AND THE COMPUTER

The Nicolet 4094 digital oscilloscope was interfaced to the CDC-CYBER computer so that recorded waveforms could be transferred to the mainframe computer and compared with theoretical predictions. This appendix summarizes the procedure for the data transfer.

The output labeled "TERMINAL" on the back panel of the Nicolet should be connected to a CYBER terminal. The switch labeled "GPIB-RS 232", located also on the back panel of the Nicolet, should be placed in the position "RS 232". The actual transfer of data is done via that RS 232 interface. The software for the data transfer is a program called "NICL" (binary version: "NICOLT"), which was written by D. Gallant-Offer. This program must be run interactively from the CYBER terminal connected to the oscilloscope. To run the program, type:

/GET,NICOLT/UN=GQ
/NICOLT

The message "ENTER COMMAND" will appear. There are six possible commands:

148

DM	transfer waveform from diskette to Nicolet's memory
MD	transfer waveform from Nicolet's memory to diskette
MC	transfer waveform from Nicolet's memory to CYBER
DC	transfer waveform from diskette to CYBER
WF	display data about waveforms in the Nicolet's memory
QU	quit the program

An invalid command causes the message "INVALID COMMAND" to appear before it again prompts for a command. A carriage return without command aborts the program with an end-of-file error. Each command prompts the information it needs. Typing while the Nicolet is communicating with the CYBER usually aborts the program and requires that the Nicolet be reset. (To reset the Nicolet, switch back and forth the RS 232/GPIB switch on the back panel of the Nicolet). While the program is running, it will display error codes from the Nicolet. An error code of zero means that no error occurred. The explanation for the other error codes is given on pp.13-60 (Table 13-25) in the Nicolet 4094 waveform analysis manual.

The following messages appear before the transfer of data.

Message	Explanation
ENTER COMMAND	enter one of the 6 commands (usually MC)
WAVEFORM NUMBER	enter the number of the waveform to be transferred (usually 1).
RECORD NUMBER	enter diskette record number to read from or save to.
MEMORY SECTION	enter the segment of memory to read from or save to.
0	all of memory (ALL)
1	first quarter (Q1)
2	second quarter (Q2)
3	third quarter (Q3)
4	fourth quarter (Q4)
5	first half (H1)
6	second half (H2)
STARTING POINT	first point to be transferred from the waveform (1 to 15871)
TOTAL NUMBER OF POINTS	total number of points to be transferred (1 to 15871)
FILENAME	name of file to write data to.

The output of "NICOLT" is a file on the CYBER in free format, called "filename". It contains the values of the data points of the waveform, in integer values. In order to convert this set of data into their real values, a program called "CONVERT" ("CVRT" in binary) has been written. Note that both "CONVERT" and "NICL" have to be compiled in Fortran 5. The input file (tape2) of "CONVERT" should be "filename". The output file (tape3) of "CONVERT" is "PEXP". It contains the waveform transferred from the Nicolet, in the following format:

```
            WRITE(3,100) TIME(I),VOLT(I)
      100    FORMAT(2(5X,E12.4))
```

where TIME(I) and VOLT(I) are the coordinates of the i-th data point. A listing of "NICL" and "CONVERT" is given below.

151

```fortran
      PROGRAM NICL(TAPE2,PSAVE,TAPE3=PSAVE)
C
C THIS PROGRAM ALLOWS THE TRANSFER OF DATA FROM A NICOLET DIGITAL
C OSCILLISCOPE 4094 WITH ONE DISK DRIVE TO A CYBER.
C
C A PROCEDURE IS CREATED WHICH WILL SAVE ALL LOCAL WAVEFORM FILES AS
C PERMANENT WAVEFORM FILES WHEN IT IS EXECUTED.
C
C SEE NOS 2.1, VOL. 4, CH. 12 FOR AN EXPLANATIION OF TRANSPARENT OUTPUT
C (:@) AND TERMINAL REDEFINITION (HALF).
C
      LOGICAL CONT
      CHARACTER CMD*2,OPER*4
      WRITE(3,'(".PROC,SPROC.",/,"CTIME.")')
C
C INITIATE HALF DUPLEX TO PREVENT THE CYBER FROM ECHOING THE NICOLET'S
C OUTPUT.
C
      HALF = O"001640614000000000000"
      WRITE(*,'(A10)') HALF
C
C TURN THE NICOLET ON WITH A CTL-A. CHANGE THE COMMAND DELILMITER TO A "!"
C AND CHANGE THE DEFAULT SPACING OF DATA.
C
      WRITE(*,'(":@5A",">C,13,33!")')
      READ *,LERR1
      WRITE(*,'("C,4,1,32!")')
      READ *,LERR2
      WRITE(*,'("@!")')
      READ *,LERR3
      WRITE(*,55) LERR1,LERR2,LERR3
55    FORMAT("ERROR CODES ",3I3)
      CONT = .TRUE.
30    WRITE(*,'("ENTER COMMAND")')
      READ(*,15) CMD
15    FORMAT(A2)
      IF (CMD.EQ.'DM') THEN
         OPER = 'R,O,'
         CALL DISKM(OPER,MEMSEC)
      ELSE IF (CMD.EQ.'DC') THEN
         CALL DISKC
      ELSE IF (CMD.EQ.'MD') THEN
         OPER = 'S,O,'
         CALL DISKM(OPER,MEMSEC)
      ELSE IF (CMD.EQ.'MC') THEN
         WRITE(*,'("ENTER WAVEFORM NUMBER")')
         READ(*,35) NWAVEN
35       FORMAT(I2)
         CALL MEMC(NWAVEN)
      ELSE IF (CMD.EQ.'WF') THEN
         CALL WAVEF
      ELSE IF (CMD.EQ.'QU') THEN
         CONT = .FALSE.
      ELSE
         WRITE(*,'("INVALID COMMAND")')
      END IF
      IF (CONT) GOTO 30
      WRITE(3,'("REVERT. PSAVE.")')
      END
C
C DISK TO MEMORY OR MEMORY TO DISK TRANSFER
C
      SUBROUTINE DISKM(OPER,MEMSEC)
      CHARACTER OPER*4
      WRITE(*,'("RECORD NUMBER")')
      READ *,NREC
      WRITE(*,'("MEMORY SECTION")')
      READ *,MEMSEC
      WRITE(*,'(":@5A>      ")')
      WRITE(*,40) OPER,NREC,MEMSEC
40    FORMAT(A4,I2,",",I2,"!")
      READ *,LERR
      WRITE(*,'("@!")')
      READ *,LERR2
      WRITE(*,15) LERR,LERR2
15    FORMAT("ERROR CODES ",2I3)
      RETURN
      END
```

152

```
C
C  MEMORY TO CYBER TRANSFER
C
       SUBROUTINE MEMC(NWAVEN)
       DIMENSION IDATA(16000), IWDAT(35,7)
       CHARACTER FLNM*6, F*22
C
C  READ PARAMETERS FROM USER
C
       WRITE(*, '("STARTING POINT")')
       READ *, ISTART
       WRITE(*, '("TOTAL NUMBER OF POINTS")')
       READ *, ITOTAL
       WRITE(*, '("FILENAME")')
       READ(*, '(A6)') FLNM
       WRITE(*, '(": 05A>        ")')
C
C  READ DATA ABOUT WAVES FROM THE NICOLET.
C
       WRITE(*, '("C,4,0!")')
       READ *,LCS1
       WRITE(*, '("C,0,1,13!")')
       READ *,LCS2
       WRITE(*, '("W!")')
       READ *, LWR1
       READ(*, '(I2)') ITOT
       ITEN = ITOT/10 + ICHAR('0')
       IONE = MOD(ITOT,10) + ICHAR('0')
       F = '('//CHAR(ITEN)//CHAR(IONE)//'(I2,I6,2I2,3I1),I2)'
       READ(*,F) ((IWDAT(I,K),K=1,7),I=1,ITOT),LWR2
       WRITE(*, '("C,0,0!")')
       READ *,LCS3
       WRITE(*, '("C,4,1,32!")')
       READ *,LCS4
       ISTEP = 1
C
C  READ DATA FROM NICOLET TO CYBER 20 VALUES AT A TIME (120 CHARACTERS).
C  THE CYBER'S BUFFER IS ONLY 150 CHARACTERS LONG AND IT NEEDS TIME TO
C  PROCESS DATA FROM THAT BUFFER.
C
       ITL = 20
       IST = ISTART
       ILP = ITOTAL / ITL
       IREM = ITOTAL - ILP*ITL
       DO 35 I=1,ILP
         WRITE(*,25) NWAVEN,IST,ITL,ISTEP
25       FORMAT("D,0,",I2,",",I6,",",I6,",",I3,"!")
         READ *,LERR1
         READ *,(IDATA(K),K=IST+1,IST+ITL),LERR2
35     IST = IST + ITL
       IF (IREM.EQ.0) GO TO 45
       WRITE(*,25) NWAVEN,IST,IREM,ISTEP
       READ *,LERR
       READ *,(IDATA(I),I=IST+1,IST+IREM),LERR
C
C  READ NORMALIZATION DATA
C
45     WRITE(*,30) IWDAT(NWAVEN,3)
30     FORMAT("N,",I2,"!")
       READ *,LERR3
       READ *,IVAL,ISWEEP,ICHANL,IDISP,VNORM,HNORM,IVZERO,IHZH,IHZL,
     1 IRNVZ,IRNHZ,LERR4
       WRITE(*, '("Q!")')
       READ *,LERR5
       WRITE(*,50) LWR1,LWR2,LERR1,LERR2,LERR3,LERR4,LERR5
50     FORMAT("ERROR CODES ",7I3)
C
C  WRITE ALL DATA OUT TO FLNM
C
       OPEN(2,FILE = FLNM)
       REWIND(2)
       WRITE(2,*) NWAVEN,ISTART,ITOTAL,ISTEP,IWDAT(NWAVEN,3),
     1 (IDATA(I),I=ISTART+1,ISTART+ITOTAL),IVAL,ISWEEP,ICHANL,IDISP,
     2 VNORM,HNORM,IVZERO,IHZH,IHZL,IRNVZ,IRNHZ
       CLOSE(2,STATUS = 'KEEP')
       WRITE(3,40) FLNM
40     FORMAT("REPLACE,",A,",")
       RETURN
       END
```

153

```
c
c   DISK TO CYBER TRANSFER
c
        SUBROUTINE DISKC
        DIMENSION IWDAT(35,7)
        LOGICAL FOUND
        CHARACTER OPER*4, F*22
c
c   READ WAVE FROM DISK TO NICOLET
c
        OPER = 'R,0,'
        CALL DISKM(OPER,MEMSEC)
c
c   AFTER THE WAVE HAS BEEN READ IN, ITS WAVEFORM NUMBER HAS TO BE FOUND
c   SO ITS DATAPOINTS CAN BE TRANSFERRED TO THE CYBER.
c
        GO TO (10,20,30,30,10,20),MEMSEC
10      NWAVEN = 1
        GO TO 70
20      NWAVEN = 2
        GO TO 70
30      WRITE(*,'(":05A>       ")')
        WRITE(*,'("C,4,0!")')
        READ *,LCS1
        WRITE(*,'("C,0,1,13!")')
        READ *,LCS2
        WRITE(*,'("W!")')
        READ *, LWR1
        READ(*,'(I2)') ITOT
        ITEN = ITOT/10 + ICHAR('0')
        IONE = MOD(ITOT,10) + ICHAR('0')
        F = '('//CHAR(ITEN)//CHAR(IONE)//'(I2,I6,2I2,3I1),I2)'
        READ(*,F) ((IWDAT(I,K),K=1,7),I=1,ITOT),LWR2
        WRITE(*,'("C,0,0!")')
        READ *,LCS3
        WRITE(*,'("C,4,1,32!")')
        READ *,LCS4
        WRITE(*,'("G!")')
        READ *, LERR
        WRITE(*,50) LWR1,LWR2,LERR
50      FORMAT("ERROR CODE ",3I3)
        FOUND = .FALSE.
        DO 35 I=1,ITOT
          IF(IWDAT(I,7).EQ.MEMSEC) THEN
            NWAVEN = IWDAT(I,1)
            FOUND = .TRUE.
          ENDIF
35      CONTINUE
        IF (.NOT.FOUND) GO TO 80
70      CALL MEMC(NWAVEN)
        RETURN
80      WRITE(*,'("INVALID WAVEFORM NUMBER")')
        RETURN
        END
```

154

```
C
C  DISPLAY DATA ABOUT WAVEFORMS IN MEMORY
C
       SUBROUTINE WAVEF
       CHARACTER F*22
       DIMENSION IWDAT(35,7)
       WRITE(*,'(":05A>      ")')
       WRITE(*,'("C,4,0!")')
       READ *,LCS1
       WRITE(*,'("C,0,1,13!")')
       READ *,LCS2
       WRITE(*,'("W!")')
       READ *, LWR1
       READ(*,'(I2)') ITOT
       ITEN = ITOT/10 + ICHAR('0')
       IONE = MOD(ITOT,10) + ICHAR('0')
       F = '(('//CHAR(ITEN)//CHAR(IONE)//'(I2,I6,2I2,3I1),I2)'
       READ(*,F)((IWDAT(I,K),K=1,7),I=1,ITOT),LWR2
       WRITE(*,'("C,0,0!")')
       READ *,LCS3
       WRITE(*,'("C,4,1,32!")')
       READ *,LCS4
       WRITE(*,'("Q!")')
       READ *,LERR
       WRITE(*,15) LWR1,LWR2,LERR
15     FORMAT("ERROR CODE ",3I3)
       WRITE(*,20) ITOT
20     FORMAT('TOTAL NUMBER OF WAVES ',I3,/)
       WRITE(*,30)
30     FORMAT('WAVE  NO. OF POINTS  NORM. SET  NORM. STEP   CHANNEL
      1REFERENCE   TITLE')
       WRITE(*,40) ((IWDAT(I,K),K=1,7),I=1,ITOT)
40     FORMAT(1X,I2,6X,I6,9X,I2,10X,I2,9X,I1,9X,I1,8X,I1)
       RETURN
       END
11.41.56.UCLP, AA. PTRLO5,      0.282KLNS.        ** END OF LISTING **
```

155

```
          PROGRAM CONVERT(PNIC, TAPE2=PNIC, PEXP, TAPE3=PEXP)
C
C         THIS PROGRAM IS USED WHEN TRANSFERRING DATA FROM THE
C         NICOLET TO THE CYBER , IE AFTER USING PROGRAM NICOLT.
C         THE PURPOSE OF THIS PROGRAM IS TO READ THE OUTPUT FILE
C         GENERATED BY NICOLT IN FREE FORMAT ( HERE IT IS CALLED PNIC)
C         AND TO CONVERT IT TO REAL VALUES IN A DESIRED FORMAT.
C         THE OUTPUT FILE OF THIS PROGRAM IS CALLED HERE PEXP
C
C         THIS PROGRAM HAS TO BE WRITTEN  IN FTN5
C
C         NOTATION:
C         TIME(I)= REAL TIME
C         VOLT(I)= REAL AMPLITUDE OF THE SIGNAL
C         RTIME(I)= RESET TIME (IE WHEN USING THE RESET ON NICOLET)
C         RVOLT(I)= RESET VOLTAGE AMPLITUDE  (IE     IDEM   )
C
C         DIMENSION I SHOULD BE GREATER THAN NF
C         NF=NO+N
C         NO= NUMBER OF THE FIRST DATA POINT TRANSFERRED (SEE NICOLT)
C         N=TOTAL NUMBER OF DATA POINTS TO BE TRANSFERRED.
C
          DIMENSION TIME(5000), VOLT(5000), RTIME(5000), RVOLT(5000)
          DIMENSION IDATA(5000)
C
C         READ OUTPUTFILE (TAPE2) FROM NICOLT
C
          READ(2, *) NWAVEN, ISTART, ITOTAL, ISTEP, NRSET,
         1(IDATA(I), I=ISTART, ISTART+ITOTAL-1), IVAL, ISWEEP,
         2ICHANL, IDISP, VNORM, HNORM, IVZERO, IHZH, IHZL,
         3IRNVZ, IRNHZ
C
C         CONVERT TO REAL VALUES
C
          DO 1 I=ISTART, ISTART+ITOTAL-1
          TIME(I)=((I-1)-(65536*IHZH+IHZL))*HNORM
          VOLT(I)=(IDATA(I)-IVZERO)*VNORM
          RTIME(I)=((I-1)-IRNHZ)*HNORM
          RVOLT(I)=(IDATA(I -IRNVZ)*VNORM
    1     CONTINUE
C
C         WRITE IN FORMAT 100 THE OUTPUT FILE (TAPE3) (HERE PEXP)
C         CONTAINING ONLY TIME(I) AND VOLT(I)
C
          DO 2 I=ISTART, ISTART+ITOTAL-1
          WRITE(3, 100)TIME(I), VOLT(I)
    2     CONTINUE
  100     FORMAT(5X, E12. 4, 5X, E12. 4)
          STOP
          END
10. 43. 07. UCLP, AA, PTRL05,      0. 086KLNS.         ** END OF LISTING **
```

156

APPENDIX D

THE INHOMOGENEOUS VISCOUS WAVE EQUATION FOR
LASER-INDUCED SOUND

The wave equation describing the pressure field of a lossless medium containing a heat source was first derived by Ingard[7]. Starting from this linear inviscid thermoacoustic wave equation, Westervelt and Larson studied[8] the special case of a sound field generated by the heating of a laser beam penetrating into a liquid, and they discovered the fascinating properties of what is now called a thermoacoustic array. In this appendix, we rederive from the hydrodynamical equations of motion the so-called Westervelt-Larson wave equation for laser-induced sound, including now the effect of viscosity.

Let $p = p_0 + p$ be the total pressure in the medium, where p_0 is the ambient pressure and p is the acoustic pressure generated through the thermal mechanism. Similarly, let $\varrho = \varrho_0 + \varrho$ be the total density of the medium, $T = T_0 + T$ be the total temperature, and $s = s_0 + s$ be the total entropy in the fluid medium. The subscript o refers to an undisturbed quantity.

Since the acoustic disturbances generated by the thermal mechanism are expected to be small, we start directly from the linearized hydrodynamical equations of motion: the conservation of mass, and the conservation of linear momentum.

mass:
$$\rho_t + \rho_0 \, \nabla \cdot u = 0 \qquad\qquad (D1)$$

momentum:
$$\rho_0 \, u_t + \nabla p = (\lambda + 2\mu) \, \nabla^2 u \qquad . \qquad (D2)$$

Here u denotes the particle velocity, $(\lambda + 2\mu)$ represents the viscosity of the medium, and the subscript t denotes a time derivative. It is implicitly assumed in Eqs. (D1) and (D2) that the medium is at rest, steady, uniform, and irrotational, and that heat conduction can be neglected.

The thermal input from the laser intensity induces a change in entropy in the system, so that an adequate equation of state describing the process is

state:
$$\rho = \rho \, (p, s) \qquad . \qquad (D3)$$

Forming a Taylor series expansion of Eq. (D3) about the equilibrium quantities ρ_0, p_0, and s_0, we have

$$\rho = \rho_0 + \left(\partial \rho / \partial p \right)_s (p - p_0) + \left(\partial \rho / \partial s \right)_p (s - s_0) + \dots \qquad . \qquad (D4)$$

By definition the small signal sound speed is $c = \sqrt{(\partial p / \partial \rho)_s}$, so that Eq. (D4) can be rewritten as

$$\rho = p/c^2 + s \, (\partial \rho / \partial s)_p \qquad . \qquad (D5)$$

The partial derivative in Eq. (D5) is the result of the change in density due

158

to the change in entropy induced by the laser heating. It is therefore related to the coefficient of thermal expansion β of the medium. By definition[45]

$$\beta = - (1/\rho) \, (\partial\rho/\partial T)_p \qquad\qquad\qquad (D6)$$

or

$$\beta = - (1/\rho) \, (\partial\rho/\partial s)_p \, (\partial s/\partial T)_p \quad . \qquad\qquad (D7)$$

But it is well known from thermodynamics[46] that the specific heat at constant pressure c_p can be expressed as

$$c_p = T \, (\partial s/\partial T)_p \qquad . \qquad\qquad\qquad (D8)$$

Combining Eq. (D8) with (D7), and linearizing the result about the undisturbed values, yields

$$(\partial\rho/\partial s)_p = - \rho_0 \, \beta \, T_0 \, / \, c_p \qquad . \qquad\qquad (D9)$$

Therefore Eq. (D5) becomes

$$\rho = p/c^2 - s \, \rho_0 \, \beta \, T_0 \, / \, c_p \qquad , \qquad\qquad (D10)$$

and the last term in Eq. (D10) represents the effect of the laser heating on the change of density in the medium. Since we seek a wave equation for the acoustic pressure p, we eliminate u between Eqs. (D1) and (D2). It is found that

159

$$\nabla^2 p - \rho_{tt} + (\lambda + 2\mu)/\rho_0 \ \nabla^2 \rho_t = 0 \qquad . \qquad \text{(D11)}$$

Eliminating ρ between Eq. (D10) and Eq. (D11) yields a wave equation in terms of the acoustic pressure p and the input entropy disturbance s,

$$\nabla^2 p - (c^{-2}) p_{tt} - (\rho_0 \beta T_0/c_p) s_{tt} +$$

$$(\lambda + 2\mu)/\rho_0 \ \nabla^2 [(c^{-2}) p_t - (\rho_0 \beta T_0/c_p) s_t] = 0 \qquad . \qquad \text{(D12)}$$

Now let us relate the change in entropy to the heat q added to the medium by the laser beam. The conservation law which governs that relation is the second law of thermodynamics for a reversible process,

$$\rho \ T \ ds = q \ dt \qquad \qquad \text{(D13)}$$

or, in linearized form,

$$\rho_0 \ T_0 \ s_t = q \qquad . \qquad \text{(D14)}$$

Combining Eq. (D14) with Eq. (D12) to eliminate the entropy fluctuation s, we obtain

$$\nabla^2 p - c^{-2} p_{tt} + (\lambda + 2\mu)/\rho_0 c^2 \ \nabla^2 p_t =$$

$$- (\beta/c_p) q_t + (\beta/c_p) (\lambda + 2\mu)/\rho_0 \ \nabla^2 q \qquad . \qquad \text{(D15)}$$

160

This is the Westervelt-Larson wave equation for a viscous (but non-heat-conducting) irrotational fluid medium containing a heat source of strength q. For a lossless medium, Eq. (D15) reduces to its standard form

$$\Box^2 p = \nabla^2 p - c^{-2} p_{tt} = -(\beta/c_p) q_t \quad , \qquad (D16)$$

where $\Box^2$ denotes the D'Alembertian operator.

It is also convenient to relate the energy q added to the medium to the intensity of the laser beam illuminating the medium. Let us denote by $< I >$ the intensity of the laser beam averaged over a period of the very rapid ($\sim 10^{-14}$ s) optical oscillation of the laser light. $< I >$ is the Poynting vector of the process, and the flux of intensity $\nabla \cdot < I >$ represents the heat absorbed by the medium per unit time and unit volume. In other words

$$q = - \nabla \cdot < I > \quad . \qquad (D17)$$

In practice the laser beam is shining in, say the +z direction, so that $q = - \partial I / \partial z$. Equations (D16) and (D17) are the starting point of Chapter III.

It is interesting to note that Eq. (D16) has the same form as the Westervelt inhomogeneous wave equation[47] describing parametric end-fire radiation. In the wave equation for the parametric array, however, the source term represents virtual sources generated by nonlinear interaction in the medium, whereas, in Eq. (D16), the source term represents the time

161

and spatial derivative of the laser intensity distribution in the laser beam. There is nevertheless a close mathematical analogy between the parametric array and the thermoacoustic array, and this analogy has been used by Novikov, Rudenko, and Timoshenko[48] to study the pressure waveform radiated by a transonic thermoacoustic array.

APPENDIX E

HALF-ORDER DERIVATIVE AND IMPULSE RESPONSE $h_L(t)$
AND CONNECTION WITH THE PARABOLIC CYLINDER FUNCTION

The concept of half-order derivatives appears as early as 1695, in a letter from Leibniz to L'Hospital, opening thus the avenue to what is now called fractional calculus. A complete historical survey of the main contributions to fractional calculus can be found in reference 49. In this appendix, it is shown that the half-derivative operator is closely related to the vertical impulse response $h_L(t)$ defined in Chapter III. It is also shown that the half-order derivative can be expressed in terms of a parabolic cylinder function.

1. Half-order derivatives

It has been shown[50] that the acoustic pressure response $p(t)$ of an infinite line source producing a uniform mass outflow $I(t)/h$ per unit length h is given by

$$p(t) = (2\pi h)^{-1} \int_{s}^{\infty} I_t(t-r/c) \, [r^2-s^2]^{-1/2} \, dr \qquad , \quad (E1)$$

where $s = r_0 \sin\theta_0$ (see Fig. 9), and where the subscript t denotes a time derivative. If it is assumed that most of the contributions come from the point of the line source right in front of the receiver (i.e., from r=s), then

163

$r^2-s^2 \approx 2s(r-s)$, and Eq. (E1) can be rewritten in the form

$$p(t) = (2\pi h)^{-1} (c/2s)^{1/2} \int_{-\infty}^{t-s/c} I_t(T) \left[(t-s/c)-T \right]^{-1/2} dT \qquad . \qquad \text{(E2)}$$

Using the identity[50]

$$(d/dt)^{1/2} I(t) = \int_{-\infty}^{t} I_t(T) \left[\pi(t-T) \right]^{-1/2} dT \qquad , \qquad \text{(E3)}$$

the acoustic pressure p can be expressed in terms of the half-order derivative $(d/dt)^{1/2}$ of the source function I, as follows.

$$p(t) = (2h)^{-1} (c/2\pi s)^{1/2} (d/dt)^{1/2} I(t-s/c) \qquad . \qquad \text{(E4)}$$

The notation $(d/dt)^{1/2}$ for the integral defined by Eq. (E3) comes from the fact that

$$(d/dt)^{1/2} \left[(d/dt)^{1/2} (I) \right] = dI/dt \qquad . \qquad \text{(E5)}$$

Note from Eq. (E3) that $(d/dt)^{1/2} I(t)$ can be expressed as a convolution between $I_t(t)$ and a half-order delta function $\delta^{1/2}(t)$ or "half-order derivative operator".

164

$$p(t) = \delta^{1/2}(t-s/c) * I_t(t) \qquad (E6)$$

But we recall from Chapter III that the impulse response $h_L(t)$ is defined as

$$p(t) = h_L(t) * I_t(t) \qquad (E7)$$

Equations (E6) and (E7) show that there is a correspondence between the impulse response $h_L(t)$ and the half-order derivative operator. It should be emphasized however, that the infinite line source model used to introduce the concept of a half-order derivative in Eq. (E1) differs in two ways from the physical problem of a thermoacoustic source as discussed in this study. First, we are dealing in our experiment with a thermoacoustic source over a pressure release boundary, and not with an infinite line source. Second, we are dealing with an exponentially shaded line source, and not with a uniform line source. This means that the analogy between the impulse response $h_L(t)$ and the half-order derivative operator is strictly applicable only for the case of very weakly absorbing media.[51]

2. Connection between the half-order derivative and the parabolic cylinder function

An equation which occurs often (see for instance reference 52) in describing the pressure field of a cylindrical line source of Gaussian cross section distribution is

$$F(g) = \int_0^\infty \sigma^{-1/2} \exp[-(\sigma-g)^2] \, d\sigma \quad . \qquad (E8)$$

It can be shown that in fact $F(g)$ is related to both the half-order derivative of a Gaussian function, and to the parabolic cylinder function. This provides a connection between these two functions.

Combining Eqs. (E3) and (E8), we obtain

$$F(g) = (\pi/2) \, (d/dg)^{-1/2} \exp(-g^2) \quad . \qquad (E9)$$

Using the identity[53]

$$D_{-1/2}(z) = \pi^{-1/2} \exp(-z^2/4) \int_0^\infty \exp[-zx - x^2/2] \, x^{-1/2} \, dx \quad , \qquad (E10)$$

where $D_{-1/2}$ is the parabolic cylinder function of order $-1/2$ and combining Eqs. (E8) and (E10) yields

$$F(g) = (2)^{-1/4} \, \pi^{1/2} \exp(-g^2/2) \, D_{-1/2}(-g\sqrt{2}) \quad . \qquad (E11)$$

Combining Eqs. (E9) and (E11) gives an expression which relates the half-order derivative of a Gaussian to the parabolic cylinder function $D_{-1/2}$.

APPENDIX F

DETERMINATION OF THE OPTICAL COEFFICIENT OF ABSORPTION

The optical coefficient of absorption α dictates the penetration depth of the laser beam in the water, according to an exponential law of attenuation

$$I(z) = I_0 \, e^{-\alpha z} \qquad , \qquad \text{(F1)}$$

where I is the laser intensity of the laser beam, and z is the vertical axis of penetration of the laser beam. Therefore $1/\alpha$ is a measure of the 1/e length of the thermoacoustic source. This means that it is necessary to determine α for both optical wavelengths used in our experiment: 1.06 µm (Nd:Glass) and 0.6943 µm (ruby).

This was done in reference 14 for the case of absorption of light in distilled water and fresh lakewater. In our study, the same experiment was repeated for the case of absorption of light in the fresh water of the tank in which the experiments were made. The details of the experimental procedure used to measure α can be found in reference 14. The method is based on measuring the attenuation of light for different widths of the sample of water. The value of α, in nepers per meter, is obtained by measuring the slope of the attenuation versus distance on a logarithmic scale.

Figure 41(a) shows that the absorption of light at an optical

wavelength of 1.06 μm is in the water tank about 13.7 Np/m. Similarly, Fig. 41(b) shows that α is about 1.5 Np/m for attenuation of ruby light in the same water. Note that the numerical values of α can differ significantly from one study to another.[10,14,15,54] This variation is attributed to the fact that α is highly dependent on the optical properties of the medium being used.
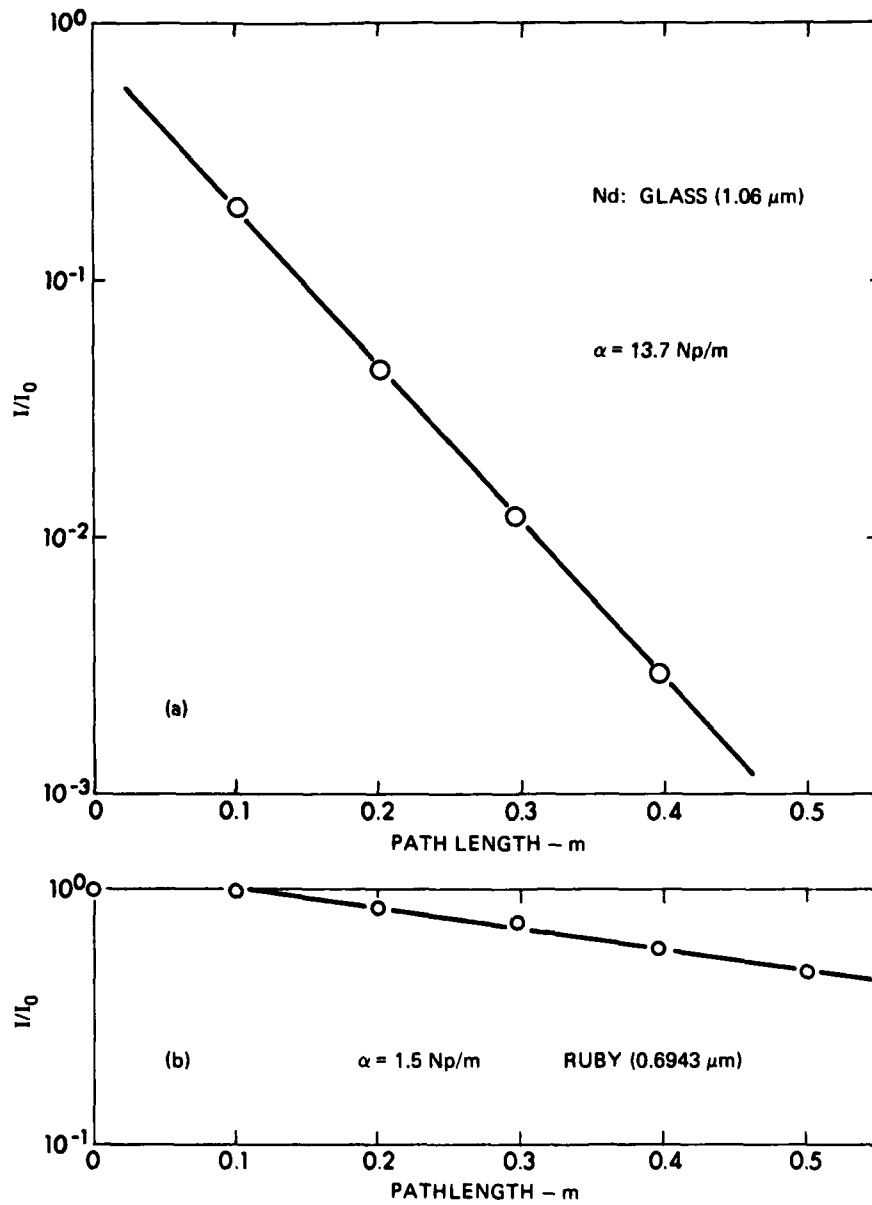
FIGURE 41
OPTICAL ABSORPTION COEFFICIENT IN WATER TANK

APPENDIX G

NUMERICAL PROGRAM "MTS"

A computer program called "MTS" has been written in Fortran, in order to compute the pressure radiated by a moving thermoacoustic source. The numerical code is based on the analysis presented in Section IV.A.

The input data to the program are variables such as the geometry between the source and the receiver, the optical coefficient of absorption, the source velocity, the modulation frequency of the laser intensity, the laser pulse duration and the optical energy going into the water, the laser beam radius on the water surface and the intensity distribution (either Gaussian or uniform) across a section of the laser beam. The output of the program is a plot of the pressure waveform at the receiver, with its corresponding acoustic level in decibels, from either peak to peak or rms pressure.

A listing of the program "MTS" is given below.

```
          PROGRAM MTS(OUT,INPUT,OUTPUT,TAPE2=OUT,RESULT,TAPE3=RESULT,
     8PLOT,TAPE5=PLOT)
          DIMENSION TIME(5000),H(100),P(5000),PT(5000)
          DIMENSION PULSE(5000),TIME2(5000),P2(5000),PLSDOT(5000)
          EXTERNAL PLS
          COMMON DT,RF,TT,T,XIO
          DATA LABX/"TIME(MS)"/
          DATA LABY/"PRESSURE"/
          LUNP=6LOUTPUT
C
C
C******************************************************************
C     THIS PROGRAM COMPUTES THE PRESSURE WAVEFORM RADIATED BY A
C     MOVING THERMOACOUSTIC ARRAY.
C      (SEE NOTES  5/18/83)  3-D PROBLEM
C
C******************************************************************
C      REVISED 02/07/85
C
C
C     PLS DEFINES LASER PULSE; STORED IN PULSE
C     MAX NUMBER OF POINTS=500
C     TIME DERIVATIVE OF LASER PULSE IS STORED IN PLSDOT
C     P(J)=PRESSURE RADIATED BY ARRAY IN POSITION I  WHEN
C     EXCITED BY AN IMPULSE PLSDOT(I)
C      P(J) IS COMPUTED INSIDE A LOOP ON THE POSITION I ,
C      AND EACH CONTRIBUTION IS PROGRESSIVELY ADDED IN AN
C      ARRAY PT(J).
C
C     J REPRESENTS THE (HORIZONTAL) TIME. .
C     PT(J)=TOTAL PRESSURE RADIATED BY THE MOVING SOURCE.
C
C     N=NUMBER OF POINTS REPRESENTING PULSE
C     TT=TOTAL TIME DURATION OF THE PULSE
C     DT=TT/N=TIME RESOLUTION
C     RF=RADIAN FREQUENCY (FACTOR OF 2 BECAUSE MODULATION IS A SIN**2)
C******************************************************************
C
C
C      INPUT VARIABLES
C
          PRINT*,"****  WELCOME AND BONJOUR ****"
          PRINT*," "
          PRINT*,"   PRESSURE RADIATED BY A M.T.A. "
          PRINT*," "
          PRINT*,"ENTER THE FOLLOWING PARAMETERS"
C
          PRINT*,"INITIAL RANGE R (M)   ="
          READ*,R
          PRINT*,"INITIAL THETA (DEG)="
          READ*,TETAD
          PRINT*,"INITIAL PHI (DEG) ="
          READ*,PHID
          PI=3.141592654
          TETAR=TETAD*PI/180.
          PHIR=PHID*PI/180.
          PRINT*,"ABSORPTION (/M)="
          READ*,ALFA
          PRINT*,"MACH NUMBER="
          READ*,XM
          PRINT*,"MODULATION FREQUENCY (KHZ)"
          READ*,F
          F=F*1000.
          PRINT*,"PULSE DURATION (MS)="
          READ*,TT
          TT=TT/1000.
          PRINT*,"AMPLITUDE AT PHOTODETECTOR (V)="
          READ*,APHID
          PRINT*,"BEAM RADIUS (CM)="
          READ*,ACM
          A=ACM*0.01
          C=1486.
```

171

```
C----------------------------------------------------------------
C       ESTIMATE THE IMPORTANCE OF FINITE BEAMWIDTH EFFECTS.
C
        PRINT*,"DO YOU WANT TO INCLUDE FINITE BEAMWIDTH EFFECTS?"
        PRINT*,"      YES=1   NO=0      (DEFAULT=1)"
        READ*, IB
        IF(IB.EQ.0)GO TO 1
C
        DT=A/(5.*C)
        IF(IB.EQ.1)PRINT*,"TIME RESOL. DT SHOULD BE LESS THAN   ",DT
C       IF BEAMWIDTH EFFECTS IMPORTANT, NEED 10 POINT/CROSS SECTION
1       PRINT*,"TIME RESOLUTION (MICROSEC) ="
        READ*, DT
        DT=DT*1.E-06
        IF(F.EQ.0.)GO TO 2
        DTLIM=1./(5.*F)
C       IF THERE IS LESS THAN 5 POINTS PER MODULATION PERIOD
C       A WARNING IS PRINTED
        IF(DT.LE.DTLIM)GO TO 2
        PRINT*,"***WARNING - DT IS TOO LARGE"
        GO TO 1
C----------------------------------------------------------------
2       RF=2.*PI*F
        V=XM*C
        EO=1.03*APHID
        SO=PI*A*A
        PO=EO/TT
        ATRANS=0.98
        XIO=PO/SO
        BETA=2.07*1.E-04
        CP=4190.
        XKC=ATRANS*BETA*ALFA*C/(4.*PI*CP)
        IF(IB.EQ.0)XKC=XKC*SO
        IFLAG=0
C----------------------------------------------------------------
C
C        COMPUTE RN,TETAN (FINAL RANGE AND ANGLE AT END OF PULSE)
C        DT=TIME RESOLUTION
C        N=NUMBER OF POINTS IN LASER PULSE
C        N2=NUMBER OF POINTS TO BE STORED FOR ANY P(J)
C        SEE NOTES FOR THE NOTATION
C
        RN=SQRT((R*R)+(V*TT)**2-(2.*V*TT*R*SIN(TETAR)*COS(PHIR)))
        TETAN=ACOS(R*COS(TETAR)/RN)
        N=INT(TT/DT)
        IF(XM-1.)6,6,7
6       AP=R*SIN(TETAR)/C
        EPS=1.
        GO TO 8
7       AP=(RN*SIN(TETAN)/C)+TT
        EPS=-1.
8       PRINT*,"TIME WINDOW FOR THE COMPUTATION"
        PRINT*,"INITIAL TIME (MS)="
        READ*, TO
        PRINT*,"FINAL TIME (MS)="
        READ*, TF
        TO=TO*0.001
        TF=TF*0.001
        TF=TF+DT
        IF(TO.LE.AP)GO TO 11
        PRINT*,"INIT.TIME SHOULD BE LESS THAN ",AP
        GO TO 8
11      N3=INT((TF-TO)/DT)+1
```

172

```
          NZERO=INT((AP-TO)/DT)
          NZEROP=NZERO+1
          N2=N3-NZERO
          IF(N.GT.5000.OR.N2.GT.5000)IFLAG=1
C         N SHOULD BE LESS THAN 5000  (VERTICAL NUMBER OF POINTS)
C         N2 SHOULD BE LESS THAN 5000 (HORIZONTAL NUMBER OF POINTS)
C
          PRINT*," "
          PRINT*,"RESOLUTION=",DT
          PRINT*,"N (VERTICAL TIME) =",N
          PRINT*,"N2 (HORIZONTAL TIME) =",N2
          PRINT*,"NZERO =",NZERO
          ENDFILE LUNP
          IF(IFLAG.EQ.1)GO TO 999
          PRINT*,"IS THAT OK? (YES=1,NO=0)"
          READ*,ISTOP
          IF(ISTOP.EQ.0)GO TO 999
C
C-----------------------------------------------------------------
C         PRINT HEADINGS
C
          PRINT(2,100)
100       FORMAT(20X,"MOVING THERMOACOUSTIC ARRAY")
          PRINT(2,101)R,TETAD,PHID,ALFA,XM
          PRINT(2,102)F,N,TT,DT
101       FORMAT(///,5X,"R=",E8.2,5X,"THETA (DEG)=",E8.2,5X,
         8"PHI=",E8.2,5X,"ABSORPTION=",E8.2,5X,"MACH=",E8.2)
102       FORMAT(5X,"MOD. FREQ. =",E8.2,5X,"N=",I4,5X,
         8"TT=",E8.2,5X,"DT=",E8.2)
          PRINT(2,103)
103       FORMAT(///,9X,"TIME",10X,"PRESSURE")
C
C-----------------------------------------------------------------
C         COMPUTE PLSDOT
C
          DO 3 M=1,N
          X=FLOAT(M)
          IF(M.GE.2)GO TO 52
          PLSDOT(1)=0.
          GO TO 3
52        PLSDOT(M)=(PLS(X)-PLS(X-1.))/DT
          PULSE(M)=PLS(X)
3         CONTINUE
C-----------------------------------------------------------------
C
C         INITIALIZE ARRAY PT(J)
C
          DO 30 J=1,N3
          PT(J)=0.
30        CONTINUE
C
C-----------------------------------------------------------------
C
C         COMPUTE RI,THETAI FOR EACH POSITION OF THE ARRAY.
C         THEN COMPUTE P(I,J)    LOOP5
C
          DO 5 I=1,N
          RI=(R*R)+(V*I*DT)**2
          RI=SQRT(RI-(2.*V*I*DT*R*SIN(TETAR)*COS(PHIR)))
          TETI=ACOS(R*COS(TETAR)/RI)
          RCI=RI*COS(TETI)
          RSI=RI*SIN(TETI)
C         THE IMPULSE RESPONSE IS INDEPENDANT OF PHI
C         EXCEPT THROUGH RI
```

```
C-------------------------------------------------------------
C
C     COMPUTE THE IMPULSE RESPONSE
C
      KFLAG=0
      T2I=(RSI/C)+(I*DT)
      T1I=AP
      T3I=(RI/C)+(I*DT)
      T3MI=T3I-DT
      DO 10 J=1,N2
      T=T1I+(J*DT)
      TIME(J)=T-(I*DT)
      IF(T.LT.T2I)GO TO 36
      IF((T-T2I).GE.1.E-08)GO TO 31
      P(J)=(X C*EXP(-ALFA*RCI))*PLSDOT(I)/RSI
      GO TO 10
36    P(J)=0.
      GO TO 10
31    ROOT=SQRT(((C*TIME(J))**2)-(RSI*RSI))
      IF(ROOT.GE.1.E-06)GO TO 32
      PRINT*,"****   ROOT=0   *****"
32    IF(T.GT.T3MI)GO TO 33
      P(J)=2.*XKC*EXP(-ALFA*RCI)*COSH(ALFA*ROOT)/ROOT
      P(J)=P(J)*PLSDOT(I)
      GO TO 10
33    KFLAG=KFLAG+1

      IF(KFLAG.NE.1)GO TO 34
C  IF KFLAG=1, T=RI/C, AND P=P(RI/C)
      P(J)=XKC*EXP(-2.*ALFA*RCI)*PLSDOT(I)/RI
      GO TO 10
34    P(J)=-2.*XKC*EXP(-ALFA*ROOT)*SINH(ALFA*RCI)/ROOT
      P(J)=P(J)*PLSDOT(I)
10    CONTINUE
C-------------------------------------------------------------
C
C     ADD SUCCECSSIVELY IN PT(J), ALL THE ELEMENTARY
C     CONTRIBUTIONS P(J), AS I IS INCREASED (IE AS THE
C     SOURCE IS MOVING).
C
      DO 35 J=1,N2
      PT(J)=PT(J)+(P(J)*DT)
35    CONTINUE
C
C     MOVE TO THE NEXT POSITION OF THE ARRAY (NEXT I)
C-------------------------------------------------------------
C
5     CONTINUE
C
C-------------------------------------------------------------
C
C
C
C     ADD NZERO ZEROES AT THE BEGINNING OF THE RECORD
C     (IE FROM T=TO TO T=AP)
C
      DO 600 KK=1,N3
      TIME(KK)=(TO+((KK-1)*DT))*1000.
      IF(KK.GT.NZERO)GO TO 601
      P2(KK)=0.
      GO TO 600
601   P2(KK)=PT(KK-NZERO)
600   CONTINUE
      DO 606 I=1,N3
      PT(I)=P2(I)*EPS
606   CONTINUE
C-------------------------------------------------------------
C
C
C     FINITE BEAMWIDTH EFFECTS
C
      IF(IB.EQ.0)GO TO 699
      PRINT*,"CROSS SECTION INTENSITY SHADING="
```

174

```
            PRINT*,"   GAUSSIAN (1)   OR   UNIFORM (2)"
            READ*,ISHADE
            CONST=SQRT(PI)*C*A*SIN(TETAR)
            TBO=(R-(A*SIN(TETAR)))/C
            TBF=(R+(A*SIN(TETAR)))/C
            I=0
            T=TBO-DT
    45      T=T+DT
            I=I+1
            IF(T.GT.TBF)GO TO 41
            O=(R-(C*T))/(A*SIN(TETAR))
            IF(ISHADE.EQ.2)H(I)=1.*CONST
            IF(ISHADE.EQ.1)H(I)=CONST*EXP(-O*O)
            GO TO 45
    41      NPB=I-1
    C
    C         CONVOLUTION FOR FINITE BEAMWIDTH
    C
            DO 42 I=1,N3
            SUM=0.
            DO 43 J=1,NPB
            IF(J.GE.I)GO TO 44
            SUM=(PT(I-J)*H(J))+SUM
            GO TO 43
    44      SUM=0.
    43      CONTINUE
            P2(I)=SUM*DT
    42      CONTINUE
    C
            DO 46 I=1,N3
            PT(I)=P2(I)
    46      CONTINUE
    C
    C         PT INCLUDES NOW THE FINITE BEAMWIDTH EFFECTS.
    C
    C------------------------------------------------------
    C
    C         COMPENSATE FOR THE PHASE SHIFT OF THE CONVOLUTION
    C
            DO 614 I=1,N3
            IF(I.NE.N3)GO TO 615
            PT(I)=0.
            GO TO 614
    615     PT(I)=PT(I+1)
    614     CONTINUE
    C
    C         PRINT THE RESULT
    C
    699     DO 602 I=1,N3
            WRITE(2,300)TIME(I),PT(I)
            WRITE(3,300)TIME(I),PT(I)
    602     CONTINUE
    300     FORMAT(2(5X,E12.4))
    C
    C------------------------------------------------------
    C         COMPUTE THE RMS PRESSURE AND THE ACOUSTIC LEVEL
    C
            PRINT*,"COMPUTATION OF THE ACOUSTIC LEVEL"
            PRINT*," (1) PEAK TO PEAK    OR  (2) RMS  ?"
            READ*,IDB
            IF(IDB.EQ.1)GO TO 613
    C
            PRINT*,"DO YOU WANT TO SPECIFY A NEW TIME WINDOW FOR THE"
            PRINT*,"COMPUTATION OF THE RMS PRESSURE? (YES=1,NO=0)"
            READ*,IRMSW
            IF(IRMSW.EQ.1)GO TO 611
            TWO=TO
            TWF=TF
            GO TO 612
```

175

```
611     PRINT*,"WINDOW FOR THE COMPUTATION OF THE RMS PRESSURE"
        PRINT*,"INITIAL TIME (MS) FOR THE WINDOW="
        READ*,TWO
        TWO=TWO/1000.
        PRINT*,"FINAL TIME(MS) FOR THE WINDOW="
        READ*,TWF
        TWF=TWF/1000.
612     TW=TWF-TWO
        NPO=INT((TWO-TO)/DT)+1
        NPF=INT((TWF-TO)/DT)+1
        RMS=0.
        DO 603 I=NPO,NPF
        RMS=RMS+(PT(I)**2)
603     CONTINUE
        RMS=SQRT(RMS*DT/TW)
        PRINT*,"*********  RMS PRESSURE = ",RMS
613     PMAX=-100.
        PMIN=100.
        DO 39 I=1,N3
        IF(PT(I).LE.PMIN)PMIN=PT(I)
        IF(PT(I).GE.PMAX)PMAX=PT(I)
39       CONTINUE
        PAMP=PMAX-PMIN
        IF(IDB.EQ.1)ARGMT=PAMP
        IF(IDB.EQ.2)ARGMT=RMS
        DB=20.*ALOG10(ARGMT*1.E+06)
        PRINT*,"*********  ACOUSTIC LEVEL=",DB
        PRINT*," "
        PRINT*,"DO YOU WANT A PLOT (YES=1;NO=0)?"
        READ*,IPLOT
        IF(IPLOT.EQ.0)GO TO 999
C--------------------------------------------------------
C
        PRINT*,"   PMAX=",PMAX
        PRINT*,"   PMIN=",PMIN
        PRINT*,"DO YOU WANT A NORMALIZED PLOT? (YES=1,NO=0)"
        READ*,INORM
        IF(INORM.EQ.0)GO TO 995
        PNORM1=ABS(PMIN)
        PNORM=AMAX1(PNORM1,PMAX)
        DO 40 I=1,N3
        PT(I)=PT(I)/PNORM
40      CONTINUE
C--------------------------------------------------------
C
C       PLOT ROUTINE
C
995     XORG=6.
        YORG=6.
        PRINT*,"DO YOU WANT TO SPECIFY A TIME WINDOW"
        PRINT*,"FOR THE PLOT  ? (YES=1; NO=0)"
        READ*,IPW
        IF(IPW.EQ.1)GO TO 996
        XMIN=TIME(1)
        XMAX=TIME(N3)
        IMAX=N3
        GO TO 997
C
996     PRINT*,"TMIN FOR PLOT (MS)"
        READ*,TPO
        PRINT*,"TMAX FOR PLOT (MS)="
        READ*,TPF
        TPO=TPO*0.001
        TPF=TPF*0.001
        NDL=INT((TPO-(TIME(1)*0.001))/DT)
```

176

```
        IMAX=INT((TPF-TPO)/DT)
        DO 993 I=1,IMAX
        P2(I)=PT(I+NDL)
        TIME2(I)=TIME(I+NDL)
993     CONTINUE
        DO 994 I=1,IMAX
        PT(I)=P2(I)
        TIME(I)=TIME2(I)
994     CONTINUE
        XMIN=TPO*1000.
        XMAX=TPF*1000.
997     IF(INORM.EQ.1) GO TO 991
        PRINT*,"YMIN="
        READ*,YMIN
        PRINT*,"YMAX="
        READ*,YMAX
        GO TO 992
991     YMIN=-1.5
        YMAX=1.5
992     XDEL=(XMAX-XMIN)/10.
        YDEL=(YMAX-YMIN)/8.
        AXL=5.
        AYL=3.
        XTITL=AXL/2.
        YTITL=AYL+0.5
        DX=(XMAX-XMIN)/AXL
        DY=(YMAX-YMIN)/AYL
        CALL PLTLFN(4LPLOT)
        CALL PLTORG(XORG,YORG)
        CALL PLTDIM(11.,8.5,1.4.)
        CALL PLTAXIS(0.,0.,AXL,0.,XMIN,XMAX,XDEL,LABX,-8,4,-.1,-.1)
        CALL PLTAXIS(0.,0.,AYL,90.,YMIN,YMAX,YDEL,LABY,8,1,-.1,-.1)
        CALL PLTAXIS(0.,AYL,AXL,0.,XMIN,XMAX,XDEL,LABX,0,0,-.1,-.1)
        CALL PLTAXIS(AXL,0.,AYL,90.,YMIN,YMAX,YDEL,LABY,0,0,.1,.1)
        CALL PLTDATA(TIME,PT,IMAX,0.,0,XMIN,DX,YMIN,DY,0.)
        CALL PLTLINE(XTITL,YTITL,-.14)
        WRITE(5,1000)
1000    FORMAT("LASER-INDUCED THERMOACOUSTIC PRESSURE")
        CALL PLTLINE(XTITL,-.8,-.1)
        WRITE(5,1001)R,TETAD,PHID,XM
1001    FORMAT("R (M)=",F6.2,4X,"THETA(D)=",F4.1,4X,"PHI(D)=",F6.1,
       84X,"MACH=",F4.1)
        F=F/1000.
        TT=TT*1000.
        CALL PLTLINE(XTITL,-1.,-.1)
        WRITE(5,1002)ALFA,F,TT
1002    FORMAT("ABS. (NP/M)=",F6.2,4X,"FREQ. (KHZ)=",F6.2,4X,
       8"TP(MS)=",F6.2)
        IF(IDB.EQ.1)GO TO 990
        TW=1000.*(TW-DT)
        CALL PLTLINE(XTITL,-1.2,-.10)
        WRITE(5,1003)PAMP,DB,TW
1003    FORMAT("PAMP (PA) =",F8.4,3X,"LEVEL (DB) =",F6.2,3X
       8,"TAVE (MS) =",F6.3)
        GO TO 989
990     CALL PLTLINE(XTITL,-1.2,-.10)
        WRITE(5,1004)PAMP,DB
1004    FORMAT("PAMP (PA)=",F6.3,9X,"LEVEL (DB)=",F6.2)
C
989     CALL PLTEND(0.,0.)
999     STOP
        END
C
C       DEFINE EXTERNAL LASER PULSE
C
        FUNCTION PLS(Y)
        COMMON DT,RF,TT,T,XIO
        T=Y*DT
989     PI=3.141592654
        A=10.8
        B=5.0
        ENVLP=XIO*(A*T/TT)*EXP(-B*T/TT)
        PLS=((SIN(RF*T/2.))**2)*ENVLP
        IF(RF.EQ.0.)PLS=ENVLP
        RETURN
        END

11.43.39.UCLP. AA. PTRLO5,       0.519KLNS.       ** END OF LISTING **
```

177

APPENDIX H

SIMPLIFIED ANALYSIS FOR A LASER-INDUCED MACH WAVE

The case of a thermoacoustic source moving at transonic velocity deserves special attention because it yields very high pressure transients. In this appendix we seek an analytical expression for the pressure waveform radiated by an MTS moving at velocity $v = c/\sin\theta_0 \cos\phi_0$ towards the receiver.

In order to simplify the analysis, it is assumed that the sound field radiated by the transonic source is the same as the one radiated by a stationary source excited by a short impulse of light. The reason for this similarity lies in the fact that all the acoustic disturbances emitted by a source moving at the speed of sound arrive nearly simultaneously at the fixed receiver, so that the receiver sees in fact the result of an instantaneous input of heat in the medium. This approximation, which is valid only in the farfield so that the angle of observation between the source and the receiver remains approximatively constant, has been discussed in the Soviet literature.[10,12,26]

It has been shown (Eq. 3.4) that the acoustic pressure seen at the receiver, is

$$p(t) = h_L(t) * h_a(t) * I_t(t) \quad , \tag{H1}$$
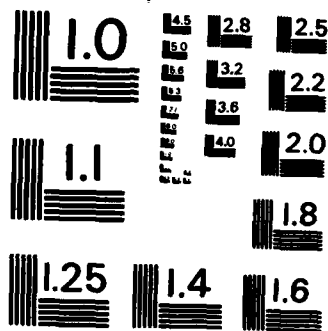
MICROCOPY RESOLUTION TEST CHART

NATIONAL BUREAU OF STANDARDS-1963-A

where the asterisk denotes a convolution and the subscript t, a time derivative.

Assuming that the effect of moving the source at transonic velocity is simply to shrink the effective laser pulse as seen by the receiver at the retarded time r_0/c, to a very short impulse of light, we rewrite Eq. (H1) as,

$$p(t) \sim h_L(t) * h_\theta(t) * \delta_t(t-r_0/c) \qquad , \qquad (H2)$$

where δ is the Dirac delta function. It has been shown in Section III.B that, in the farfield, $h_L(t)$ tends to behave like the time derivative of a delta function, so that Eq. (A2) becomes

$$p(t) \sim d^2/dt^2 [h_\theta(t)] \qquad . \qquad (H3)$$

The acoustic pressure received at the receiver is therefore proportional to the second time derivative of the impulse response of a cross section of the laser beam. Assuming a Gaussian intensity distribution, we can express the received pressure as

$$p(t) \sim (2\tau^2-1) \exp(-\tau^2) \qquad , \qquad (H4)$$

where $\tau = (r_0-ct/a \sin\theta_0)$. Taking the Fourier transform of Eq. (H3) gives an estimate of the spectrum of a laser-induced Mach wave. For a Gaussian intensity distribution, it takes the form

179

$$p(\omega) \sim \Omega^2 \exp(-\Omega^2/4) \quad , \qquad\qquad (H5)$$

where $\Omega = f_0 / (a \sin\theta_0/c)$ is a nondimensional frequency characteristic of diffraction effects imposed by the finite dimension of the laser beam cross section.

This last result is of practical importance as far as long range propagation of thermoacoustic signals under water is concerned, because it shows that the acoustic signal contains some low frequencies which will propagate long distances under water before being absorbed.

APPENDIX I

DIRECTIVITY PATTERNS AND SPREADING CURVES WITH A RUBY
LASER

In this appendix we present some experimental results that were obtained with a ruby laser. The optical coefficient of absorption of ruby light (optical wavelength 0.6943 μm) in the water tank was measured to be 1.5 Np/m (see Appendix F), so that the thermoacoustic source was fairly long.

Figure 42 shows the directivity pattern of such a source, measured in its vertical plane, at a radius of 4 m from the initial point of impact of the laser beam on the surface of the water. The modulation frequency was 9.75 kHz and the source velocity was v=0.5 c , where c is the speed of sound in the water (1486 m/s). The experimental data on Fig. 42 is compared with two theoretical models. The solid line in Fig. 42 represents the analytical expression given by Lyamshev and Sedov in reference 18. In this model, which is valid only in the farfield, the motion of the source is taken into account by a simple ad hoc Doppler shift of the modulation frequency. The dashed line in Fig. 42 was obtained from the numerical model described in Chapter IV.A. It can be noted that this model seems to predict the presence of sidelobes in the directivity pattern, whereas the prediction by Lyamshev and Sedov does not show this feature. The reason for this difference is that, contrarily to our numerical approach, their model is not valid in the
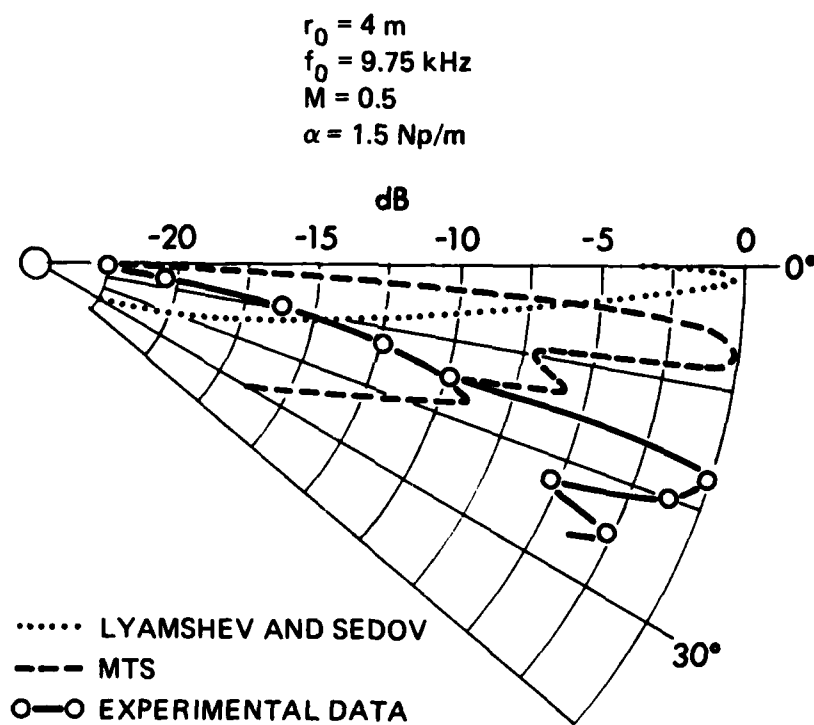
$r_0 = 4$ m
$f_0 = 9.75$ kHz
$M = 0.5$
$\alpha = 1.5$ Np/m

FIGURE 42
VERTICAL DIRECTIVITY OF AN MTS - I

nearfield. The farfield prediction for the tilt angle of the main lobe is about 89^0, whereas the experimental result indicates a value of about 72^0. The numerical model predicts a value of 82^0, and although it yields a better estimate than the farfield theory, it still overestimates the tilt angle by 10^0.

Figure 43 reports the result of a similar experiment, the major difference being that the source was moving at Mach 1. The modulation frequency was 19.5 kHz. Again the nearfield directivity pattern shows some sidelobes structure and a very large tilt angle of the main lobe, most of the acoustic radiation being radiated at 20^0 from the interface.

Figure 44 also shows a vertical directivity pattern, but this time the source was moving at supersonic velocity (M=1.5). The modulation frequency was about 29.25 kHz. The distance of observation was 9.4 m so that, in this case, the receiver was far enough from the source to ignore nearfield effects. Experimental results show that indeed the main acoustic lobe narrows significantly to only a few degrees for the half-power beamwidth, and approaches the interface between air and water. This is qualitatively confirmed by the numerical model (program MTS) but there is an unexplained significant quantitative difference between the predictions and the experimental data. A possible explanation for the presence of some irregularities in the experimental beam pattern could be the presence of some spurious harmonics in the signal.

Experimental data for a horizontal directivity pattern are shown in Fig. 45. The radius of observation was 2m, the modulation frequency was 9.75 kHz, and the source Mach number was 0.5. As discussed in

183
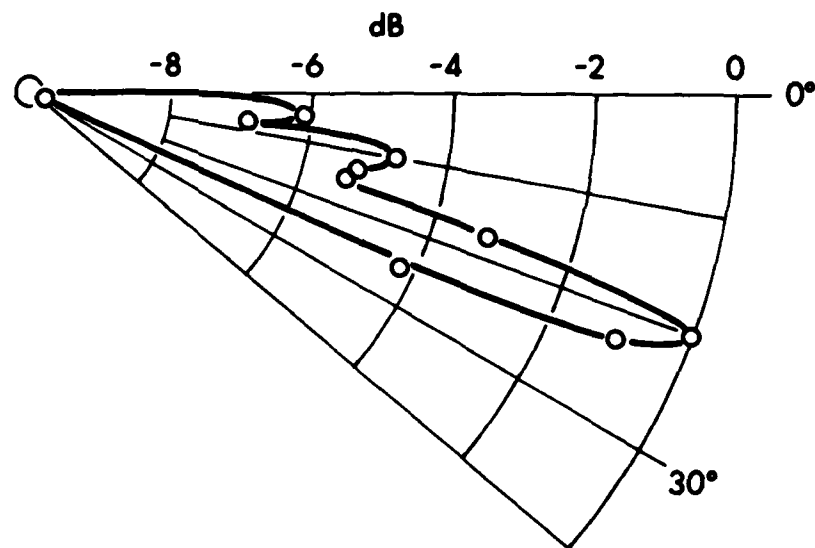
FIGURE 43
VERTICAL DIRECTIVITY OF A TRANSONIC MTS

M = 1.5
α = 1.5 Np/m
r = 9.4 m
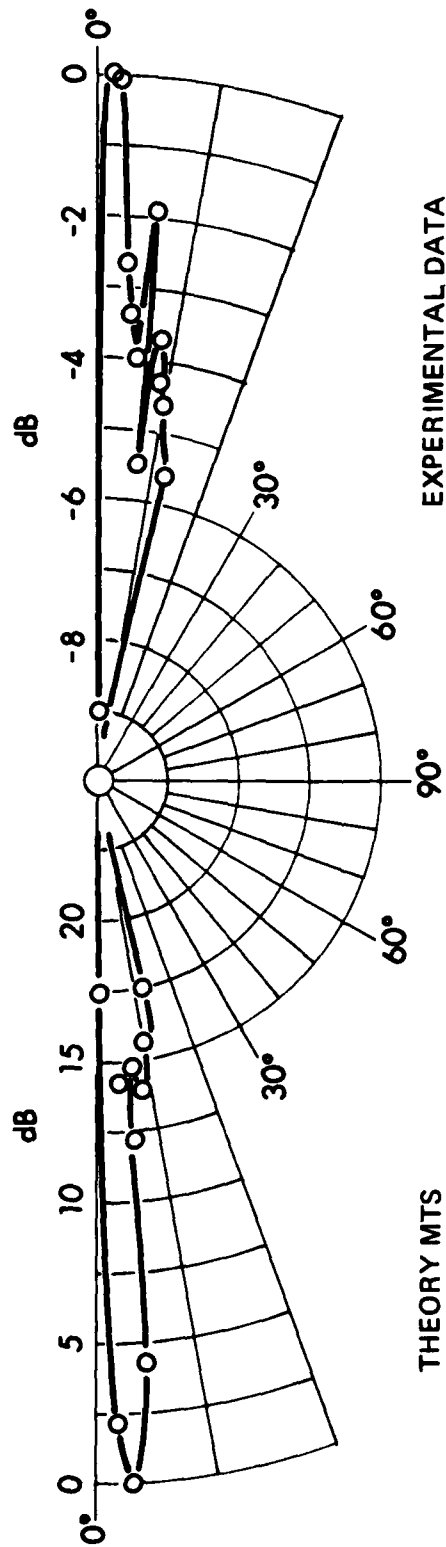f_0 = 29.25 kHz

dB

EXPERIMENTAL DATA

THEORY MTS

FIGURE 44
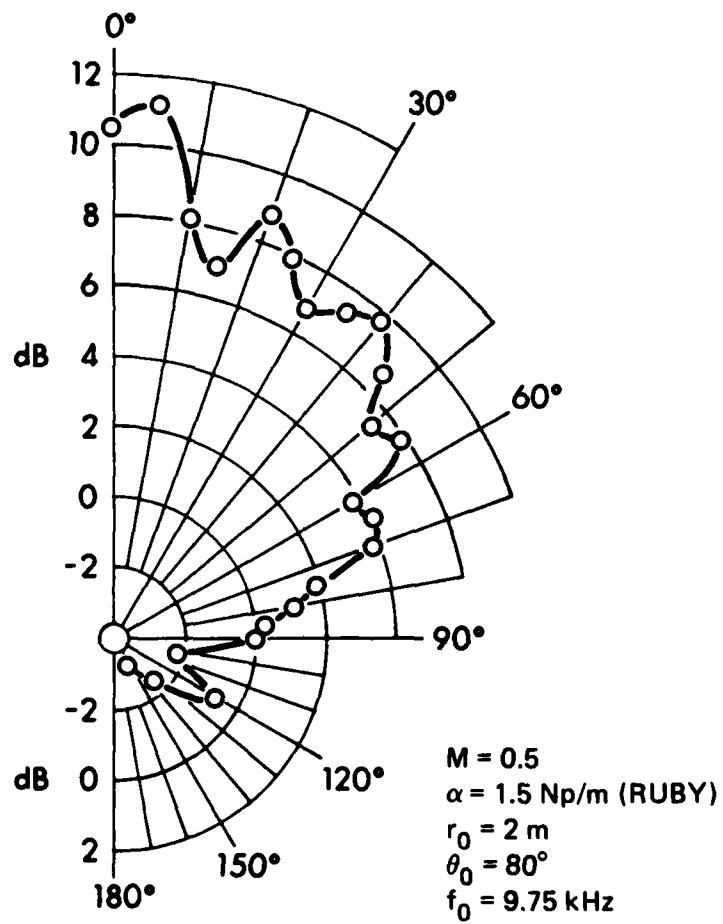VERTICAL DIRECTIVITY OF AN MTS - II

185

FIGURE 45
HORIZONTAL DIRECTIVITY OF AN MTS

Section IV.B.2, there is a strong reinforcement (more than 10 dB) of the acoustic radiation in the direction of motion of the source.

Finally, the sound level dependence on range of observation was determined for an MTS moving at Mach 1.5 towards the receiver. The results are given in Fig. 46. The Doppler shifted received frequency was about 61 kHz at all ranges. The results confirm that close enough to the source, a slope of 3 dB characteristic of cylindrical spreading can be expected. But when the receiver is far enough from the source, the classical spherical spreading law of 6 dB per doubling of distance dominates.

The experimental data presented in this appendix were obtained with a "mechanical modulator" in order to achieve the modulation of the laser beam. The optical modulation system (Pockels cell and polarizers) described in section II.A became ineffective because one of the polarizers was damaged. A mechanical modulator was built to replace the optical modulation system. The mechanical modulator consists of a series of wooden sticks placed evenly over the water surface, along the laser beam path, so that the laser beam could penetrate into the water only intermittently. The thickness of the sticks was equal to the spacing between the sticks, and this spacing was equal to the laser beam diameter on the surface of the water. This modulation system turned out to be very effective, although the modulation frequency was dictated by the laser beam scanning velocity. The relationship between the modulation frequency and the source velocity was, in our design, given by $f_0 = 19.5 M$, where M is the source Mach number and where f_0 is expressed in kHz.
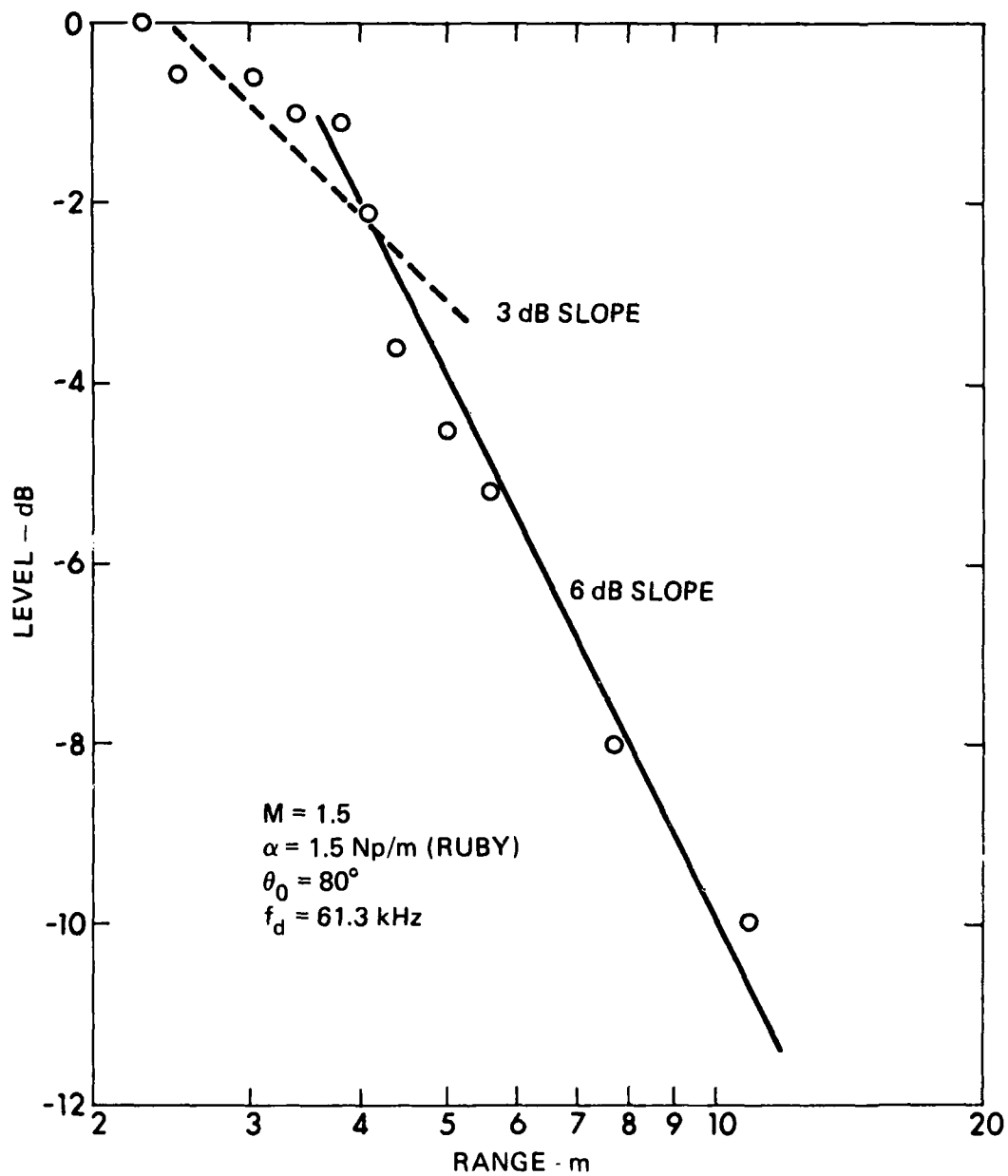
FIGURE 46
SPREADING OF AN MTS

REFERENCES

1. A. G. Bell, "Upon the production of sound by radiant energy," Philoso. Mag. (Ser.5) **11**, 510-528 (1881).

2. A. C. Tam, "Photoacoustics: Spectroscopy and other applications," in <u>Ultrasensitive Laser Spectroscopy</u>, edited by D. S. Kliger, (Academic Press, New York, 1983), chapter 1.

3. A. D. Pierce and H. A. Hsieh, "Bilbliography on Laser-induced sound," compiled for paper UU1, 109th meeting of the Acoustical Society of America, (1985).

4. M. P. Felix and A. T. Ellis, "Laser-induced liquid breakdown. A step-by-step account," Appl. Phys. Letters **19**(11), 484-486 (1971).

5. G. A. Askar'yan, et al., "The effects of a laser beam in a liquid," Sov. Phys. JETP **17**(6), 1463-1465 (1963).

6. R. M. White, "Generation of elastic waves by transient surface heating," J. Appl. Phys. **34**(12), 3559-3567 (1963).

7. U. Ingard, Acoustics, <u>Handbook of Physics</u>, edited by E. U. Condon, and H. Odishaw, (McGraw-Hill,1958), chapter 8.

8. P. J. Westervelt and R. S. Larson, "Laser-excited broadside array," J. Acoust. Soc. Am. **54**, 121-122 (1973).

9. T. G. Muir, C. R. Culbertson, and J. R. Clynch, "Experiments on thermoacoustic arrays with laser excitation," J. Acoust. Soc. Am. **59**, 735-743 (1976).

10. F. V. Bunkin, et al., "Experimental investigation of the acoustic field of a moving optoacoustic antenna," Sov. J. Quantum Electron. 8(2), 270-271 (1978).

11. A. I. Bozhkov, et al., "Moving laser thermooptical sources of ultrasound," Sov. Phys. Acoust. 26(2), 100-104 (1980).

12. F. V. Bunkin, A. I. Malyarovskii, and V. G. Mikhalevich, "Experimental study of pulsed sound fields excited by moving laser thermooptical sources," Sov. Phys. Acoust. 27(2), 98-102 (1981).

13. C. R. Culbertson, N. P. Chotiros, and Y. H. Berthelot, "Experimental apparatus for studying moving thermoacoustic sources," Applied Research Laboratories Technical Report No. 83-24, (ARL-TR-83-24), Applied Research Laboratories, The University of Texas at Austin (1983).

14. C. R. Culbertson, "Experimental investigation of the laser-excited thermoacoustic array in water," Applied Research Laboratories Technical Report No. 75-51, (ARL-TR-75-51), Applied Research Laboratories, The University of Texas at Austin (1975).

15. Y. H. Berthelot and I. J. Busch-Vishniac, "Laser-induced thermoacoustic radiation," submitted to J. Acoust. Soc. Am. (1985).

16. R. S. Larson, "Optoacoustic interactions in fluids," Applied Research Laboratories Technical Report No. 74-21, (ARL-TR-74-21), Applied Research Laboratories, The University of Texas at Austin (1974).

17. P. M. Morse, Vibration and Sound, published by the American Institute of Physics for the Acoustical Society of America, (1976). See chapter VII, pp. 344-346. In Fig. 77, p. 345, r-y cosθ should be read as r-y sinθ.

18. L. M. Lyamshev and L. V. Sedov, "Optical generation of sound in a liquid: Thermal mechanism (review)," Sov. Phys. Acoust. **27**(1), 4-18 (1981).

19. The minus sign in the right-hand side of Eq. (12) in reference 18 should be read as a plus sign.

20. A typographical error appears in Eq. (13) of reference 18. In Lyamshev and Sedov's notation, the exponent of the exponential should be divide by τ_μ. However, it turns out that the exponential term is of negligible order and should be discarded to be consistent with other approximations assumed in the derivation.

21. Sir H. Lamb, Hydrodynamics, 6th edition, (Dover publications, New York, 1945), Chapter XIII, art. 196 and 197, pp. 298-299.

22. Y. H. Berthelot and I. J. Busch-Vishniac, "Thermoacoustic radiation of sound by a moving laser source," submitted to J. Acoust. Soc. Am. (1985).

23. C. Doppler, "Bemerkungen zu meiner theorie des farbigen lichtes der doppelsterne etc. mit vorzuglicher rucksicht auf die von Herrn Dr. Ballot zu Utrecht dagegen erhobenen bedenken," Ann. Phys. Chem. **68**, 1-35 (1846). (in German).

24. Y. H. Berthelot and I. J. Busch-Vishniac, "The Doppler shift of an acoustic source moving at transonic velocity," submitted to J. Acoust. Soc. Am. (1985).

25. Lord Rayleigh, _The Theory of Sound_, (Dover publications, New York, 1945), Vol. 2, art. 298.

26. L. M. Lyamshev and L. V. Sedov, "Generation of sound by a moving pulsed optoacoustic source," Sov. Phys. Acoust. **25**(6), 510-514 (1979).

27. L. M. Lyamshev and K. A. Naugol'nykh, "Optical generation of sound: Nonlinear effects. (Review)," Sov. Phys. Acoust. **27**(5), 357-371 (1981)

28. A. A. Karabutov, "Nonlinear limit on the efficiency of an optoacoustic exciter," Sov. Phys.Tech. Lett. **5**(4), 174-175 (1979).

29. A. A. Karabutov and O. V. Rudenko, "Nonlinear plane waves excited by volume sources in a medium moving with transonic velocity," Sov. Phys. Acoust. **25**(4), 306-309 (1979).

30. A. I. Bozhkov, F. V. Bunkin, and Al. A. Kolomenskii, " Acoustic perturbations in a medium in connection with the restricted motion of a thermal source having the speed of sound," Sov. Phys. Acoust. **25**(5), 443-445 (1979).

31. V. E. Gusev and A. A. Karabutov, "Excitation of acoustic pulses by distributed sources moving with transonic velocity," Sov. Phys. Acoust. **27**(2), 117-120 (1981).

32. V. E. Gusev and A. A. Karabutov, "Transonic flow of relaxing gas past a heat-release layer," Sov. Phys. Acoust. **28**(2), 108-111 (1982).

33. Eq. (5.18) is valid only if the slope of the characteristic is monotonic between the limit of integration.

34. N. P. Chotiros, "The moving thermoacoustic array: A theoretical feasibility study," Applied Research Laboratories Technical Report No. 85-3, (ARL-TR-85-3), Applied Research Laboratories, The University of Texas at Austin (1985).

35. B. S. Maccabee and C. E. Bell, "Acoustic pressure scaling of laser-induced sound," Naval Surface Weapons Center, Technical Report No. 82-122, (NSWC-TR-82-122) (1982).

36. B. S. Maccabee and C. E. Bell, Naval Surface Weapons Center, Technical Report No. 83-130, (NSWC-TR-83-130) (1983).

37. V. S. Teslenko, "Investigation of photoacoustic and photohydrodynamic parameters of laser breakdown in liquids", Sov. J. Quantum Electron. 7(8), 981-984 (1977).

38. L. M. Lyamshev, V. G. Mikhalevich, and G. P. Sipulo, "Thermooptical excitation of acoustic fields in a liquid by a periodic train of laser pulses," Sov. Phys. Acoust. 26(2), 126-130 (1980).

39. A. D. Pierce and H. A. Hsieh, "Achievement of substantially higher source levels for airborne-laser-induced sound," J. Acoust. Soc. Am. 77, S104 (1985).

40. A. D. Pierce, "Energy partitoning and optical-to-acoustical conversion efficiency during laser generation of underwater sound," J. Acoust. Soc. Am., Suppl. 1, 74, S78 (1983).

41. T. McKee and J. A. Nilson, "Excimer applications," Laser focus, Vol.18, 51-55, June 1982.

42. J. M. Lourtioz, "Le laser NH3: Un rendement record," La Recherche Vol. 16, No.162, 108-111, January 1985. (in French).

43. C. A. Robinson, Jr., "Defense dept. backs space-based missile defense," Aviation Week and Space Technology, 14-16, September 1982.

44. <u>Underwater electroacoustic standard transducers</u>, published by Naval Research Laboratory, Underwater Sound Reference Detachment, Orlando , Florida. (1982).

45. G. Van Wylen and R. Sonntag, <u>Fundamentals of Classical Thermodynamics</u>, second edition, (John Wiley and sons, Inc, 1973), Chapter 10, Eq. (10.39) p. 390.

46. See reference 45, Chapter 10, Eq. (10.21), p 378.

47. P. J. Westervelt, "Parametric end-fire array," J. Acoust. Soc. Am. **32**(A), 934-935 (1960). Also see "Parametric acoustic array," J. Acoust. Soc. Am. **35**, 535-537 (1963).

48. B. K. Novikov, D. V. Rudenko, and V. I. Timoshenko, <u>Nonlinear Hydroacoustics</u>, (Sudostroyeniye, Leningrad,1981), Chapter 9. (in Russian).

49. K. B. Oldham and J. Spanier, <u>The Fractional Calculus</u>, (Academic Press, New York, 1974), Chapters 1, 3, and 7.

50. J. Lighthill, <u>Waves in Fluids</u>, (Cambridge University Press, 1978), Chapter 1, pp. 20-21.

51. P. L. Marston, "Half-order derivative of a sine-wave burst: Applications to two-dimensional radiation, photoacoustics, and focused scattering from spheres and a torus," J. Acoust. Soc. Am. **76**(1), 291-295 (1984).

52. A. D. Pierce and H. A. Hsieh, "Multi-dimensional acoustic transients created by laser beams moving over water surfaces at supersonic speeds," <u>Multi-Dimensional Fluid Transients</u>, ASME winter annual meeting, New Orleans (1984).

53. I. S. Gradshteyn and I. M. Ryzhik, <u>Table of Integrals, Series, and Products</u>, second edition, (Academic Press, inc, New York, 1980). see art. 9.241.2 p 1064.

54. V. M. Zolotarev, et al., "Dispersion and absorption of liquid water in the infrared and radio regions of the spectrum," Opt. Spectrosc. **27**, 430-432 (1969).

DISTRIBUTION LIST FOR
ARL-TR-85-21
UNDER CONTRACT N00014-82-K-0425

<u>Copy No.</u>

Director
Office of Naval Research
Department of the Navy
Arlington, VA 22217
1   Attn: R. M. Fitzgerald, Code 425UIA
2   L. E. Hargrove, Code 412

Director
Naval Research Laboratory
455 Overlook Ave., S. W.
Washington, DC 20375
3   Attn: Code 2627

4 - 15 Commanding Officer and Director
Defense Technical Information Center
Bldg. 5, Cameron Station
Alexandria, VA 22314

New London Laboratory
Naval Underwater Systems Center
New London, CT 06320
16   Attn: Bill Roderick

17   Commander
Naval Ocean Systems Center
San Diego, CA 92152

Director
Naval Surface Weapons Center
White Oak Laboratory
Silver Spring, MD 20910

| 18 | Attn: | C. Bell |
| 19 | | B. Maccabee |

Naval Postgraduate School
Department of Physics
Monterey, CA 93940

| 20 | Attn: | S. Garrett |
| 21 | | S. W. Yoon |

Chief
Defence Research Establishment Atlantic
P. O. Box 1012
Dartmouth, Nova Scotia
CANADA

| 22 | Attn: | H. M. Merklinger |

Applied Research Laboratory
The Pennsylvania State University
P. O. Box 30
State College, PA 16801

23	Attn:	Librarian
24		J. Hughes
25		M. Josserand

School of Mechanical Engineering
Georgia Institute of Technology
Atlanta, GA 30332

26	Attn:	Y. H. Berthelot
27		H. A. Hsieh
28		J. H. Ginsberg
29		A. D. Pierce
30		P. H. Rogers

Department of Physics
Brown University
Providence, RI 02912

31   Attn: R. T. Beyer
32   P. J. Westervelt

Department of Physics
University of Mississippi
University, MS 38677

33   Attn: H. E. Bass
34   L. A. Crum

Department of Physics
Washington State University
Pullman, WA 99164

35   Attn: P. L. Marston

Department of Physics
Kalamazoo College
Kalamazoo, MI 49007

36   Attn: W. M. Wright

Department of Engineering
Yale Univerisity
Mason Laboratory
9 Mill House Avenue
New Haven , CT 06520

37   Attn: R. E. Apfel

Department of Physics
The Pennsylvania State University
104 Davey Laboratory
University Park, PA 16802

38   Attn: J. D. Maynard

Department of Mechanical Engineering
The Pennsylvania State University
213 Unit E
University Park, PA 16802

39   Attn: G. Reethof
40   F. Pla

Department of Ocean Engineering
Florida Atlantic University
Boca Raton, FL 33431

41   Attn: J. Cuschieri
42   B. Davidson
43   D. Dunn
44   S. Glegg

Department of Physics
Hendrix College
Conway, AR 72032

45   Attn: R. Rolleigh

Mechanical Engineering Department
The University of Texas at Austin
Austin, TX 78713

46 - 49 Attn: I. Busch-Vishniac
50   M. Hamilton
51   D. Wilson

Electrical Engineering Department
The University of Texas at Austin
Austin, TX 78713

52   Attn: M. Becker
53   E. Hixson

Distribution List for ARL-TR-85-21 under Contract N00014-82-K-0425
(cont'd)
<u>Copy No.</u>

             Institute of Sound and Vibration Research
             The University
             Southampton S09 5NH
             ENGLAND
54   Attn: C. L. Morfey

             Matematisk Institutt
             University of Bergen
             Allegaten 53-55
             5014 Bergen-U
             NORWAY
55   Attn: Sigve Tjøtta
56   Jacqueline Naze Tjøtta

             Department of Physics
             University of Bergen
             Allegaten 53-55
             5000 Bergen
             NORWAY
57   Attn: H. Hobaek

             Physics Department
             The University of Auckland
             Private Bag, Auckland
             NEW ZEALAND
58   Attn: A. C. Kibblewhite
59   C. T. Tindle

             Groupe d'Etude et de Recherche
              de Detection Sous-Marines
             Le Brusc
             B.C.A.N. Toulon
             FRANCE
60   Attn: B. Lucas

Universite de Technologie de Compiegne
Génie Mécanique (AVI)
B.P. 233
Compiegne, 60206 - CEDEX
FRANCE

61   Attn: J. F. Amphoux de Bellevel

62   J. M. Ville

AT&T Bell Laboratories
Acoustics Research Department
Murray Hill, NJ 07974

63   Attn: J. E. West

Hoover, Keith and Bruce, Inc.
9730 Town Park
Houston, TX 77036

64   Attn: H. Kuntz

Tracoustics, Inc.
P. O. Box 3610
Austin, TX 78764

65   Attn: D. Nelson

Wyle Laboratories
128 Maryland St.
El Segundo, CA 90245

66   Attn: L. Sutherland

IBM Research Laboratory
San Jose, CA 95193

67   Attn: A. Tam (K46/282)

68   Union Carbide Corporation
Parma Technical Center
Electrode Systems Division
P. O. Box 6116
Cleveland, OH 44101

Distribution List for ARL-TR-85-21 under Contract N00014-82-K-0425
(cont'd)

<u>Copy No.</u>

69	W. James Hadden 2400 Westover Austin, TX 78703
70	Advanced Sonar Division, ARL:UT
71	Garland R. Barnard, ARL:UT
72 - 92	Yves H. Berthelot, ARL:UT
93	David T. Blackstock, ARL:UT
94	Nicholas P. Chotiros, ARL:UT
95	Frederick D. Cotaras, ARL:UT
96	Charles R. Culbertson, ARL:UT
97	James M. Estes, ARL:UT
98	Thomas A. Griffy, ARL:UT
99	Loyd D. Hampton, ARL:UT
100	James A. Hawkins, ARL:UT
101	John M. Huckabey, ARL:UT
102	Thomas G. Muir, ARL:UT
103	John D. Sample, ARL:UT
104	Stephen C. Schreppler, ARL:UT
105	James A. TenCate, ARL:UT

Distribution List for ARL-TR-85-21 under Contract N00014-82-K-0425
(cont'd)

106   Reuben H. Wallace, ARL:UT

107   Library, ARL:UT

END

FILMED

12-85

DTIC